

## The *R*-Process Alliance: Chemo-Dynamically Tagged Groups of Halo *r*-Process-Enhanced Stars Reveal a Shared Chemical-Evolution History

DMITRII GUDIN,<sup>1,2,3</sup> DEREK SHANK,<sup>1,2</sup> TIMOTHY C. BEERS,<sup>1,2</sup> ZHEN YUAN,<sup>4</sup> GUILHERME LIMBERG,<sup>5</sup> IAN U. ROEDERER,<sup>6,2</sup> VINICIUS PLACCO,<sup>1,2,7</sup> ERIKA M. HOLMBECK,<sup>1,2,8</sup> SARAH DIETZ,<sup>1,2</sup> KAITLIN C. RASMUSSEN,<sup>1,2,6</sup> TERESE T. HANSEN,<sup>9,10</sup> CHARLI M. SAKARI,<sup>11</sup> RANA EZZEDDINE,<sup>12,2,13</sup> AND ANNA FREBEL<sup>12,2</sup>

<sup>1</sup>*Department of Physics, University of Notre Dame, Notre Dame, IN 46556, USA*

<sup>2</sup>*Joint Institute for Nuclear Astrophysics – Center for the Evolution of the Elements (JINA-CEE), USA*

<sup>3</sup>*Department of Mathematics, University of Maryland, College Park, MD 20742, USA*

<sup>4</sup>*Key Laboratory for Research in Galaxies and Cosmology, Shanghai Astronomical Observatory, Chinese Academy of Sciences, 80 Nandan Road, Shanghai 200030, China*

<sup>5</sup>*Universidade de São Paulo, Instituto de Astronomia, Geofísica e Ciências Atmosféricas, Departamento de Astronomia, SP 05508-090, São Paulo, Brazil*

<sup>6</sup>*Department of Astronomy, University of Michigan, 1085 S. University Ave., Ann Arbor, MI 48109, USA*

<sup>7</sup>*NSF's National Optical-Infrared Astronomy Research Laboratory, Tucson, AZ 85719, USA*

<sup>8</sup>*Center for Computational Relativity and Gravitation, Rochester Institute of Technology, Rochester, NY 14623, USA*

<sup>9</sup>*George P. and Cynthia Woods Mitchell Institute for Fundamental Physics and Astronomy, Texas A&M University, College Station, TX 77843, USA*

<sup>10</sup>*Department of Physics and Astronomy, Texas A&M University, College Station, TX 77843, USA*

<sup>11</sup>*Department of Physics and Astronomy, San Francisco State University, San Francisco, CA 94132, USA*

<sup>12</sup>*Department of Physics and Kavli Institute for Astrophysics and Space Research, Massachusetts Institute of Technology, Cambridge, MA 02139, USA*

<sup>13</sup>*Department of Astronomy, University of Florida, Bryant Space Science Center, Gainesville, FL 32611, USA*

### ABSTRACT

We derive dynamical parameters for a large sample of 446 *r*-process-enhanced (RPE) metal-poor stars in the halo and disk systems of the Milky Way, based on data releases from the *R*-Process Alliance, supplemented by additional literature samples. This sample represents more than a ten-fold increase in size relative to that previously considered by Roederer et al., and, by design, covers a larger range of *r*-process-element enrichment levels. We test a number of clustering analysis methods on the derived orbital energies and other dynamical parameters for this sample, ultimately deciding on application of the HDBSCAN algorithm, which obtains 30 individual Chemo-Dynamically Tagged Groups (CDTGs); 21 contain between 3 and 5 stars, and 9 contain between 6 and 12 stars. Even though the clustering was performed solely on the basis of their dynamical properties, the stars in these CDTGs exhibit *statistically significant similarities* in their metallicity ([Fe/H]), carbonicity ([C/Fe]), and neutron-capture element ratios ([Sr/Fe], [Ba/Fe], and [Eu/Fe]). These results demonstrate that the RPE stars in these CDTGs have likely experienced common chemical-evolution histories, presumably in their parent satellite galaxies or globular clusters, prior to being disrupted into the Milky Way's halo. We also confirm the previous claim that the orbits of the RPE stars preferentially exhibit pericentric distances that are substantially lower than the present distances of surviving ultra-faint dwarf and canonical dwarf spheroidal galaxies, consistent with the disruption hypothesis. The derived dynamical parameters for several of our CDTGs indicate their association with previously known substructures, Dynamically Tagged Groups, and RPE Groups.

*Keywords:* galaxies: dwarf — Galaxy: halo — stars: kinematics and dynamics — stars: abundances — stars: Population II

### 1. INTRODUCTION

The origin of the heaviest elements ( $Z \gtrsim 30$ ) found in our Milky Way has been debated for over half a century, beginning with the pivotal works of [Burbidge et al.](#)

(1957) and [Cameron \(1957\)](#). These elements, the great majority of which were formed by neutron-capture processes, have been measured for numerous individual

stars in the halo and disk populations of the Galaxy, as well as in dwarf satellite galaxies and globular clusters.

The astrophysical site(s) of the slow neutron-capture process (*s*-process) are reasonably well understood – the thermal pulses of asymptotic giant-branch stars (in some cases preserved on an observed companion due to subsequent mass transfer across a binary system; see, e.g., Herwig 2005; Bisterzo et al. 2010; Abate et al. 2015), or in massive, rapidly rotating, extremely low-metallicity stars (e.g., Meynet et al. 2006; Pignatari et al. 2008; Choplin et al. 2018). Recent work has provided evidence for the likely operation of the so-called intermediate neutron-capture process (*i*-process; Cowan & Rose 1977), the astrophysical site(s) for which are still under study (Dardelet et al. 2014; Hampel et al. 2016; Denissenkov et al. 2017). Heavy elements that were produced by the rapid neutron-capture process (*r*-process) have had multiple proposed astrophysical sites (e.g., Arnould et al. 2007; Frebel 2018), including neutron star mergers (NSMs; Lattimer & Schramm 1974; Thielemann et al. 2017), magneto-rotational supernovae jets (Winteler et al. 2012; Nishimura et al. 2015), core-collapse supernovae (CCSNe; Arcones et al. 2006; Wanajo 2013), and collapsars (Siegel et al. 2019).

Recent observations of highly *r*-process-enhanced (hereafter, RPE) stars in the satellite ultra-faint dwarf (UFD) galaxy Reticulum II (Ji et al. 2016, 2019; Roederer et al. 2016), coupled with the gravitational-wave detection of a NSM by LIGO/VIRGO (GW 170817; Abbott et al. 2017), with subsequent photometric and spectroscopic analysis of its associated kilonova (SSS17a; e.g., Drout et al. 2017; Kilpatrick et al. 2017; Shappee et al. 2017; Watson et al. 2019), provided strong evidence for two key pieces of the puzzle for the astrophysical origin of the *r*-process elements. First, that NSMs can plausibly be the dominant source of the heavy ( $Z > 52$ ) *r*-process elements (e.g., Hotokezaka et al. 2018; Horowitz et al. 2019) – although it is important to note that theoretical predictions of the NSM yields and frequencies vary, leading to significant uncertainties in the predicted amounts of expected *r*-process elements produced (e.g., Côté et al. 2019; Keegans et al. 2019; Siegel et al. 2019). Secondly, that dwarf spheroidal (dSph) galaxies and UFDs may be the primary birth places of the metal-poor RPE stars in the halo of the Milky Way, which were later distributed

throughout it when their parent dwarfs were disrupted during accretion (see, e.g., Brauer et al. 2019)<sup>1</sup>.

This opens the exciting possibility of grouping RPE stars on the basis of the similarity in their dynamical properties, which are expected to be approximately conserved even after their parent galaxy (or globular cluster) is destroyed (see, e.g., Roederer et al. 2018a). Alternatively, identification of Dynamically Tagged Groups (DTGs) in large catalogs of very metal-poor (VMP;  $[\text{Fe}/\text{H}] < -2.0$ ) stars, followed by “mapping” of the derived dynamical parameters of individual RPE stars onto the identified DTGs, provides another means to investigate their likely progenitor environments (see, e.g., Yuan et al. 2020 and Limberg et al. 2020). We distinguish between these approaches by noting that the stellar DTGs are identified without knowledge of the detailed chemistry of their individual members, while the identification of dynamical groups of *previously known* chemically peculiar stars (such as RPE stars or carbon-enhanced metal-poor, CEMP, stars) produces Chemo-Dynamically Tagged Groups (CDTGs).

Application of mathematical clustering algorithms to the space of orbital energies and other suitable dynamical parameters will result in stars being grouped based on the similarity of their orbits around the Galaxy. Although such clustering is made without relying on knowledge of their chemistry, if the stars in a given CDTG indeed originated in a common progenitor galaxy or globular cluster, then they might be expected to exhibit smaller dispersions in their metallicities and other chemical species, including *r*-process-element abundances, than expected by chance. In the work of Roederer et al. (2018a), based on a relatively small sample of 35 RPE stars judged to have suitably accurate estimates of distances (out of an initial sample of 83 RPE stars), the metallicity spread for member stars in their individual RPE Groups was indeed shown to be smaller than expected for random draws from the full sample. The mean metallicities of their eight RPE Groups indicated likely association with low-mass dwarf galaxy parents, based on the metallicity-luminosity relationship (Kirby et al. 2013). We note that tests on the similarity of the reported  $[\text{Eu}/\text{Fe}]$  ratios are somewhat compromised for this sample, since they are relatively few in number, and the range of the  $[\text{Eu}/\text{Fe}]$  ratios

<sup>1</sup> Globular clusters also possess RPE stars (e.g., Sneden et al. 2000; Sobeck et al. 2011), and since they may be accreted by the halo as well, could contribute a number of RPE stars to the halo system. Sakari et al. (2018) identify the RPE star J2116-0213 as one possible example, based on its distinctive elevated  $[\text{Na}/\text{Fe}]$  and low  $[\text{Mg}/\text{Fe}]$  abundances.

**Table 1.** RPA  $r$ -Process-Enhanced Star Classifications

Sub-class	Abundances
$r$ -II	$[\text{Eu}/\text{Fe}] > +0.7$ , $[\text{Ba}/\text{Eu}] < 0$
$r$ -I	$+0.3 < [\text{Eu}/\text{Fe}] \leq +0.7$ , $[\text{Ba}/\text{Eu}] < 0$
limited- $r$	$[\text{Sr}/\text{Ba}] > +0.5$ , $[\text{Eu}/\text{Fe}] \leq +0.3$
CEMP- $r$	$[\text{C}/\text{Fe}] > +0.7$ , $[\text{Eu}/\text{Fe}] > +0.3$ , $[\text{Ba}/\text{Eu}] < 0$

covered by their stars ( $[\text{Eu}/\text{Fe}] > +0.7$ ) does not include the moderately  $r$ -process-enhanced  $r$ -I stars with  $+0.3 < [\text{Eu}/\text{Fe}] \leq +0.7$ . We address this difficulty in the present paper, based on consideration of a significantly larger sample of RPE stars, including the known  $r$ -I stars, spanning a wider range of  $[\text{Eu}/\text{Fe}]$ .

The RPE stars can be split into multiple subclasses, based on their light-element and neutron-capture-element abundances (see Table 1). For the purpose of the current effort, we make use of the classifications employed by the  $R$ -Process Alliance (RPA), which are a subset of the original classifications from Beers & Christlieb (2005), with an extension from Frebel (2018). Note that the recent work of Holmbeck et al. (2020) has advocated, from a statistical analysis of the complete set of RPA abundances measured to date, that the most appropriate division between the moderately enhanced  $r$ -I stars and the highly enhanced  $r$ -II stars is at  $[\text{Eu}/\text{Fe}] > +0.7$  (rather than  $[\text{Eu}/\text{Fe}] > +1.0$  in common previous use), which we have adopted here.

The  $r$ -II and  $r$ -I stars are thought to have been enriched primarily by the main  $r$ -process. Some  $r$ -II and  $r$ -I stars exhibit enhanced abundances of the actinide elements, such as uranium and thorium (Hill et al. 2002; Mashonkina et al. 2014; Holmbeck et al. 2018). The origin of this ‘‘actinide boost’’ (Schatz et al. 2002) is not known with certainty, but its presence hints at the possibility of fundamental differences in the nature of the  $r$ -process (Holmbeck et al. 2019a), even within a single progenitor population (see, e.g., Holmbeck et al. 2019b). There are insufficient numbers of actinide-boost stars known to confidently assign them into a separate class at present. The limited- $r$  stars exhibit enhanced light  $r$ -process elements (e.g., Sr, Y, Zr) relative to heavy ones (e.g., Ba, Eu), while the heavier elements are not enhanced (Frebel 2018)<sup>2</sup>. These stars

may have received significant contributions from CC-SNe. The CEMP- $r$  stars exhibit carbon enhancement ( $[\text{C}/\text{Fe}] > +0.7$ ), along with  $r$ -process-element enrichment (see, e.g., Beers & Christlieb 2005).

In this work, we consider the dynamical properties of a large sample of 446  $r$ -II and  $r$ -I stars from the RPA and other literature sources. This paper is arranged as follows. Section 2 describes the assembly of our sample, their derived distance estimates, and the available chemical-abundance information. In Section 3, we derive orbital energies and other dynamical parameters for each of these stars, making use of parallaxes, proper motions, and radial velocities from *Gaia* Data Release 2 (DR2) (Gaia Collaboration et al. 2016, 2018; Lindegren et al. 2018; Sartoretti et al. 2018), supplemented by kinematic data available in the literature, as needed. Section 4 describes the application of the HDBSCAN (McInnes et al. 2017) clustering algorithm to identify 30 CDTGs, populated with between 3 and 12 stars each. In Section 5, we investigate the distributions of various elemental abundances within each CDTG, and demonstrate that their dispersions are significantly smaller and globally inconsistent with random draws from the full population of RPEs. Section 6 provides a discussion of the possible associations of our identified CDTGs with previously known substructures and DTGs, as well as how the pericentric distances of our RPEs (and CDTGs) compare with those of surviving dSph and UFD galaxies, and the implications of our CDTG chemistry on the nature of their birth environments and  $r$ -process progenitor(s). Section 7 summarizes our results, and provides perspectives on future samples of RPE stars and their dynamical analyses, and how new approaches to chemical-evolution modeling may help refine our understanding of nature and origin of the astrophysical  $r$ -process.

## 2. DATA ASSEMBLY, DISTANCES, AND ELEMENTAL ABUNDANCES

We select 141  $r$ -II, 332  $r$ -I, and 46 limited- $r$  stars from a number of sources: the first four data releases from the RPA (Hansen et al. 2018; Sakari et al. 2018; Ezzeddine et al. 2020; Holmbeck et al. 2020), the

<sup>2</sup> We point out that the limited- $r$  process has been recognized, under various names, over the past few decades. See, e.g., McWilliam (1998), Travaglio et al. (2004), and Hansen et al. (2012), and references therein.

**Table 2.** Positions, Magnitudes, Distances, Radial Velocities, and Proper Motions for the Initial Sample

Name	RA	DEC	$V$ mag	$d_{Gaia}$ (err)	$d_{SH}$ (err)	Rad Vel	PM <sub>RA</sub>	PM <sub>DEC</sub>
	(J2000)	(J2000)		(kpc)	(kpc)	(km s <sup>-1</sup> )	(mas yr <sup>-1</sup> )	(mas yr <sup>-1</sup> )
2MASS J00002259–1302275	00:00:22.60	–13:02:27.5	12.88	5.71 (1.54)*	4.78 (1.47)**	–104.4	–2.61	–9.45
2MASS J00002416–1107454	00:00:24.16	–11:07:45.4	12.04	3.76 (0.68)	3.51 (0.79)*	–110.4	–0.63	–23.48
SMSS J000113.96–363337.9	00:01:13.99	–36:33:38.1	13.91	8.02 (2.24)*	7.28 (2.03)*	243.3 <sup>a</sup>	8.35	–5.16
HD 224930	00:02:11.18	+27:04:40.0	5.67	0.01 (0.00)	0.01 (0.00)	–35.6	723.11	–933.75
2MASS J00021668–2453494	00:02:16.70	–24:53:49.5	13.49	4.86 (0.74)	5.11 (1.36)*	80.1	–3.61	–8.09
BPS CS 22957–0036	00:03:31.20	–04:44:19.0	14.41	1.26 (0.09)	1.20 (0.15)	–154.5 <sup>b</sup>	38.64	–22.27
HD 20	00:05:15.48	–27:16:18.8	9.01	0.50 (0.01)	0.50 (0.02)	–56.5	132.43	–39.92
2MASS J00073817–0345509	00:07:38.17	–03:45:50.9	11.65	2.86 (0.56)	2.72 (0.65)*	–146.3	2.30	–16.04
BPS CS 31070–0073	00:08:51.83	+05:26:17.1	14.53	...	1.44 (0.57)**	–86.0 <sup>c</sup>	19.87	–12.43
2MASS J00093394–1857008	00:09:33.94	–18:57:00.8	11.18	1.26 (0.08)	1.29 (0.08)	–71.4	39.33	–37.43

NOTE—Sources for (non-*Gaia*) radial-velocity information:

NOTE—<sup>a</sup> Jacobson et al. (2015), <sup>b</sup> Roederer et al. (2014), <sup>c</sup> T.C. Beers, private comm., <sup>d</sup> Hansen et al. (2015), <sup>e</sup> Beers et al. (1992), <sup>f</sup> Beers & Sommer-Larsen (1995), <sup>g</sup> Barklem et al. (2005), <sup>h</sup> Ezzeddine et al. (2020), <sup>i</sup> Hansen et al. (2018), <sup>j</sup> Aoki et al. (2002), <sup>k</sup> Bonifacio et al. (2009), <sup>l</sup> Kunder et al. (2017), <sup>m</sup> Xing et al. (2019), <sup>n</sup> Carrera et al. (2013), <sup>o</sup> Cohen et al. (2013), <sup>p</sup> Holmbeck et al. (2020), <sup>q</sup> Aoki et al. (2005), <sup>r</sup> Frebel et al. (2006), <sup>s</sup> Sakari et al. (2018), <sup>t</sup> Howes et al. (2015), <sup>u</sup> Howes et al. (2016), <sup>v</sup> Allende Prieto et al. (2000), <sup>w</sup> Aoki et al. (2010)

NOTE—Source for (non-*Gaia*) proper motions: <sup>1</sup> Kharchenko & Roeser (2009)

NOTE—Single (\*) and double (\*\*) marks indicate stars with relative distance errors in the range  $20\% < \epsilon \leq 30\%$ , and  $\epsilon > 30\%$ , respectively.

NOTE—This table is a stub; the full table is available in electronic form.

JINAbase literature compilation (Abomalima & Frebel 2018), and a few additional stars from the recent literature that are not yet in the JINAbase compilation. These are then cross-matched with *Gaia* DR2 (Gaia Collaboration et al. 2016, 2018; Lindegren et al. 2018; Sartoretti et al. 2018) in order to obtain parallaxes, proper motions, and radial velocities, where available. When this information is not available from *Gaia*, we supplement it with radial velocities from RAVE DR5, where available (Kunder et al. 2017), as well as from other literature sources. A minority of our stars ( $\sim 3\%$ ) only had negative parallaxes from *Gaia*; their distance estimates are obtained as described below. We further require that each of the stars have spectroscopic determinations of [Fe/H], [Ba/Fe], and [Eu/Fe], as these are required to make confident sub-class assignments. Stars with only reported upper limits on [Eu/Fe] are rejected, as are stars with [Fe/H]  $> -1.0$ . Application of these cuts reduces our sample to 519 stars, which we refer to below as the Initial Sample.

Distance estimates for our stars were obtained from inversion of the reported *Gaia* DR2 parallax, with a positive correction of 0.054 mas added to the parallax value, as recommended by Everall et al. (2019) and Schönrich et al. (2019). We also calculate distances using the Bayesian tool *StarHorse* (Queiroz et al. 2018, 2020; Anders et al. 2019), one advantage of which is *StarHorse*'s ability to provide reasonable estimates of

distances even for stars with negative (or missing) parallax values reported by *Gaia* DR2. The *StarHorse* algorithm uses  $T_{\text{eff}}$ ,  $\log g$ , relative chemical abundances, photometric magnitudes, and parallaxes, when available, as inputs, but it does not explicitly apply a correction to the *Gaia* parallax values.

The resulting basic information for our program stars is listed in Table 2. Stars with relative errors in their derived distances ( $\epsilon = \Delta d/d$ ) in the range  $20\% < \epsilon \leq 30\%$ , and those with  $\epsilon > 30\%$ , are indicated in the table. We also list our adopted radial velocities, taken from *Gaia* DR2 (with accuracy typically better than 1 km s<sup>-1</sup>), where available. When not, we adopt the radial velocities reported by high-resolution spectroscopic studies (with accuracy no worse than 1–2 km s<sup>-1</sup> (Holmbeck et al. 2020), or, in two cases, from medium-resolution studies (with accuracy no worse than 10 km s<sup>-1</sup>) for each star, as indicated in the table. Note that our preference for the choice of radial velocities from *Gaia*, as opposed to other sources, is that we wished to preserve the homogeneity of our uncertainties, to the extent possible. All but one of our stars have proper motions available from *Gaia* DR2; in this one case we adopt a measurement from an alternative source, as indicated in the table.

Figure 1 shows a comparison between the derived *Gaia* DR2 and *StarHorse* distances. The top panel shows the stars with *Gaia* relative distance errors in the range

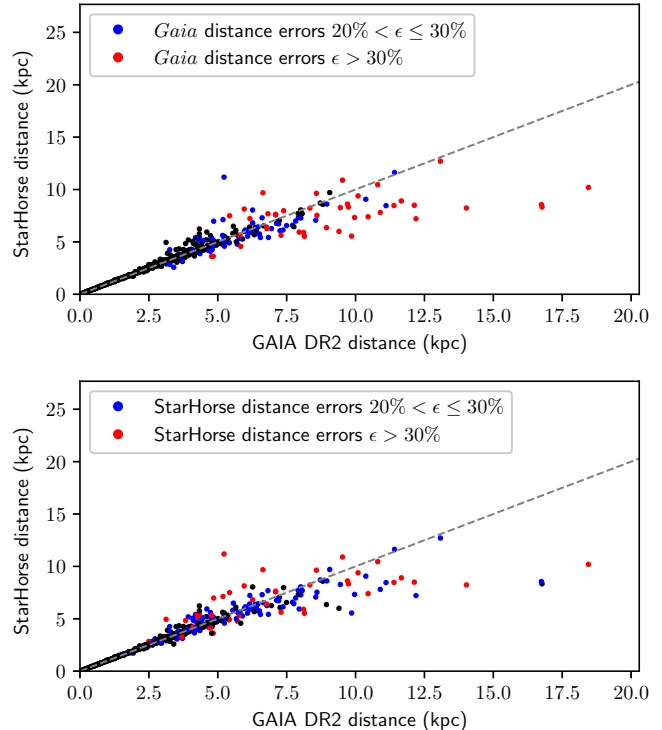
$20\% < \epsilon \leq 30\%$  with blue dots, and those with  $\epsilon > 30\%$  with red dots, respectively. The bottom panel shows the same information, but with the blue and red dots reflecting the stars with  $20\% < \epsilon \leq 30\%$  and  $\epsilon > 30\%$  in the **StarHorse** distances, respectively. From inspection, the two sets of distances are quite close to one another in the distance range  $d < 5$  kpc, and reasonably consistent for  $d < 7.5$  kpc. If a star has an available distance estimate from **StarHorse** with  $\epsilon \leq 30\%$  (which applies to  $\sim 95\%$  of the stars), we adopt it; otherwise we adopt the parallax-corrected *Gaia* distance estimate, provided its  $\epsilon \leq 30\%$ . We remove all stars for which our best available distance estimate has  $\epsilon > 30\%$ . This results in a total of 466 stars. We carry the stars with relative distance errors  $20\% < \epsilon \leq 30\%$  through our dynamical analysis below, but point out a number of stars (113) that may be suspect, due to the errors in their derived dynamical quantities arising from their uncertain distances. We have gone to some length to preserve the stars with larger distance errors in our sample, in the expectation that improved distance estimates for most of them will come available in future *Gaia* releases.

Table 3 lists the  $r$ -process-enhancement classes used by the RPA (as in Table 1), the reported effective temperatures ( $T_{\text{eff}}$ ), and selected elemental abundances, along with the primary references used for their determination. The last column provides an indicator, set to 1, if the star is included in the RPA data releases (or other RPA papers), or set to 0, if not.

For the measured carbon abundances reported in Table 3 ( $[\text{C}/\text{Fe}]$ ), we apply the evolutionary correction developed by Placco et al. (2014) in order to approximate the initial carbon abundance that occurs due to CN processing during the upper red giant-branch stage. The corrected abundance is referred to as  $[\text{C}/\text{Fe}]_c$  in this and later tables.

For the remaining analysis we remove the limited- $r$  stars, which are relatively few in number (46), and may have nucleosynthetic origins that differ from the  $r$ -I and  $r$ -II stars (Frebel 2018). This rejection, along with the removal of stars having high relative distance errors described above, results in a final sample of 127  $r$ -II and 319  $r$ -I stars (for a total of 446 stars), which we refer to as the RPE Sample.

Figure 2 shows the adopted distances for our RPE Sample stars. More than 75% of our stars are located within 5 kpc of the Sun; only four have distances more than 10 kpc. We recognize that estimates of the energies and other dynamical parameters based on poorly estimated distances can lead to significant errors. For this reason, Roederer et al. (2018a) employed a conservative relative-parallax error cut of 12.5%, reducing their orig-



**Figure 1.** Comparison of *Gaia* DR2 inverse-parallax distances and Bayesian **StarHorse** distances. The top panel marks stars with relative distance errors in the range  $20\% < \epsilon < 30\%$  with blue dots, and those with  $\epsilon > 30\%$  with red dots, respectively. The bottom panel shows the same information, but with the blue and red colored dots reflecting the stars with  $20\% < \epsilon \leq 30\%$  and  $\epsilon > 30\%$  in the **StarHorse** distances, respectively.

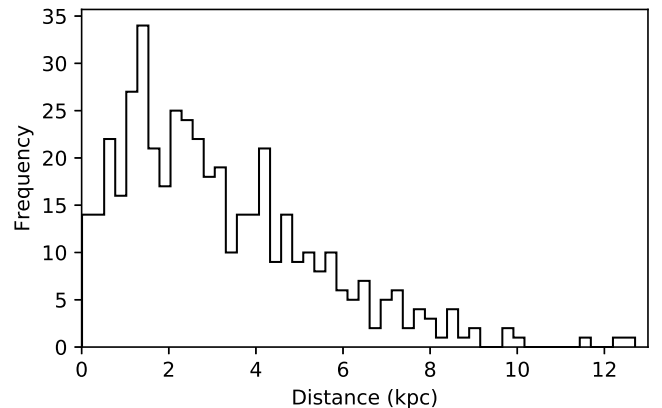


**Figure 2.** Adopted distances for the 446 stars in the RPE Sample, based on the **StarHorse** or *Gaia* DR2 estimates. See text for details.

inal sample from 83 to 35 stars. As mentioned above, we have chosen to retain stars with relative distance errors  $20\% < \epsilon \leq 30\%$ , but removed stars with relative distance errors  $\epsilon > 30\%$ .

**Table 3.** RPA Classes, Temperatures, and Elemental Abundances for the Initial Sample

Name	RPA Class	$T_{\text{eff}}$ (K)	[Fe/H]	[C/Fe]	[C/Fe] <sub>c</sub>	[Sr/Fe]	[Ba/Fe]	[Eu/Fe]	Reference	RPA
2MASS J00002259–1302275	<i>r</i> -I	4576	−2.90	−0.65	−0.65	−1.20	−0.38	+0.58	<sup>a</sup>	1
2MASS J00002416–1107454	<i>r</i> -I	4693	−2.43	−0.27	+0.30	−0.04	−0.24	+0.51	<sup>b</sup>	1
SMSS J000113.96–363337.9	limited- <i>r</i>	4810	−2.32	−0.33	+0.09	−0.04	−1.21	−0.55	<sup>c</sup>	0
HD 224930	<i>r</i> -I	5275	−1.00	...	...	...	−0.19	+0.34	<sup>d</sup>	0
2MASS J00021668–2453494	<i>r</i> -I	5020	−1.81	−0.88	−0.57	+0.59	+0.10	+0.52	<sup>a</sup>	1
BPS CS 22957–0036	<i>r</i> -I	5970	−2.28	+0.04	+0.04	+0.20	−0.22	+0.55	<sup>e</sup>	0
HD 20	<i>r</i> -II	5445	−1.58	−0.34	−0.32	+0.13	+0.32	+0.80	<sup>f</sup>	0
2MASS J00073817–0345509	<i>r</i> -II	4663	−2.09	−0.32	+0.17	+0.41	+0.11	+0.73	<sup>g</sup>	1
BPS CS 31070–0073	<i>r</i> -II / CEMP- <i>r</i>	6190	−2.55	+1.34	+1.34	−0.04	+2.42	+2.83	<sup>h</sup>	0
2MASS J00093394–1857008	<i>r</i> -I	4815	−1.88	−0.17	+0.06	+0.13	+0.23	+0.46	<sup>b</sup>	1

NOTE—The code in the column RPA indicates if the reported information is drawn from papers from the RPA (1) or other sources (0).

NOTE—Sources for chemical-abundance information:

NOTE—<sup>a</sup> Hansen et al. (2018), <sup>b</sup> Holmbeck et al. (2020), <sup>c</sup> Jacobson et al. (2015), <sup>d</sup> Fulbright (2000), <sup>e</sup> Roederer et al. (2014), <sup>f</sup> Barklem et al. (2005), <sup>g</sup> Sakari et al. (2018), <sup>h</sup> Allen et al. (2012), <sup>i</sup> Ezzeddine et al. (2020), <sup>j</sup> Hansen et al. (2015), <sup>k</sup> Christlieb et al. (2004), <sup>l</sup> Siqueira Mello et al. (2014), <sup>m</sup> Hansen et al. (2012), <sup>n</sup> Lai et al. (2008), <sup>o</sup> Rasmussen et al. (2020), <sup>p</sup> Preston et al. (2006), <sup>q</sup> Hollek et al. (2011), <sup>r</sup> Cayrel et al. (2004), <sup>s</sup> Cain et al. (2018), <sup>t</sup> Holmbeck et al. (2018), <sup>u</sup> Mardini et al. (2019), <sup>v</sup> Li et al. (2015), <sup>w</sup> Xing et al. (2019), <sup>x</sup> Valentini et al. (2019), <sup>y</sup> Hayek, W. et al. (2009), <sup>z</sup> Ishigaki et al. (2013), <sup>aa</sup> Johnson & Bolte (2002), <sup>ab</sup> Cohen et al. (2013), <sup>ac</sup> Westin et al. (2000), <sup>ad</sup> Roederer et al. (2010), <sup>ae</sup> Aoki et al. (2005), <sup>af</sup> Hawkins & Wyse (2018), <sup>ag</sup> Burris et al. (2000), <sup>ah</sup> Honda et al. (2004), <sup>ai</sup> Cain et al. (2020), <sup>aj</sup> Cowan et al. (2002), <sup>ak</sup> Howes et al. (2015), <sup>al</sup> Johnson et al. (2013), <sup>am</sup> Placco et al. (2020), <sup>an</sup> Howes et al. (2016), <sup>ao</sup> McWilliam et al. (1995), <sup>ap</sup> Placco et al. (2017), <sup>aq</sup> Sneden et al. (2003), <sup>ar</sup> Mashonkina et al. (2014), <sup>as</sup> Ivans et al. (2006), <sup>at</sup> Ryan et al. (1996), <sup>au</sup> Roederer et al. (2018b), <sup>av</sup> Masseron et al. (2012), <sup>aw</sup> Aoki et al. (2010)

NOTE—This table is a stub; the full table is available in electronic form.

Figure 3 shows the distribution of [Eu/H] and [Eu/Fe] for the RPE Sample, as a function of [Fe/H], color-coded by  $T_{\text{eff}}$ . The metallicity range of our stars extends over  $-3.7 < [\text{Fe}/\text{H}] < -1.0$ . Most stars have  $T_{\text{eff}}$  in the range [4400, 5200] K, which is essentially set by our demand for a measured [Eu/Fe]; there are a few *r*-II stars in the RPE sample with temperatures as high as  $T_{\text{eff}} \sim 6650$  K. The coolest stars included in the RPE sample have  $T_{\text{eff}} \sim 4150$  K. Note that, because of the inclusion of *r*-I stars, the range in [Eu/Fe] we consider in the RPE Sample,  $+0.30 < [\text{Eu}/\text{Fe}] \leq +2.28$ , is substantially larger than that considered by Roederer et al. (2018a).

### 3. ESTIMATED DYNAMICAL PARAMETERS

We derive orbital energies and other integrals of motion (actions) for the RPE sample, along with other dynamical parameters, using the AGAMA package (Vasiliev 2018) and the MW2017 potential (McMillan 2017)<sup>3</sup>. These results are listed in Table 4. We note that there

<sup>3</sup> We used the axisymmetric potential, not accounting for the central rotating bar.

exist a number of sources of errors, both statistical and systematic, that contribute to the overall uncertainty in the estimation of these parameters. This list includes, but is not limited to, the measurement errors in the distance estimates to each star, errors in the reported proper motions, errors in the radial velocities, and covariances between these quantities, as well as systematics arising from the choice of Galactic potential, and other unrecognized systematic errors. Errors in the distance estimates are very likely, however, to be the dominant contributor. These are listed, star-by-star, in Table 2.

Figure 4 shows histograms of the pericentric distances,  $r_{\text{peri}}$ , apocentric distances,  $r_{\text{apo}}$ , and the maximum distance from the Galactic plane achieved during the stars' orbits,  $Z_{\text{max}}$ . AGAMA calculates the stellar orbits by integrating the motions of each star over a period of 3 Gyr (from its present position), from which these values are obtained. The orbital eccentricity is obtained from  $e = (r_{\text{apo}} - r_{\text{peri}})/(r_{\text{apo}} + r_{\text{peri}})$ .

It is noteworthy that all of the pericentric distances of the RPE stars are within 20 kpc, as was also pointed

**Table 4.** Derived Dynamical Parameters for the RPE Sample

Name	Energy $\times 10^5$ ( $\text{km}^2 \text{s}^{-2}$ )	Ecc	$J_r$ $\times 10^3$ ( $\text{kpc km s}^{-1}$ )	$J_\phi$ $\times 10^3$ ( $\text{kpc km s}^{-1}$ )	$J_z$ $\times 10^3$ ( $\text{kpc km s}^{-1}$ )	$r_{\text{peri}}$ (kpc)	$r_{\text{apo}}$ (kpc)	$Z_{\text{max}}$ (kpc)
2MASS J00002259–1302275*	−1.50	0.79	0.74	+0.57	0.34	1.68	14.46	9.65
2MASS J00002416–1107454*	−1.39	0.73	0.85	−0.87	0.46	2.85	18.29	12.07
HD 224930	−1.68	0.25	0.07	+1.41	0.01	4.86	8.13	0.42
2MASS J00021668–2453494*	−1.42	0.40	0.25	+0.92	1.07	6.18	14.51	12.61
BPS CS 22957–0036	−1.72	0.84	0.58	−0.32	0.10	0.82	9.44	4.26
HD 20	−1.57	0.98	1.15	+0.06	0.01	0.15	13.44	5.68
2MASS J00073817–0345509*	−1.71	0.86	0.75	+0.04	0.10	0.73	10.08	3.45
2MASS J00093394–1857008	−1.74	0.64	0.37	−0.74	0.04	1.96	8.96	1.37
2MASS J00101758–1735387	−1.54	0.04	0.00	+0.68	1.14	7.97	8.64	7.95
2MASS J00154806–6253207	−1.69	0.85	0.52	−0.16	0.40	0.79	9.53	8.25

NOTE—Single (\*) mark indicates the 16 stars with relative distance errors in the range  $20\% < \epsilon < 30\%$ . See text for details.

NOTE—This table is a stub; the full table is available in electronic form.

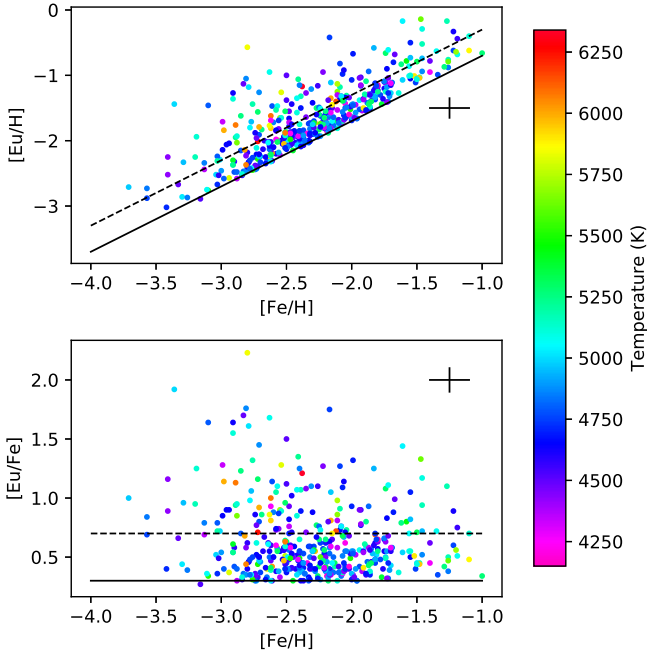


**Figure 3.** Europium abundances ( $[\text{Eu}/\text{H}]$ , upper panel;  $[\text{Eu}/\text{Fe}]$ , lower panel), as a function of metallicity ( $[\text{Fe}/\text{H}]$ ), for the RPE Sample. The solid black line denotes the  $[\text{Eu}/\text{Fe}] = +0.3$  cutoff used by the RPA to include  $r$ -I stars; the dashed black line indicates the adopted division line for  $r$ -II stars,  $[\text{Eu}/\text{Fe}] = +0.7$ . Effective temperatures ( $T_{\text{eff}}$ ) are color-coded using the scale shown in the right margin. Representative error bars on the abundances are shown in each panel.

out by Roederer et al. (2018a) for their much smaller sample. This has clear implications for the likely birth environments of the RPE stars, as discussed in more detail below.

Figure 5 is the Toomre diagram for the stars in the RPE Sample. From inspection, all but 51 of the stars are clearly kinematically associated with the halo system, and lie outside the semi-circular region indicating a  $100 \text{ km s}^{-1}$  velocity difference from the Local Standard of Rest, within which stars are potentially members of the disk system (all but 7 of these potential disk-system stars have  $Z_{\text{max}} < 4 \text{ kpc}$ ). Considering only the clear halo-system stars, those on prograde orbits (201; 51%) are roughly equal in numbers to those on retrograde orbits (194; 49%).

The energies and the other integrals of motion (actions) are defined (Binney 2012) as:

- $E$ , the specific orbital energy, defined as the full orbital energy of the star divided by its mass.
- $J_r$ , the orbital action due to oscillations along the orbital radius, is defined to be non-negative. For a given  $E$ ,  $J_r = 0$  for circular orbits and is large for eccentric orbits.
- $J_\phi$ , the action due to orbital motions, is taken to be the reverse projection of the angular momentum on the axis perpendicular to the Galactic plane,  $-L_z$ . In our adopted coordinate system, positive and negative values of  $J_\phi$  (and  $V_\phi$ ) corre-

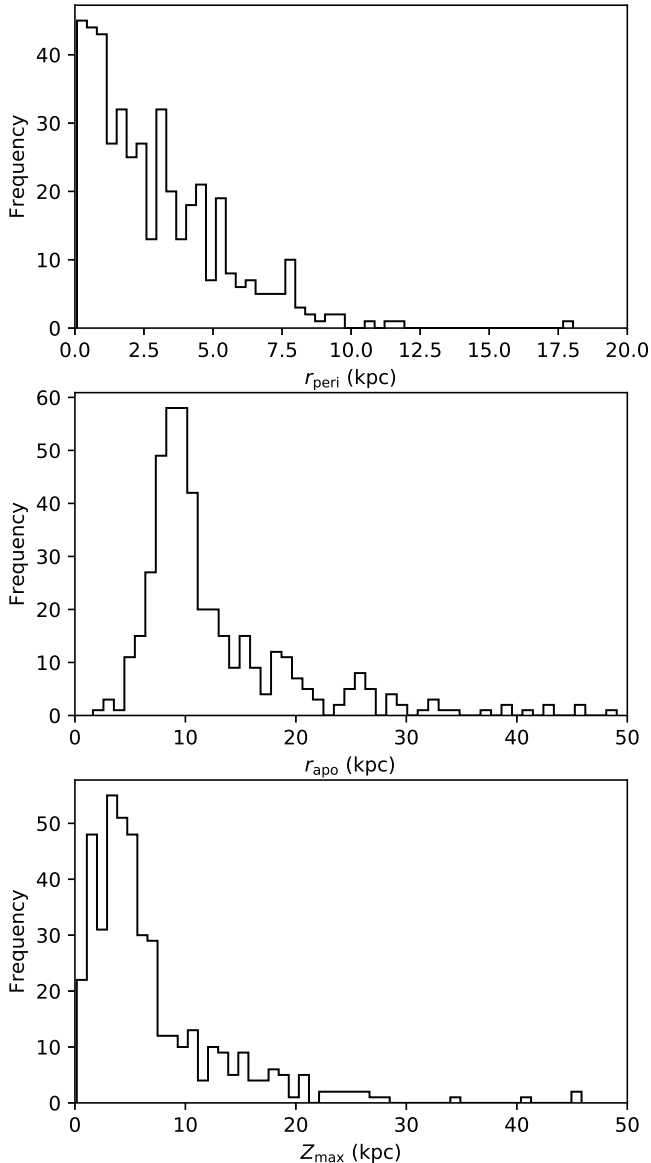


**Figure 4.** Distribution of pericentric distances,  $r_{\text{peri}}$  (top panel), apocentric distances,  $r_{\text{apo}}$  (middle panel), and maximum distance from the Galactic plane achieved during the stars’ orbits,  $Z_{\text{max}}$  (bottom panel), for stars in the RPE Sample. Note that 10 stars with  $r_{\text{apo}} > 50$  kpc and 7 stars with  $Z_{\text{max}} > 50$  kpc are not shown.

spond to prograde and retrograde motions about the Milky Way’s center, respectively.

- $J_z$ , the action due to oscillations along the axis perpendicular to the Galactic plane, is defined to be non-negative.  $J_z = 0$  for planar orbits, and is large for orbits with large  $Z_{\text{max}}$ .

Figure 9 shows the distributions of the derived energies and other integrals of motions (actions) for the RPE Sample, along with several additional dynamical

parameters, as a function of  $[\text{Fe}/\text{H}]$ . From inspection of this figure, even though the RPE Sample comprises relatively bright stars (which was preferable in order to obtain high-resolution spectroscopic follow-up), the derived dynamical parameters cover a wide range of values, and also span a large range of  $[\text{Fe}/\text{H}]$ . If this were not the case, it would be unsurprising to find clusters in the dynamical parameters and low dispersions in  $[\text{Fe}/\text{H}]$ , due to random selection alone.

We note that, for the actual clustering procedure described in the next section, we remove four additional stars (BPS CS 29526-110, BPS BS 15621-047, BPS BS 16929-005, and BPS BS 16033-081) from the sample due to their abundances strongly varying across different studies, putting their classification shown in Table 3 into question.

#### 4. CLUSTERING PROCEDURE

A number of clustering approaches have been explored in the past for considering the dynamical groupings of halo stars. For example, [Helmi & de Zeeuw \(2000\)](#) ran theoretical simulations, and found that a Friends of Friends (FoF) approach, clustering over  $E$ ,  $L_z$ , and total orbital momentum,  $L$ , can recover over 50% of all galactic accretion events, indicating low variability over time of these integrals of motion. Other observational works employed a number of alternatives. These include: (1) density analysis and subsequent application of a so-called watershed algorithm ([Roerdink & Meijster 2000](#)) in the space of  $E$  and  $J_\phi$  ([Helmi et al. 2017](#)), (2) visual density-map analysis in the space of  $E$ ,  $J_\phi$ , and  $L_\perp$  (the component of  $L$  perpendicular to  $L_z$ ) ([Koppelman et al. 2018](#)), (3) HDBSCAN ([McInnes et al. 2017](#); [Malzer & Baum 2019](#)), used to explore clustering applied to the space of  $E$ ,  $J_\phi$ ,  $e$ , and  $[\text{Fe}/\text{H}]$  ([Koppelman et al. 2019a](#)), and (4) the four approaches explored by the [Roederer et al. \(2018a\)](#) analysis of RPE stars – K-means clustering ([Lloyd 1982](#); [Arthur & Vassilvitskii 2007](#)), agglomerative clustering ([Ward 1963](#)), affinity propagation clustering ([Frey & Dueck 2007](#)), and mean-shift clustering ([Comaniciu & Meer 2002](#)), all applied to the space of  $E$  and the orbital actions  $J_r$ ,  $J_\phi$ , and  $J_z$ . Most recently, [Yuan et al. \(2020\)](#) applied the neural-network based method STARGO ([Yuan et al. 2018](#)) to the  $E$ ,  $L$ ,  $\theta$ , and  $\phi$  space, where the latter two angular parameters characterize the directions of the orbital poles.

Each of the above clustering approaches have advantages and disadvantages, and different algorithms may be useful for different applications, and for data sets of varying size and possible cluster shapes. For example, STARGO appears to be particularly suitable for large



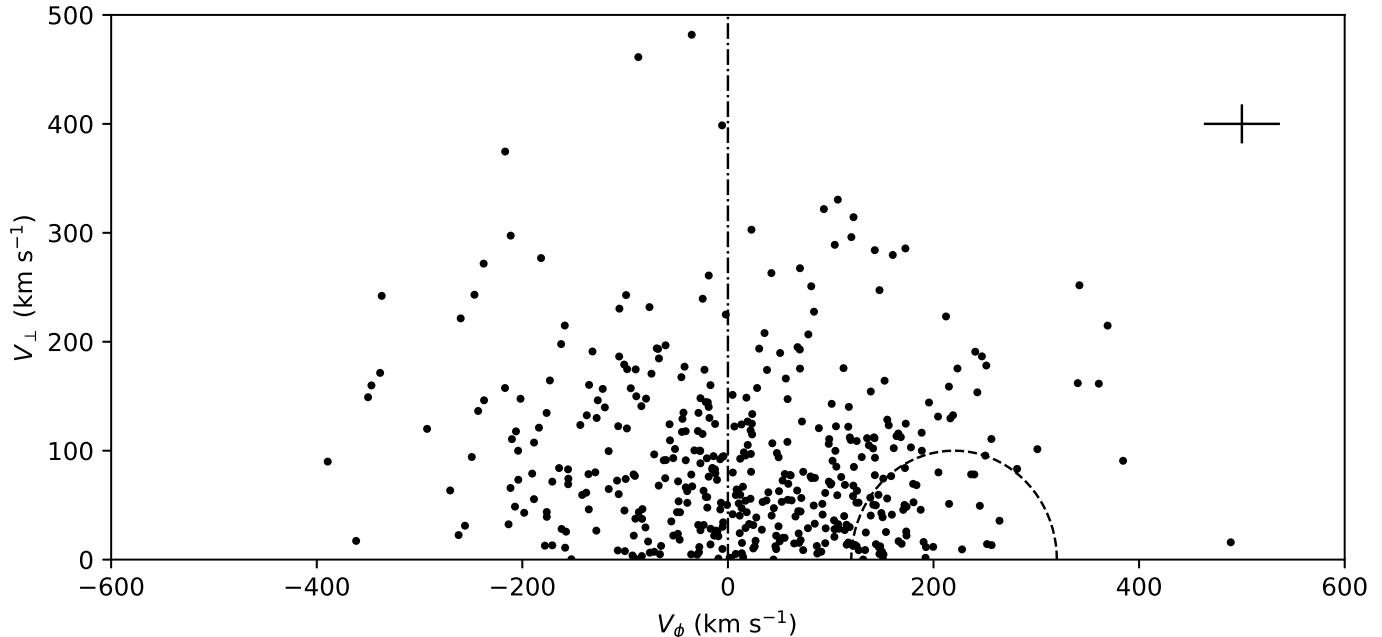


**Figure 5.** Toomre diagram for the RPE Sample. The dashed semi-circle denotes the radius of  $100 \text{ km s}^{-1}$  from the approximate location of the Local Standard of Rest,  $V_\phi \approx 220 \text{ km s}^{-1}$ . The vertical dash-dotted line separates stars with prograde ( $V_\phi > 0$ ) orbits from those with retrograde ( $V_\phi < 0$ ) orbits. A representative error bar is shown in the upper right of this figure, multiplied by a factor of 5 for better visibility.

( $N > 1000$ ) data sets, and in particular, provides an objective means for assessing the confidence (and possible contamination) of the various clusters it identifies. The methods employed by Roederer et al. (2018a) were chosen because they were thought to be best for smaller ( $N < 100$ ) data sets. Whatever approach is taken, there is always some subjective set of choices that must be made by the user, which can lead to complexity in the interpretation of the final results.

After conducting experiments with a number of the above techniques, we initially decided, in the interest of simplicity and reproducibility, as well as our concern over the limited size of the RPE Sample, to employ a FoF<sup>4</sup> algorithm in the space of  $E$ ,  $J_\phi$ , and  $e$ . The FoF results depend on the choice of a single parameter,  $l$ , the linking length, which allowed us to explore how the elemental-abundance dispersions of the resulting dynamical clusters depended on this parameter. The results clearly indicated a statistically significant reduction of abundance dispersions in the identified dynamical clusters compared to clusters formed from random selections. We were somewhat concerned (as was an anonymous referee), however, that our optimal choice of  $l$  led to several very large dynamical clusters “tied

together” by single stars in low-density regions of the dynamical space.

We thus chose to implement a more powerful clustering algorithm, HDBSCAN, which has recently been employed to find DTGs of VMP stars from the HK (Beers et al. 1985, 1992) and Hamburg/ESO (Christlieb et al. 2008) surveys by Limberg et al. (2020). Here, we combine the DTG-search methodology presented by these authors with our statistical tools (described below) to evaluate the chemical nature of the identified CDTGs. For application of HDBSCAN, we employed the same input dynamical parameters as used by Roederer et al. (2018a) and Limberg et al. (2020): energy,  $E$ , and the three actions,  $J_r$ ,  $J_\phi$  and  $J_z$ . Note that we specifically *did not* choose to include  $[\text{Fe}/\text{H}]$ , or any other chemical information, among the input parameters for this exercise, as we wished to quantitatively test the similarities of the elemental abundances for the members of a given cluster. This allows us to evaluate the hypothesis that the cluster members share a common chemical-evolution history.

The result of this procedure is the identification of 30 CDTGs, ranging in size from 3 to 12 stars, with 21 of the CDTGs containing between 3 and 5 stars each, and 9 containing between 6 and 12 stars each. The RPE stars in these CDTGs are listed in Table 6. In this table, the identified CDTGs are listed in order of declining confidence level (CL, described below). Within each

<sup>4</sup> The particular implementation used was the *pyfof* Python library (<https://github.com/simongibbons/pyfof>).

CDTG, the member stars are listed in order of increasing  $[\text{Eu}/\text{Fe}]$ . We discuss these CDTGs in more detail below.

For convenience (e.g., for matching the CDTGs to other known substructures or dynamical groups), and for future reference, Table 5 lists the average energy, actions, eccentricity, and orbital rotation,  $V_\phi$ , along with the means and dispersions of the elemental abundances considered here.

Figure 8 shows plots of  $E$  vs.  $J_\phi$  for the CDTGs and non-clustered stars in the RPE Sample, as such plots have been used by numerous previous studies of DTGs, and are useful for comparisons with those works, as well as with future studies. Although the plots are split into four individual panels, some apparent overlap in this dynamical space is unavoidable. These are relieved for most cases in the projected action-space figures described below.

Figure 7 shows projected action-space maps for the CDTGs and the non-clustered stars in the RPE Sample. From inspection of this figure, it is clear that the RPE CDTGs exhibit a variety of orbital behaviors, and variations in their degree of clustering (“tight” vs. “relaxed”). Note that stars with prograde and retrograde orbits, and stars with radial and polar orbits, always appear together in the same CDTGs, with the exception of CDTG-29, which exhibits a noticeable spread in its orbital characteristics, from mildly retrograde to mildly prograde orbits.

For each of the obtained CDTGs, we also investigate their significance against the uncertainties of the dynamical parameters of their respective member stars. Mean errors for energies and actions are 1.3% for  $E$ , 8.9% for  $J_r$ , 2.3% for  $J_\phi$ , and 7.0% for  $J_z$ . We assume normal distributions for these quantities with its nominal value being the mean and its error the standard deviation of the distribution. We first produce 1,000 sets of the 4-D energy-action vector of each star with a Monte Carlo procedure. Then, we re-evaluate the cluster assignment of these generated sets, and calculate the fraction of instances that each given star was attributed to the same CDTG. We take these fractions as representative of the membership probability of each star belonging to their assigned CDTG. Finally, for each CDTG, we average the resulting probabilities over all its member stars, and define this as the confidence level (CL) of the CDTG. The complete methodology for the HDBSCAN algorithm and CL estimation are described in Limberg et al. (2020).

The CL values are indicated for each CDTG in Table 6, where CDTGs are ordered by these values. Most of the CDTGs (23 out of 30) have CL values above 75%, and only 4 of them have CL values below 50%. This in-

dicates the relative stability of our CDTGs to errors in the dynamical parameters, although improved distance estimates will certainly improve the accuracy of our results.

## 5. THE CHEMICAL NATURE OF THE IDENTIFIED CDTGS

We now explore the chemical properties of the identified CDTGs listed in Table 6, based on the limited set of elemental abundances provided for each star in the RPE Sample listed in Table 3. Our search is for evidence whether or not stars in the individual CDTGs exhibit elemental abundances that are more similar to one another than would have been obtained from considering the chemical behavior of similar-sized groups of stars chosen from the RPE Sample at random (that is, without considering their dynamical behavior). For this exercise, we obtain large numbers of mock groupings ( $10^6$  per abundance per cluster size) of  $N$  stars (matching the numbers of stars in the full set of CDTGs), randomly selected from the RPE Sample (where  $3 \leq N \leq 12$ ), and derive the means and sample standard deviations of the elements considered (When the number of available measured elemental abundances is 4 or more, biweight estimates (see, e.g., Beers et al. (1990)) of these quantities are reported, in order to decrease the influence of potential outliers). Since the clustering was based entirely on dynamical parameters, and did not involve the stellar elemental abundances, we can quantify the degree to which the elemental abundances among members of each CDTG are more similar to one another than expected by chance by comparing to the sample standard deviations of the mock groups, as described below. Note that, although we report values of the original measured carbonicity,  $[\text{C}/\text{Fe}]$ , for all of stars in the CDTGs listed in Table 6, for the statistical analysis reported below we used the evolutionary-stage corrected value of the carbonicity,  $[\text{C}/\text{Fe}]_c$ , calculated following Placco et al. (2014).

Figure 6 shows the cumulative distribution functions (CDFs) of the sample standard deviations (which we refer to as dispersions below) in these abundances for randomly drawn groups of 3, 4–5 and 6–12 stars, respectively, from the 442 stars analyzed in the RPE Sample (Recall that four stars were dropped from consideration due to doubts about the reliability of their abundance determinations; see Section 3), indicated by the curved dashed lines in each panel (in the last two rows the boundaries of the region occupied by all the CDFs are shown). Each panel also indicates the numbers of stars in the CDTGs that are considered for each element. The horizontal dashed lines indicate the CDF

values of 0.50, 0.33, and 0.25 (corresponding to one-half, one-third, and one-quarter of the full CDF), respectively. We can then ask, element-by-element, whether or not the observed dispersions for stars in the CDTGs are distributed throughout the CDFs obtained for the full RPE Sample with these measurements (which varies slightly depending on the element under consideration) in a manner expected from chance, as described below.

For the elemental-abundance dispersions selected at random for CDTGs of a given size, the probability of the number of clusters lying below a given CDF value (from 0 to 1) is described by the binomial distribution. For  $N$  total random-abundance dispersions, the probability that exactly  $n$  of their CDF values lie below the value  $v$  is:

$$p_v(k = n, N) = C_N^n v^n (1 - v)^{N-n}, \quad (1)$$

where

$$C_N^n = \frac{N!}{(N-n)!n!}. \quad (2)$$

The cumulative probability that  $n$  or more CDF values lie below the value  $v$  is found by summation of these probabilities over all values  $k = n, n+1, \dots, N$ :

$$p_v(k \geq n, N) = \sum_{k=n}^N C_N^k v^k (1 - v)^{N-k}. \quad (3)$$

We refer to these probabilities as the Individual Elemental-Abundance Dispersion (IEAD) probabilities – these are just the binomial probabilities for each element for the levels  $v = 0.50, 0.33,$  and  $0.25,$  respectively. If the resulting IEAD probabilities for our observed numbers of clusters lying below certain values,  $v,$  are significantly below 50%, this is a strong indication that the abundance dispersions for a given element in our CDTGs do not result from chance.

Table 7 summarizes the CDF statistics for all of the relevant abundances: [Fe/H], [C/Fe]<sub>c</sub>, [Sr/Fe], [Ba/Fe], and [Eu/Fe]. The first column lists the abundance under consideration, the second displays the number of CDTGs that have a measured dispersion of this abundance (the requirement for which is the presence of at least three stars in a given CDTG with available measurements), the third shows the numbers of CDTGs with abundance-dispersion values in the CDF of dispersions obtained from the full RPE Sample below  $v = 0.50, 0.33,$  and  $0.25,$  respectively, and the last columns list the various probabilities of obtaining these (or larger) numbers of such CDTGs from random selection, as described below.

### 5.1. Individual Elemental-Abundance Behavior

Here we consider the behavior of the individual elements within the CDTGs, on an element-by-element basis.

**[Fe/H]** – The first row of Table 7 and the first row of panels in Figure 6 summarize the dispersions of [Fe/H] within the CDTGs. The dispersions are notably lower, compared to randomly drawn groups of stars from the CDFs of the full RPE Sample. All three IEAD (binomial) probabilities are below 10%, as 21 of the 30 identified CDTGs have CDF values below the 0.50 level, 14 are lower than the 0.33 level, and 12 of them are below the 0.25 level.

We can directly compare the more selective and smaller Roederer et al. (2018a) sample and our more inclusive and larger sample using the above metric. In the smaller sample, the binomial probability of finding 6 of 6 (5 of 6) groups with  $N_{\text{star}} \geq 3$  with [Fe/H] dispersions < 0.50 (0.25) in the CDF is 1.6% (0.4%) by chance. Only for the smallest [Fe/H] dispersions (< 0.25 in the CDF) do those probabilities differ meaningfully from the ones found here with the expanded sample.

**[C/Fe]<sub>c</sub>** – The second row of Table 7 and the second row of panels in Figure 6 summarize the dispersions of [C/Fe]<sub>c</sub> within the CDTGs. The dispersions for most of the CDTGs (17/26) are lower than the 0.50 level for randomly drawn groups of stars from the CDFs of the full RPE Sample, resulting in a binomial probability of 11.5%. Half of them are below the 0.33 level, and a bit under half are below the 0.25 level, resulting in small binomial probabilities of 8.4% and 5.4%.

**[Sr/Fe]** – The third row of Table 7 and the third row of panels in Figure 6 summarize the dispersions of [Sr/Fe] within the CDTGs. The dispersions for most of the CDTGs with measured [Sr/Fe] dispersions (16/26) are lower than the 0.50 level, compared to randomly drawn groups of stars from the CDFs of the full RPE Sample, resulting in a binomial probability of 16.3%. There are 15 with dispersions lower than the 0.33 level, resulting in a tiny binomial probability of 0.8%, and 9 of them are below 0.25, resulting in a binomial probability of 18.0%.

**[Ba/Fe]** – The fourth row of Table 7 and the fourth row of panels in Figure 6 summarize the dispersions of [Ba/Fe] within the CDTGs. The dispersions for 60% of the CDTGs (18/30) are lower than the 0.5 level for randomly drawn groups of stars from the CDFs of the full RPE Sample, resulting in a binomial probability of 18.1%. Half of the CDTGs (15/30) are lower than the 0.33 level, resulting in a binomial probability of 4.0%, and 12 of them are also below the 0.25 level, with a corresponding binomial probability of 5.1%.

**[Eu/Fe]** – The fifth row of Table 7 and the fifth row of panels in Figure 6 summarize the dispersions of [Eu/Fe] within the CDTGs. The dispersions for the majority of the CDTGs (17/30) are lower than the 0.50 level for randomly drawn groups of stars from the CDFs of the full RPE Sample, resulting in a binomial probability of only 29.2%. Less than a third of the CDTGs (9/30) are lower than the 0.33 level, resulting in a statistically insignificant binomial probability of 70.1%. Almost a third (8/18) of them are below the 0.25 level, for a binomial probability of 48.6%.

### 5.2. Full Elemental-Abundance Behavior

We can make an estimate of the probability that our full set of elemental-abundance dispersions could have been arrived at through random draws from the CDFs for stars in the RPE Sample. To accomplish this, we take the five IEAD (binomial) probabilities ( $p_1, p_2, p_3, p_4, p_5$ ), for the full set of five elements under consideration, listed in the fourth column of Table 7. The first entry in that column is the 0.50 CDF value, the second is the 0.33 CDF value, and the third entry is the 0.25 CDF value.

As these probabilities correspond to different elements, they are expected to be independent of one another. We can thus characterize the statistical significance of obtaining them by estimating the probability that a set of these or lower probabilities (meaning a set of probabilities that, when ordered from the lowest to the largest, are each smaller than the corresponding probability from the set we have obtained) is generated by random draws of five probabilities from 0% to 100%. This probability can be calculated in the same fashion as the GEAD probabilities in the next section (Eqn. 7): we simply replace  $N$  with 5,  $N_1, N_2, N_3$  with 1, 2, 3, 4, 5, and 0.50, 0.33, and 0.25 with our set of five probabilities,  $p_1, p_2, p_3, p_4, p_5$ , ordered from the smallest to the largest, to obtain the following formula for the Full Elemental-Abundance Distribution (FEAD) probability:

$$\begin{aligned}
 p_{\text{FEAD}} &= p(k_1 \geq 1, k_2 \geq 2, k_3 \geq 3, k_4 \geq 4, k_5 \geq 5) \\
 &= \sum_{\substack{n_1, n_2, n_3, n_4, n_5 \in \mathbb{Z}, \\ n_1 \geq 1, \\ n_2 \geq 2, \\ n_3 \geq 3, \\ n_4 \geq 4, \\ n_5 = 5, \\ 0 \leq n_1 \leq n_2 \leq n_3 \leq n_4 \leq n_5 = 5}} p(k_1, k_2, k_3, k_4, k_5) = (n_1, n_2, n_3, n_4, n_5),
 \end{aligned}
 \tag{4}$$

where:

$$\begin{aligned}
 &p(k_1 = n_1, k_2 = n_2, k_3 = n_3, k_4 = n_4, k_5 = n_5) \\
 &= p_{p_1}(k = n_1, 5) \\
 &\times p_{\frac{p_2 - p_1}{1 - p_1}}(k = n_2 - n_1, 5 - n_1) \\
 &\times p_{\frac{p_3 - p_2}{1 - p_2}}(k = n_3 - n_2, 5 - n_2) \\
 &\times p_{\frac{p_4 - p_3}{1 - p_3}}(k = n_4 - n_3, 5 - n_3) \\
 &\times p_{\frac{p_5 - p_4}{1 - p_4}}(k = n_5 - n_4, 5 - n_4).
 \end{aligned}
 \tag{5}$$

The quantity  $p_{\text{FEAD}}$  is the probability that the IEAD probabilities are below the respective values obtained from analysing CDTGs, when obtained by randomly drawing samples from the individual binomial distributions.

From this calculation, we obtain FEAD probabilities (shown in the last row of Table 7) of 0.03% for the 0.50 CDF values, 0.00% for the 0.33 CDF values, and 0.01% for the 0.25 CDF values. These results are all dramatically lower than the 50% probability expected randomly. We conclude that the dynamical clustering procedure used in this work produces CDTGs with significantly lower elemental-abundance dispersions than obtained from random selections of same-sized groups from the full RPE sample.

### 5.3. Statistical Significance of the Results

In the previous two subsections, we obtained IEAD probabilities describing the individual results for the numbers of CDTGs with elemental-abundance dispersions for CDF values,  $v$ , below 0.50, 0.33, and 0.25, respectively, as well as the FEAD probabilities, reflecting the full set of elemental-abundance dispersions over all three levels.

We now evaluate the statistical significance of our results for each of the individual elemental-abundance dispersions – the Global Elemental-Abundance Dispersion (GEAD) probabilities, as well as the resulting Overall Elemental-Abundance Dispersion (OEAD) probability, calculated in order to assign a single probability for our abundance-dispersion results, and defined as described below.

For this purpose, we need to assess the probability of finding the triplets of observed numbers summarized in Table 7 for the three different CDF values, by randomly drawing values from the binomial distribution. Using the definition for binomial probability  $p_\nu(k = n, N)$  from Section 4, the probability of obtaining exactly  $N_1, N_2$ , and  $N_3$  CDTGs out of  $N$  with CDF values (for a given elemental-abundance dispersion) below 0.50, 0.33,

and 0.25, respectively, is:

$$\begin{aligned}
 p(k_1 = N_1, k_2 = N_2, k_3 = N_3, N) \\
 &= p_{0.25}(k = N_1, N) \times \frac{p_{0.33-0.25}}{1-0.25}(k = N_2 - N_1, N - N_1) \\
 &\times \frac{p_{0.50-0.33}}{1-0.33}(k = N_3 - N_2, N - N_2),
 \end{aligned} \tag{6}$$

and the probability of obtaining a triplet of these or larger numbers of CDTGs below 0.50, 0.33, and 0.25 can be calculated through the conditional sum<sup>5</sup>:

$$\begin{aligned}
 p(k_1 \geq N_1, k_2 \geq N_2, k_3 \geq N_3, N) \\
 &= \sum_{\substack{n_1, n_2, n_3 \in \mathbb{Z}, \\ n_1 \geq N_1, \\ n_2 \geq N_2, \\ n_3 \geq N_3, \\ 0 \leq n_1 \leq n_2 \leq n_3 \leq N}} p(k_1 = n_1, k_2 = n_2, k_3 = n_3, N).
 \end{aligned} \tag{7}$$

Calculating this sum for the numbers from the third column of Table 7 yields the results for the GEAD probabilities, shown in the 5th column of that table. All of these probabilities are substantially below 50% – in fact, all but one of them are 2% or less, and two of them are below 1%. This indicates strong statistical significance of the elemental-abundance dispersions in our CDTGs. We note that the GEAD probability for [Eu/Fe] (22.2%), though clearly statistically significant, is large compared to the GEAD probabilities of the other abundance dispersions. From inspection of the table, this is driven primarily by the larger IEAD probabilities for the CDF levels 0.33 and 0.25, relative to the other abundance dispersions. As an experiment, we dropped the five CDTGs with the lowest CL values (retaining only those CDTGs with CL levels greater than 60%; the GEAD probability for [Eu/Fe] was reduced to 18.7%.

Finally, to obtain a single number characterizing the statistical significance of all of our results (i.e., the probability that they could have been obtained by forming clusters from randomly drawn groups of stars from the RPE Sample), we apply Eqn. 4 listed in Section 5.2 to these five probabilities. The formal result is the Overall Elemental-Abundance Dispersion (OEAD) probability,  $p_{\text{OEAD}} \ll 0.001\%$ . This extremely low probability value strongly supports the assertion that clustering on the dynamical quantities produces CDTGs with significantly lower elemental-abundance dispersions than random selection.

We note that, if the hypothesis that the RPE stars were born in dwarf galaxy-like environments holds true, we can go one step further. The [Fe/H] and [C/Fe]<sub>c</sub>

abundance ratios can be thought of as tracers of the birth environments, while [Sr/Fe], [Ba/Fe], and [Eu/Fe] can be thought of as tracers of the nature of the  $r$ -process progenitor(s). In contrast to the above, where all five abundances are considered together for calculation of the OEAD probability, we can group on these two sets of abundance dispersions; the “environmental variables” (EVs) and the “progenitor variables” (PVs), respectively. The OEAD probabilities obtained for the EVs (0.02%) and PVs (0.02%) are both extremely low, supporting both the birth-environment hypothesis and the universality of the  $r$ -process signature for the main  $r$ -process.

It is worth noting that the estimation of binomial probabilities for groups of elements (e.g., the FEAD, OEAD, EV, and PV probabilities) assumes that their individual abundances are independent. While that is certainly true for their measurement, there are physical reasons to believe that the heavy-element abundances ([Sr/Fe], [Ba/Fe], and [Eu/Fe]) may be somewhat correlated with each other. Indeed, the processes that produced sufficient Eu to enrich the stars in a given environment to the point of becoming  $r$ -process enhanced would also be expected to produce large quantities of Sr and Ba. Although this possible correlation was not taken into account in the present work, we don’t expect its presence to significantly affect the results. Formally, the results are independent of this possible correlation – high statistical significance in the case of independent abundances implies high statistical significance in the case of correlated abundances, and vice versa.

One interesting feature is the clearly less statistically significant [Eu/Fe] abundance dispersions for our CDTGs compared to the other heavy elements ([Sr/Fe] and [Ba/Fe]). We found this result to be robust when using other clustering methods, such as FoF, and when changing the HDBSCAN parameters, suggesting it may be real. This result was also found in the previous work of Roederer et al. (2018a). From the observational standpoint, Eu measurements are more challenging than either Sr or Ba, since the former is often based on fewer, weaker lines. Thus it might be expected that the Eu dispersions within CDTGs could be less consistent star-to-star for this reason alone. Larger, homogeneously analyzed, data samples with higher signal-to-noise [Eu/Fe] measurements will be required to test this hypothesis.

## 6. DISCUSSION

### 6.1. Membership of CDTGs in Known Substructures, DTGs, or Groups

We expect that many of the CDTGs we identify in this paper may be members of known substructures,

<sup>5</sup> The detailed derivation of these equations can be found in the Appendix.

and the DTGs identified by Yuan et al. (2020) and Limberg et al. (2020), or the RPE Groups identified by Roederer et al. (2018a).

Table 8 lists the dynamical properties of the known substructures and previously identified DTGs and Groups. The first column lists the substructure, DTG, or Group, along with the numbers of member stars from the RPE Sample it may be associated with. The second column lists the CDTGs which may be associated with each of these. The final columns list the average dynamical parameters (and dispersions in these quantities) for the CDTGs listed in the second column. We note that the substructures and the DTGs from Yuan et al. (2020) and Limberg et al. (2020) are of immediate interest, as they were identified without knowledge of the detailed chemistry of their stars. Given that these appear to harbor one or more RPE stars from our sample, it should prove illuminating to obtain high-resolution spectroscopic follow-up of their member stars. Matches with the Groups A-F and Group H of Roederer et al. (2018a) are satisfying (since very different clustering algorithms were used), but unsurprising, given that their stars were selected to be RPE stars.

We also note, for completeness, that a number of the DTGs identified in Table 8 were identified in both Yuan et al. (2020) and Limberg et al. (2020), but we have chosen to simply list one match. Ultimately, as ongoing and near-future investigations of DTGs and CDTGs are obtained, it will be useful to assemble a catalog of all such identifications, and their constituent stars, which we defer to a future effort.

Regarding associations with better known, prominent substructures previously identified in the halo, over 20% of the stars in the RPE Sample, and ten of our CDTGs, are apparently associated with *Gaia*-Sausage/Enceladus (GSE) (Belokurov et al. 2018; Helmi et al. 2018), based on their almost null net rotation ( $\langle V_\phi \rangle \approx -4 \text{ km s}^{-1}$ ) and high average eccentricities ( $\langle e \rangle > 0.8$ ). The presence of member stars from these CDTGs (see Table 8) in VMP DTGs from Yuan et al. (2020) and Limberg et al. (2020) corroborate this connection. The progenitor(s) of GSE is/are apparently a major contributor of RPE stars to the inner halo, confirming suggestions from both Yuan et al. (2020) and Limberg et al. (2020) based on their own DTG analyses.

Two other larger substructures have been recognized in the halo, both predominantly retrograde: Sequoia (Myeong et al. 2019) and Thamnos (Koppelman et al. 2019a). Four of our CDTGs could be associated with them (Table 8) according to the independently proposed criteria of Naidu et al. (2020). On the other hand, neither Yuan et al. (2020) nor Limberg et al. (2020) pre-

sented statistical evidence of associations between our studied RPE stars and their DTGs. It is clear that we are in urgent need of high-resolution abundance analyses of stars from Sequoia/Thamnos, particularly for those inhabiting the VMP end of their metallicity distributions, in order to understand the chemical evolution and early star-forming environments of their progenitor(s).

Three member stars from CDTG-15 ( $N = 6$ ,  $CL = 83.2\%$ ) are associated with GL20:DTG-3 (Limberg et al. 2020), and one of them (BD+30:2611; Burris et al. 2000) with ZY20:DTG-3 (Yuan et al. 2020) as well. Both of these DTGs have been attributed to the Helmi et al. (1999) stream by these authors. Limberg et al. (2020) has also suggested a connection between this stream and RPE stars based on their dynamics. It is striking that spectroscopic studies of this structure had already claimed that its stars were enriched in neutron-capture elements, primarily via the  $r$ -process, based on the close conformity among the abundances of Ba and many elements in the rare-earth domain to the scaled-solar  $r$ -process pattern (Roederer et al. 2010) or their [Sr/Ba] profiles (Aguado et al. 2021).

The metallicity values of stars from CDTG-15 are in the range  $-2.7 \lesssim [\text{Fe}/\text{H}] \lesssim -1.4$ ; its average metallicity is  $\langle [\text{Fe}/\text{H}] \rangle = -2.0$ , consistent with Aguado et al. (2021) and others in the literature (e.g., Myeong et al. 2018a,b). Additionally, the [Fe/H] dispersion of  $\approx 0.5$  dex found for CDTG-15 leads to a CDF value of 0.71 (commensurate with random draws from the full RPE Sample), consistent with its progenitor being a dwarf galaxy with extended star formation (see Koppelman et al. 2019b).

Finally, there are three CDTGs with similar dynamics to the metal-weak thick disk (MWTd) (Table 8). This component was originally proposed by Morrison et al. (1990), and recently shown to be an independent structure from the canonical thick disk by Carollo et al. (2019) and An & Beers (2020). This finding is particularly intriguing, given the recent demonstration that the disk system of the Galaxy harbors significant populations of extremely and ultra metal-poor stars (Sestito et al. 2019, 2020). These recent efforts, alongside our RPE Sample, point to a MWTd with a diverse chemical profile. Clearly, larger samples of low-metallicity stars with disk-like kinematics will be necessary to unveil the early nucleosynthesis processes that contributed to these peculiar elemental-abundance patterns.

## 6.2. Apocentric and Pericentric Distances of the RPE Sample

Roederer et al. (2018a) noted that only 20% of the RPE stars they considered have apocentric distances (or  $Z_{\max}$  distances) greater than 20 kpc. For our much larger sample of RPE stars, we obtain similar results; only 14% have apocentric distances (or  $Z_{\max}$  distances) greater than 20 kpc. These authors pointed out that the present distances to the known UFD or canonical dSph satellite galaxies are all greater than 20 kpc. The limited orbital information presently available for these galaxies (e.g., Simon 2018) indicates that only the UFD galaxy Tucana III passes within 15 kpc of the Galactic center; the rest all have pericentric distances greater than 20 kpc. From inspection of the top panel of Figure 4, all of the stars in the RPE Sample have pericentric distances  $r_{\text{peri}} < 20$  kpc. Many have pericentric distances that pass quite close to the Galactic center: 52% come within 2.5 kpc, and 26% come within 1 kpc.

The obvious implication of the above is that RPE stars once associated with parent satellite galaxies that passed too close to the Galactic center were disrupted, and strewn throughout the inner-halo region of the MW, as previously emphasized by Roederer et al. (2018a).

### 6.3. Implications of CDTG Chemistry for the Birth Environments of RPE Stars

In Section 5, we have described at length the behavior of a limited set of available elemental-abundance ratios ( $[\text{Fe}/\text{H}]$ ,  $[\text{C}/\text{Fe}]_c$ ,  $[\text{Sr}/\text{Fe}]$ ,  $[\text{Ba}/\text{Fe}]$ , and  $[\text{Eu}/\text{Fe}]$ ) for the 30 CDTGs identified in this work. We have also defined the various probabilities that can be obtained to assess whether or not the observed relatively low dispersions of these abundances are consistent with random draws from the full set of stars in the RPE Sample. The conclusion appears unavoidable that, in fact, they are not. The members of the CDTGs identified on the basis of the similarity in their dynamical parameters shared common chemical-evolution histories, strongly suggesting that they originated in parent satellite galaxies (or globular clusters), which were later disrupted into the inner-halo region of the Galaxy. Most of those parent satellite galaxies were probably not very massive. The average metallicities of most (22/30) of the CDTGs listed in Table 6 are very low ( $[\text{Fe}/\text{H}] \leq -2$ ), and the galaxy mass-metallicity relationship (Kirby et al. 2013) implies that they were likely born in relatively low-mass dwarf galaxies, consistent with the findings of Roederer et al. (2018a).

A related conclusion is reached that, although multiple astrophysical progenitors of the  $r$ -process are not strictly precluded by the present data alone, the evidence in hand is fully consistent with a universal  $r$ -process pattern, at least for the main  $r$ -process. Com-

parison with predictions from high-resolution, large-scale cosmological numerical simulations that consider multiple classes of  $r$ -process progenitors is required to further explore this hypothesis.

We note the possibility that at least a few of the CDTGs we have identified may have been born in globular clusters, rather than low-mass galaxies, on the sole basis of their small dispersions in metallicity. There are five CDTGs listed in Table 6 with  $[\text{Fe}/\text{H}]$  dispersions of 0.20 dex or less: CDTG-11 ( $-2.43 \pm 0.10$ ;  $N = 6$ , CL = 87.1%), CDTG-18 ( $-2.12 \pm 0.13$ ;  $N = 4$ , CL = 79.3%), CDTG-19 ( $-2.48 \pm 0.17$ ;  $N = 4$ , CL = 78.0%), CDTG-25 ( $-1.93 \pm 0.15$ ;  $N = 3$ , CL = 61.2%) and CDTG-27 ( $-2.11 \pm 0.08$ ;  $N = 3$ , CL = 37.4%), where the numbers in parentheses refer to the mean  $[\text{Fe}/\text{H}]$ , dispersion in  $[\text{Fe}/\text{H}]$ , number of member stars, and the CDTG confidence level, respectively. It is beyond the scope of this paper to investigate this possibility further, but these CDTGs would be of particular interest for further study in order to accept or reject such associations.

## 7. SUMMARY AND CONCLUSIONS

We have used accurate dynamical parameters, based primarily on astrometry (parallaxes and proper motions) and radial velocities from *Gaia* DR2 (supplemented by a number of other sources), for a large sample of 446  $r$ -process-enhanced stars (RPE: 127  $r$ -II and 319  $r$ -I stars) assembled by the *R*-Process Alliance (and other sources), to identify 30 Chemo-Dynamically Tagged Groups (CDTGs) in the halo of the Milky Way. A statistical analysis of the dispersions in their chemical abundances for a restricted set of elements ( $[\text{Fe}/\text{H}]$ ,  $[\text{C}/\text{Fe}]$ ,  $[\text{Sr}/\text{Fe}]$ ,  $[\text{Ba}/\text{Fe}]$ , and  $[\text{Eu}/\text{Fe}]$ ) demonstrates that the members of individual CDTGs have likely experienced common chemical-evolution histories, presumably in their parent satellite galaxies (or, in a few cases, globular clusters) prior to being dispersed into the inner-halo region of the Galaxy. Their observed apocentric and pericentric distances are consistent with this interpretation, similar to the inference drawn by Roederer et al. (2018a) based on a much smaller sample. A number of our CDTGs are associated with previously identified substructures, DTGs, and RPE groups.

We note that we have not yet explicitly considered the dynamical clustering of the limited- $r$  stars, since they still remain relatively few in number. This limitation will be lifted in the near future, based on the expected doubling or tripling of the numbers of these, and other RPE stars, once the ongoing analysis of existing and soon-to-be-acquired snapshot high-resolution spectroscopic follow-up from the RPA is completed. Further enlargement of the numbers of RPE stars will also en-

able the use of more strict dynamical clustering criteria (and hence consideration of clusters with higher confidence levels), and provide for the identification of numerous new CDTGs. Stars in the DTGs identified from lower-resolution spectroscopy that are associated with the RPE CDTGs we have identified are of particular interest as well, as they most likely harbor additional RPE stars that have yet to be recognized.

We believe that the statistical techniques we have developed in the process of the present analysis for evaluating the significance of the elemental-abundance dispersions in CDTGs will prove useful for future similar observational studies, and for comparison with predictions obtained by chemical-evolution models. Both such efforts are necessary in order to tell the full story of the nature of the astrophysical origin of the  $r$ -process, in particular the hypothesis of a single predominant astrophysical source suggested by the significantly low elemental-abundance dispersions within our CDTGs.

#### ACKNOWLEDGMENTS

The authors are thankful to an anonymous referee, who provided comments and suggestions that substantially improved this paper. D.G., D.S., T.C.B., I.U.R., V.M.P., E.M.H., S.D., K.C.R., R.E., and A.F. acknowledge partial support for this work from grant PHY 14-30152; Physics Frontier Center/JINA Center for the Evolution of the Elements (JINA-CEE), awarded by the US National Science Foundation. I.U.R. acknowledges support from grant AST-1815403 awarded by the NSF. G.L. acknowledges CAPES (PROEX; Proc. 88887.481172/2020-00). T.T.H. acknowledges generous support from the George P. and Cynthia Woods Institute for Fundamental Physics and Astronomy at Texas A&M University.



## 8. APPENDIX: DERIVATION OF THE PROBABILITY EQUATIONS

Here we provide a derivation of the two equations, Eqn. (5) and Eqn. (6), provided in Section 5.3 for calculation of the Global Elemental-Abundance Dispersion (GEAD) probabilities from basic principles of Probability Theory.

First, we are interested in the following question: In a sequence of  $N$  draws from the uniform distribution over range  $[0,1]$ , what is the probability that exactly  $N_1$  of them will take values below 0.25,  $N_2$  of below 0.33, and  $N_3$  of below 0.50? In Section 5, we provided the definition of the binomial probability:

$$p_\nu(k = n, N) = C_N^n \nu^n (1 - \nu)^{N-n} \quad (8)$$

that, with the probability  $p$  of success for an individual experiment, the total number of successes out of  $N$  experiments will be  $n$ . We can apply this probability to our present situation as well.

Figure 10 visualizes the problem when applied to cumulative fraction distributions of abundance dispersions. We need to find the probability  $p(k_1 = N_1, k_2 = N_2, k_3 = N_3, N)$  that exactly these numbers of CDF values in the specified ranges (below 0.25, below 0.33, and below 0.50) can be obtained by randomly grouping stars from the RPE Sample and calculating the CDF values of the resulting CDTGs.

First, let us find the probability that exactly  $N_1$  CDTGs will have CDF values below 0.25. Since the probability of success for each experiment here is exactly 0.25 (as the entire range of CDF values is  $[0,1]$ , we obtain  $0.25/(1 - 0) = 0.25$ ), hence the first conditional probability will simply equal the first conditional binomial probability:

$$p(k_1 = N_1, N) = p_{0.25}(k = N_1, N). \quad (9)$$

The next step is to find the probability that, given that exactly  $N_1$  values are below 0.25, that exactly  $N_2$  values are below 0.33. This means that exactly  $N_2 - N_1$  values must lie in the range  $[0.25, 0.33]$ . Since all the remaining values are only allowed to fall within the range  $[0.25, 1]$ , the entire range of allowed values is  $1 - 0.25$ , while the

range of values that must be occupied is  $0.33 - 0.25$ . Hence, the probability of one success is  $\frac{0.33-0.25}{1-0.25}$ , and, given that we have only  $N - N_1$  values left to draw from, and exactly  $N_2 - N_1$  of them must fall within this range, we obtain the second conditional binomial probability:

$$p(k_2 = N_2, N | k_1 = N_1) = p_{\frac{0.33-0.25}{1-0.25}}(k = N_2 - N_1, N - N_1). \quad (10)$$

Similarly, since exactly  $N_3 - N_2$  values must lie in the range  $[0.33, 0.50]$ , the entire allowed range being  $1 - 0.33$  and the number of values remaining being  $N - N_2$ , we obtain the third conditional binomial probability:

$$p(k_3 = N_3, N | k_1 = N_1, k_2 = N_2) = p_{\frac{0.50-0.33}{1-0.33}}(k = N_3 - N_2, N - N_2). \quad (11)$$

The full probability is then found by multiplication of these three conditional probabilities:

$$\begin{aligned} p(k_1 = N_1, k_2 = N_2, k_3 = N_3, N) &= \\ &= p(k_1 = N_1, N) \times p(k_2 = N_2, N | k_1 = N_1) \\ &\quad \times p(k_3 = N_3, N | k_1 = N_1, k_2 = N_2), \end{aligned} \quad (12)$$

which is Eqn. (5) in Section 5.3.

Now we seek the probability that this, or a higher number of abundance dispersions, fall in these ranges. That is, the probability that the number of dispersions below 0.25 is equal to or above  $N_1$ , the number of dispersions below 0.33 is equal to or above  $N_2$ , and the number of dispersions below 0.50 is equal to or above  $N_3$ . This can be found by summing over all probabilities with the respective numbers of dispersions  $n_1, n_2$ , and  $n_3$  satisfying the conditions  $n_1 \geq N_1, n_2 \geq N_2, n_3 \geq N_3$ , and such that  $N_1 + N_2 + N_3 \leq N$ . This yields the sum:

$$\begin{aligned} p(k_1 \geq N_1, k_2 \geq N_2, k_3 \geq N_3, N) &= \\ &= \sum_{\substack{n_1, n_2, n_3 \in \mathbb{Z}, \\ n_1 \geq N_1, \\ n_2 \geq N_2, \\ n_3 \geq N_3, \\ 0 \leq n_1 \leq n_2 \leq n_3 \leq N}} p(k_1 = n_1, k_2 = n_2, k_3 = n_3, N), \end{aligned} \quad (13)$$

which is Eqn. (6) in Section 5.3 (the condition  $n_1, n_2, n_3 \in \mathbb{Z}$  denotes that  $n_1, n_2, n_3$  must be integers).

## APPENDIX

### A. FULL LONG TABLES

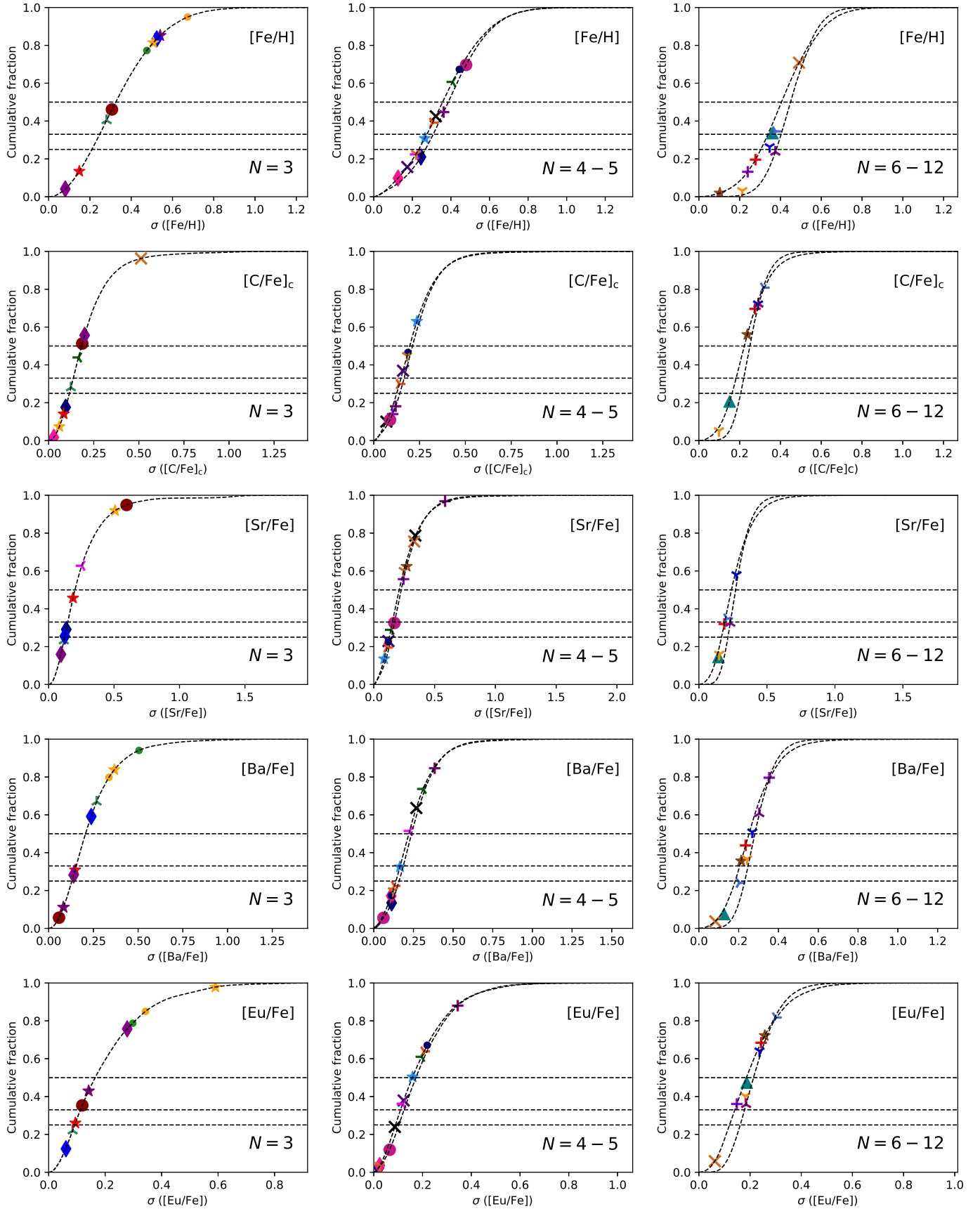


**Figure 6.** Dispersions in the elemental abundances within each CDTG, shown on the CDFs of random groupings of all stars (with the same numbers of stars as the identified CDTGs) in the full RPE Sample. The left column includes CDTGs with 3 measured abundances. The next two columns correspond to CDTGs with 4–5 and 6–12 measured abundances, respectively; all CDFs in these rows fall between the two curved dashed lines. The horizontal dashed lines show the 0.5, 0.33, and 0.25 cumulative fraction values.

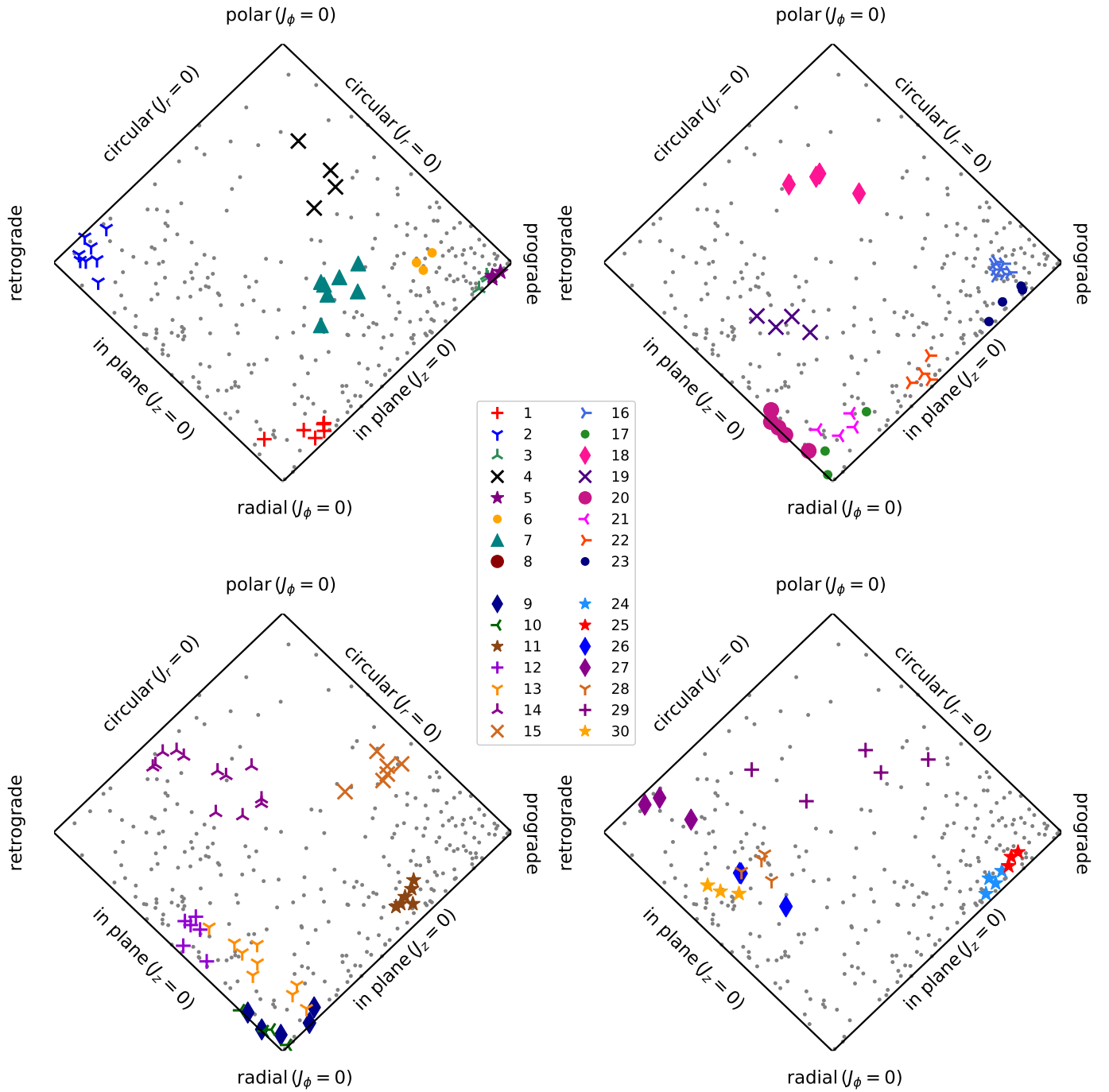


**Figure 7.** Projected action-space plots for the resulting clusters of stars from the RPE Sample. The x-axis is  $(J_\phi/J_{\text{tot}})$ , and the y-axis is  $(J_z - J_r)/J_{\text{tot}}$ , where  $J_{\text{tot}} = J_r + |J_\phi| + J_z$ . Different symbols and colors correspond to stars in different CDTGs, as shown in the legend. Small gray dots are stars from the RPE Sample that have not been assigned membership to a CDTG. The same markers are used for the same groups as in Figures 8. The CDTGs are split into four separate plots for clarity.

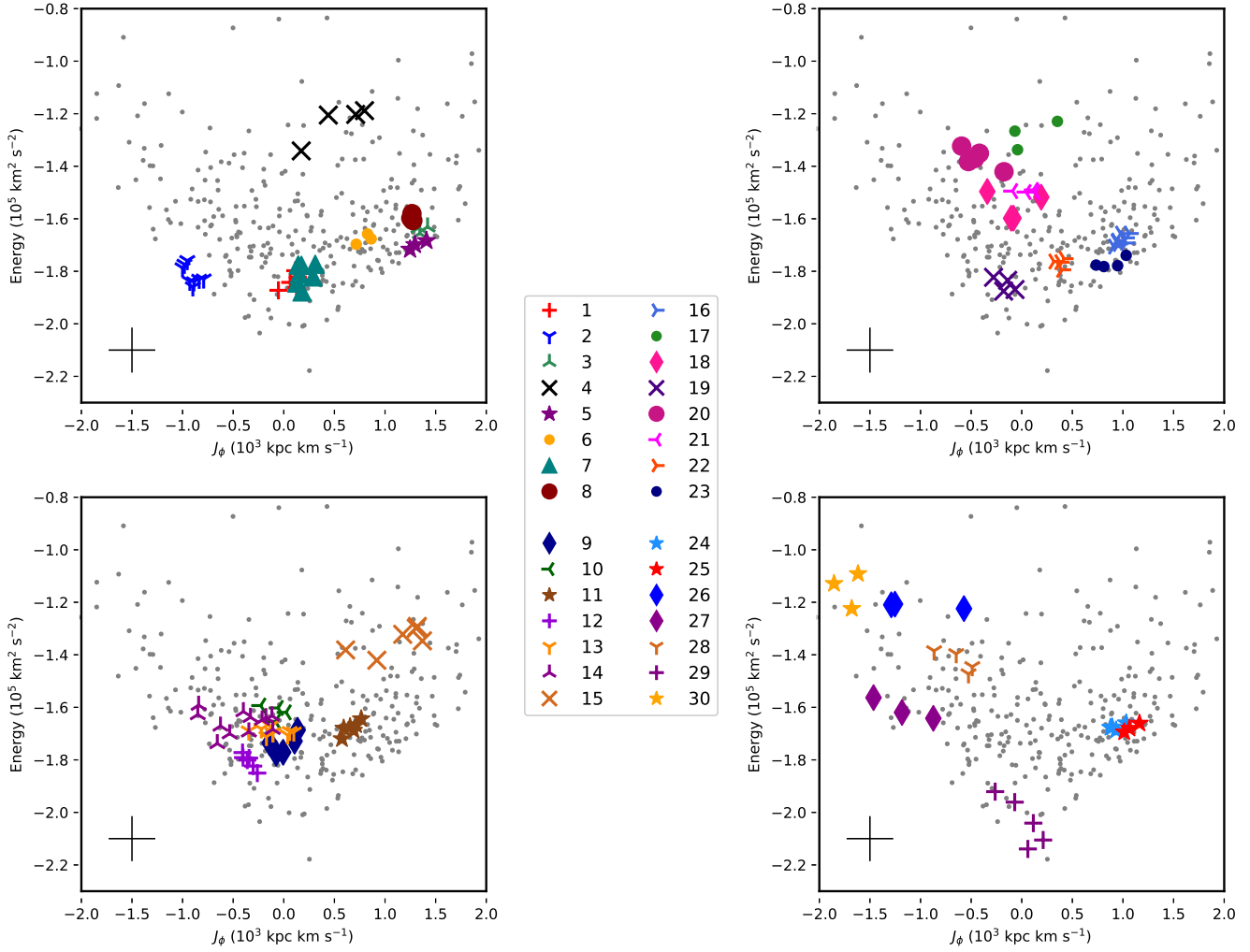


**Figure 8.** Energy vs.  $J_\phi$  plots for the CDTGs in the RPE Sample. Different symbols and colors correspond to stars in different CDTGs, as shown in the legend. Small gray dots are stars from the RPE Sample that have not been assigned membership to a CDTG. The CDTGs are split into four separate plots for clarity. The error bars in the bottom-left corners show mean uncertainties (multiplied by a factor of 5 for better visibility) of the involved quantities.

**Table 5.** Average Energies, Eccentricities, Actions, Rotational Velocities, and Elemental Abundances for the CDTGs

Name	$N$ stars	$\langle Energy \rangle$ $\times 10^5$ ( $\text{km}^2 \text{s}^{-2}$ )	$\langle J_r \rangle / \langle J_\phi \rangle / \langle J_z \rangle$ $\times 10^3$ ( $\text{kpc km s}^{-1}$ )	$\langle Ecc \rangle$	$\langle V_\phi \rangle$ ( $\text{km s}^{-1}$ )	$\langle [Fe/H] \rangle$	$\langle [C/Fe]_c \rangle$	$\langle [Sr/Fe] \rangle$	$\langle [Ba/Fe] \rangle$	$\langle [Eu/Fe] \rangle$
CDTG-1	6	-1.84	0.59 / 0.12 / 0.03	0.94	15.37	-2.19±0.28	-0.01±0.28	+0.08±0.19	+0.12±0.23	+0.57±0.24
CDTG-2	8	-1.82	0.05 / -0.91 / 0.10	0.27	-160.12	-2.35±0.35	+0.34±0.29	+0.29±0.28	-0.05±0.27	+0.51±0.24
CDTG-3	3	-1.64	0.16 / 1.37 / 0.03	0.37	159.57	-1.40±0.28	-0.07±0.12	+0.48±0.12	+0.38±0.27	+0.63±0.08
CDTG-4	4	-1.20	0.69 / 0.55 / 1.91	0.51	66.69	-2.19±0.32	+0.15±0.07	+0.48±0.34	-0.03±0.27	+0.48±0.09
CDTG-5	3	-1.70	0.09 / 1.32 / 0.01	0.30	168.90	-1.75±0.54	...	...	-0.07±0.08	+0.45±0.14
CDTG-6	3	-1.68	0.25 / 0.80 / 0.25	0.52	97.24	-2.20±0.67	...	...	+0.28±0.34	+0.80±0.34
CDTG-7	7	-1.81	0.38 / 0.17 / 0.28	0.83	22.14	-2.49±0.36	+0.50±0.15	+0.12±0.14	-0.03±0.13	+0.57±0.19
CDTG-8	3	-1.59	0.09 / 1.27 / 0.29	0.28	150.90	-2.43±0.31	+0.17±0.19	+0.21±0.60	-0.11±0.06	+0.56±0.12
CDTG-9	5	-1.74	0.77 / 0.00 / 0.01	0.95	0.23	-1.56±0.24	+0.14±0.09	+0.10±0.13	+0.07±0.11	+0.46±0.02
CDTG-10	4	-1.61	1.02 / -0.07 / 0.00	0.98	-8.90	-1.93±0.41	-0.11±0.17	+0.20±0.14	+0.21±0.31	+0.57±0.20
CDTG-11	6	-1.68	0.46 / 0.67 / 0.10	0.70	78.72	-2.43±0.10	+0.20±0.24	-0.16±0.27	-0.08±0.21	+0.59±0.13
CDTG-12	6	-1.80	0.46 / -0.35 / 0.07	0.80	-46.57	-2.06±0.24	+0.09±0.10	+0.22±0.24	-0.01±0.35	+0.44±0.15
CDTG-13	9	-1.69	0.72 / -0.10 / 0.13	0.93	-10.53	-2.20±0.21	+0.22±0.10	+0.17±0.15	+0.11±0.24	+0.53±0.18
CDTG-14	12	-1.65	0.28 / -0.42 / 0.61	0.57	-61.11	-2.39±0.38	+0.20±0.29	+0.09±0.23	-0.13±0.30	+0.54±0.18
CDTG-15	6	-1.34	0.37 / 1.25 / 1.08	0.42	148.70	-2.00±0.49	+0.15±0.51	+0.10±0.33	+0.03±0.08	+0.44±0.06
CDTG-16	8	-1.68	0.20 / 0.98 / 0.16	0.46	127.04	-2.38±0.38	+0.34±0.32	+0.13±0.21	+0.16±0.20	+0.55±0.30
CDTG-17	3	-1.28	1.85 / 0.08 / 0.11	0.97	10.33	-1.60±0.48	...	...	+0.27±0.51	+0.76±0.30
CDTG-18	4	-1.55	0.39 / -0.09 / 0.99	0.67	-15.41	-2.12±0.13	+0.44±0.03	...	-0.16±0.11	+0.37±0.02
CDTG-19	4	-1.85	0.40 / -0.16 / 0.19	0.85	-24.40	-2.48±0.17	+0.23±0.16	+0.20±0.12	-0.07±0.01	+0.52±0.12
CDTG-20	5	-1.37	1.50 / -0.48 / 0.01	0.91	-57.73	-2.00±0.48	+0.05±0.09	+0.05±0.17	+0.25±0.06	+0.54±0.07
CDTG-21	4	-1.50	1.17 / 0.07 / 0.12	0.96	8.89	-1.90±0.22	+0.34±0.02	+0.30±0.25	+0.06±0.23	+0.58±0.12
CDTG-22	4	-1.76	0.53 / 0.38 / 0.05	0.80	49.73	-2.26±0.31	+0.31±0.14	-0.03±0.11	-0.02±0.13	+0.58±0.21
CDTG-23	4	-1.78	0.22 / 0.88 / 0.03	0.50	114.55	-2.05±0.44	+0.05±0.19	+0.28±0.12	+0.14±0.11	+0.59±0.22
CDTG-24	4	-1.68	0.34 / 0.91 / 0.05	0.58	108.32	-2.38±0.26	+0.07±0.24	+0.25±0.09	+0.16±0.16	+0.61±0.16
CDTG-25	3	-1.68	0.23 / 1.08 / 0.07	0.48	137.98	-1.93±0.15	+0.29±0.08	+0.15±0.19	+0.02±0.15	+0.47±0.09
CDTG-26	3	-1.21	1.35 / -1.04 / 0.64	0.77	-144.50	-2.26±0.52	...	+0.07±0.12	-0.09±0.24	+0.59±0.06
CDTG-27	3	-1.61	0.12 / -1.17 / 0.30	0.31	-145.53	-2.11±0.08	+0.23±0.20	-0.06±0.09	-0.08±0.14	+0.54±0.28
CDTG-28	4	-1.42	0.86 / -0.60 / 0.51	0.75	-83.92	-2.54±0.22	+0.46±0.18	+0.03±0.25	-0.17±0.12	+0.48±0.02
CDTG-29	5	-2.03	0.13 / 0.03 / 0.29	0.79	22.40	-1.84±0.36	-0.09±0.12	-0.02±0.59	+0.23±0.38	+0.83±0.34
CDTG-30	3	-1.15	1.42 / -1.72 / 0.47	0.71	-281.50	-2.46±0.51	-0.01±0.06	+0.21±0.51	+0.21±0.37	+0.87±0.59

NOTE—For each of the listed elements, the table entries indicate the means and standard deviations (dispersions) of the abundances, when at least 3 measurements of that element were available for a given CDTG. When the number of available measured elemental abundances is 4 or more, biweight estimates of these quantities are reported, in order to decrease the influence of potential outliers.

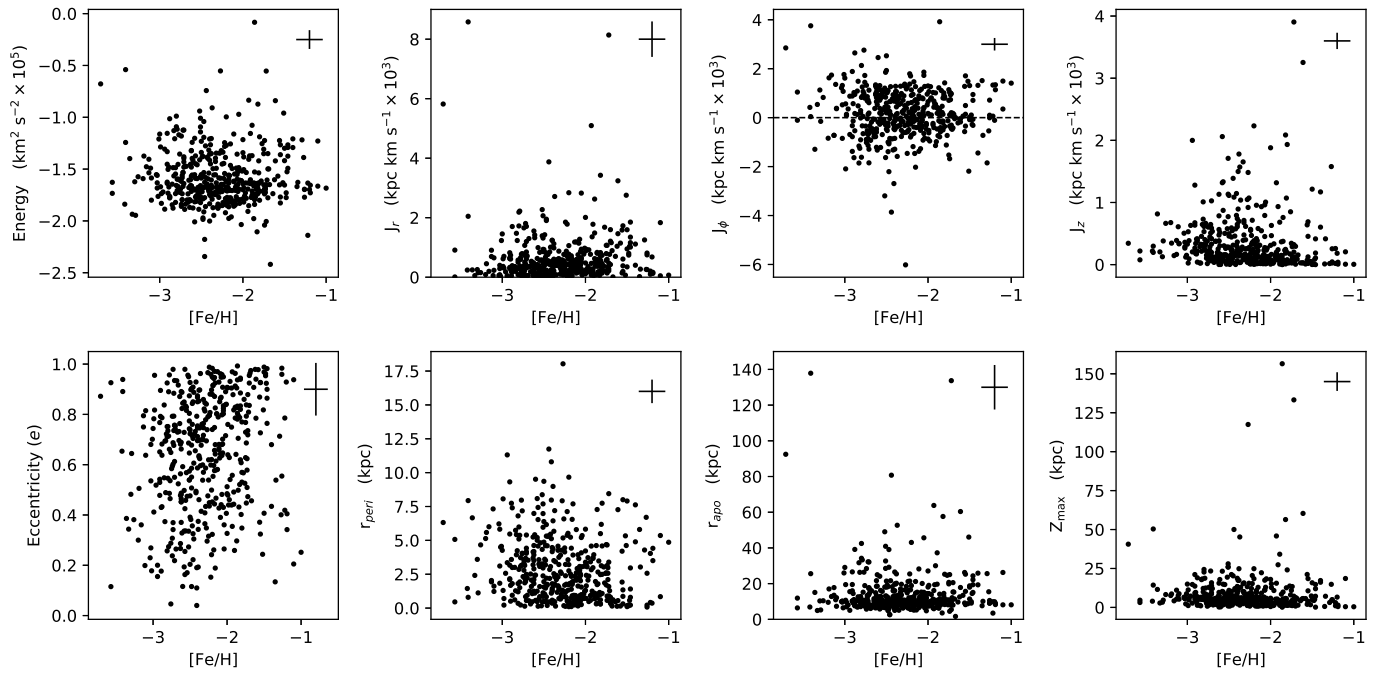


**Figure 9.** Orbital energies, actions, and other dynamical parameters for the RPE Sample, derived using **AGAMA** with the MW2017 potential, as a function of  $[\text{Fe}/\text{H}]$ . The horizontal dashed line in the  $J_\phi$  vs.  $[\text{Fe}/\text{H}]$  plot divides stars with prograde from retrograde orbits. Horizontal error bars in the upper-right corners show characteristic uncertainties in the  $[\text{Fe}/\text{H}]$  determination, and the vertical error bars show mean uncertainties (multiplied by a factor of 5 for better visibility) of the involved quantities.

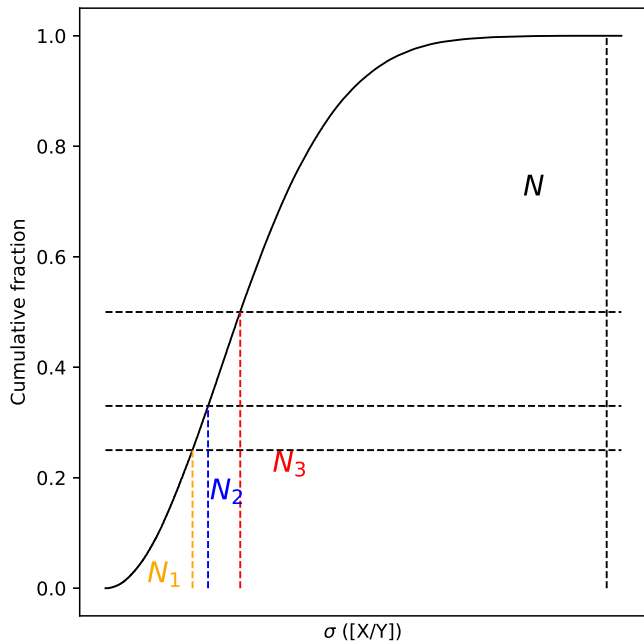


**Figure 10.** Setup for derivation of the binomial probability. The cumulative fraction distribution of some elemental-abundance dispersion is plotted versus the dispersion value. Here  $N_1$  is the number of CDF values below 0.25,  $N_2$  below 0.33, and  $N_3$  below 0.50, among the total  $N$ . We are interested in the probability that these numbers can be obtained from a binomial distribution.

**Table 6.** CDTGs Identified from the HDBSCAN Algorithm

Name	Class	[Fe/H]	[C/Fe]	[C/Fe] <sub>c</sub>	[Sr/Fe]	[Ba/Fe]	[Eu/Fe]	[Eu/H]
<i>CDTG-1</i> ( $N = 6$ , CL = 99.8%)								
2MASS J10492192–1154173	$r$ -I	–2.18	–0.42	–0.41	–0.06	–0.16	+0.33	–1.85
2MASS J20584918–0354340	$r$ -I	–2.36	0.00	+0.40	–0.24	–0.09	+0.36	–2.00
2MASS J12591462–7049592	$r$ -I	–2.45	–0.60	+0.16	+0.25	+0.25	+0.50	–1.95
2MASS J11404726–0833030	$r$ -I	–1.55	+0.03	+0.05	+0.11	+0.36	+0.55	–1.00
2MASS J00405260–5122491	$r$ -II	–2.11	–0.04	–0.04	+0.09	–0.04	+0.86	–1.25
BD+17:3248	$r$ -II	–2.09	–0.47	–0.24	+0.29	+0.40	+0.91	–1.18
$\mu \pm \sigma$ ([X/Y])		–2.19±0.28	–0.25±0.27	–0.01±0.28	+0.08±0.19	+0.12±0.23	+0.57±0.24	–1.54±0.43
Cumulative fraction value		0.20		0.70	0.32	0.44	0.68	
<i>CDTG-2</i> ( $N = 8$ , CL = 99.1%)								
2MASS J19445483–4039459	$r$ -I	–1.98	–0.27	+0.33	+0.21	+0.13	+0.33	–1.65
2MASS J15293404–3906241	$r$ -I	–2.74	...	...	–0.36	–0.16	+0.34	–2.40
RAVE J151558.3–203821	$r$ -I	–2.74	–0.15	+0.58	+0.27	–0.39	+0.36	–2.38
2MASS J20303339–2519500	$r$ -I	–2.21	–0.65	+0.10	+0.41	–0.29	+0.41	–1.80
2MASS J15133549–1244339	$r$ -I / CEMP- $r$	–2.04	+0.45	+0.75	–2.87	–0.10	+0.55	–1.49
2MASS J14232679–2834200	$r$ -I	–1.90	+0.43	+0.44	+0.44	–0.07	+0.61	–1.29
BPS CS 22896–0154	$r$ -II	–2.69	+0.27	+0.28	+0.54	+0.51	+0.86	–1.83
2MASS J14592981–3852558*	$r$ -II	–2.48	–0.95	–0.17	+0.23	+0.13	+0.93	–1.55
$\mu \pm \sigma$ ([X/Y])		–2.35±0.35	–0.12±0.52	+0.34±0.29	+0.29±0.28	–0.05±0.27	+0.51±0.24	–1.73±0.40
Cumulative fraction value		0.26		0.72	0.58	0.51	0.64	
<i>CDTG-3</i> ( $N = 3$ , CL = 97.4%)								
2MASS J16024498–1521016	$r$ -I	–1.80	–0.05	–0.05	+0.35	+0.08	+0.55	–1.25
2MASS J09284944–0738585	$r$ -I	–1.22	0.00	+0.07	+0.45	+0.32	+0.60	–0.62
2MASS J10191573–1924464	$r$ -II	–1.19	–0.32	–0.23	+0.63	+0.73	+0.75	–0.44
$\mu \pm \sigma$ ([X/Y])		–1.40±0.28	–0.12±0.14	–0.07±0.12	+0.48±0.12	+0.38±0.27	+0.63±0.08	–0.77±0.35
Cumulative fraction value		0.40		0.28	0.23	0.67	0.22	
<i>CDTG-4</i> ( $N = 4$ , CL = 93.7%)								
2MASS J00413026–4058547	$r$ -I	–2.58	–0.49	+0.20	+0.04	–0.27	+0.38	–2.20
2MASS J02274104–0519230*	$r$ -I	–2.38	–0.70	+0.08	+0.72	–0.18	+0.42	–1.96
2MASS J00453930–7457294	$r$ -I / CEMP- $r$	–2.00	+0.93	+0.98	+0.83	+0.37	+0.55	–1.45
2MASS J00182832–3900338	$r$ -I	–1.80	–0.35	+0.15	+0.28	+0.07	+0.57	–1.23
$\mu \pm \sigma$ ([X/Y])		–2.19±0.32	–0.50±0.28	+0.15±0.07	+0.48±0.34	–0.03±0.27	+0.48±0.09	–1.71±0.41
Cumulative fraction value		0.43		0.10	0.79	0.64	0.24	

NOTE—Single (\*) mark indicates the 27 stars with relative distance errors in the range  $20\% < \epsilon < 30\%$ . See text for details.

NOTE—Means ( $\mu$ ), standard deviations ( $\sigma$ ), and cumulative fraction values for the elemental abundances in each CDTG with at least 3 measured abundances are listed. When the number of available measured elemental abundances is 4 or more, biweight estimates of these quantities are reported, in order to decrease the influence of potential outliers.

NOTE—This table is a stub; the full table is available in electronic form.

**Table 7.** CDTG Elemental-Abundance Statistics

Abundance	# CDTGs	$N < 0.50, 0.33, 0.25$	IEAD Probabilities	GEAD Probabilities	OEAD Probability
[Fe/H]	30	21, 14, 12	2.1%, 8.3%, 5.5%	0.8%	
[C/Fe] <sub>c</sub>	26	17, 13, 11	11.5%, 8.4%, 5.4%	1.5%	
[Sr/Fe]	26	16, 15, 9	16.3%, 0.8%, 18.0%	0.8%	$\ll 0.001\%$
[Ba/Fe]	30	18, 15, 12	18.1%, 4.0%, 5.1%	2.0%	
[Eu/Fe]	30	17, 9, 8	29.2%, 70.1%, 48.6%	22.2%	
FEAD Probabilities			0.03%, 0.00%, 0.01%		

NOTE—The Individual Elemental-Abundance Dispersion (IEAD) probabilities represent the binomial probabilities for each element for the levels  $v = 0.50, 0.33,$  and  $0.25,$  respectively. The Full Elemental-Abundance Dispersion (FEAD) probabilities represent the probabilities (across *all* elements) for the levels  $v = 0.50, 0.33,$  and  $0.25,$  respectively. The Global Elemental-Abundance Dispersion (GEAD) probabilities represent the probabilities for the triplet of CDF levels for each element. The Overall Elemental-Abundance Dispersion (OEAD) probability represents the probability (across *all* elements) resulting from random draws from the full CDF. See text for details.



**Table 8.** Dynamical Properties of Known Substructures, DTGs, and RPE Groups

Substructure ( $n_{\text{sub}}$ )	Groups	$(\langle V_r \rangle, \langle V_\phi \rangle, \langle V_z \rangle)$	$(\langle J_r \rangle, \langle J_\phi \rangle, \langle J_z \rangle)$	$\langle E \rangle$
		$\sigma_{V_r}, \sigma_{V_\phi}, \sigma_{V_z}$	$\sigma_{J_r}, \sigma_{J_\phi}, \sigma_{J_z}$ $\times 10^3$ (kpc km s $^{-1}$ )	$\sigma_E$ $\times 10^5$ (km $^2$ s $^{-2}$ )
GSE (57)	CDTG-1,7,9,10,12,13,17,19,20,21,22	(24.91, $-3.85$ , 4.86) (178.35, 35.19, 69.69)	(0.67, $-0.04$ , 0.08) (0.37, 0.25, 0.09)	$-1.75$ 0.14
Sequoia <sup>a</sup> (6)	CDTG-26,30	( $-10.51$ , $-212.84$ , 113.44) (241.61, 98.96, 35.36)	(1.38, $-1.47$ , 0.64) (0.24, 0.42, 0.02)	$-1.21$ 0.04
Thamnos <sup>a</sup> (11)	CDTG-2,27	(1.91, $-157.80$ , $-36.46$ ) (61.88, 18.71, 89.76)	(0.05, $-0.92$ , 0.15) (0.03, 0.10, 0.10)	$-1.79$ 0.10
MWTD <sup>b</sup> (9)	CDTG-3,5,8	( $-4.30$ , 158.81, 9.20) (63.57, 13.56, 76.15)	(0.10, $+1.31$ , 0.02) (0.04, 0.07, 0.02)	$-1.64$ 0.05
ZY20:DTG-3 <sup>c</sup> (1)	CDTG-15	(44.37, 148.70, $-264.30$ ) (118.57, 53.84, 63.41)	(0.37, $+1.25$ , 1.08) (0.13, 0.25, 0.07)	$-1.34$ 0.05
ZY20:DTG-7 <sup>d</sup> (1)	CDTG-1	(27.81, 15.37, 6.98) (41.86, 4.04, 46.33)	(0.59, $+0.12$ , 0.03) (0.03, 0.03, 0.01)	$-1.84$ 0.03
ZY20:DTG-16 <sup>d</sup> (1)	CDTG-12	(39.03, $-46.57$ , 3.59) (72.13, 6.14, 50.28)	(0.46, $-0.35$ , 0.07) (0.02, 0.05, 0.03)	$-1.80$ 0.03
ZY20:DTG-46 <sup>d</sup> (1)	CDTG-28	(38.76, $-83.92$ , 8.27) (246.05, 50.62, 99.95)	(0.86, $-0.60$ , 0.51) (0.02, 0.16, 0.06)	$-1.42$ 0.04
GL20:DTG-2 (3)	CDTG-4	( $-91.85$ , 66.69, $-22.65$ ) (33.31, 36.71, 321.86)	(0.69, $+0.55$ , 1.91) (0.20, 0.26, 0.11)	$-1.20$ 0.01
GL20:DTG-3 <sup>c</sup> (3)	CDTG-15	(44.37, 148.70, $-264.30$ ) (118.57, 53.84, 63.41)	(0.37, $+1.25$ , 1.08) (0.13, 0.25, 0.07)	$-1.34$ 0.05
GL20:DTG-7 (2)	CDTG-28	(38.76, $-83.92$ , 8.27) (246.05, 50.62, 99.95)	(0.86, $-0.60$ , 0.51) (0.02, 0.16, 0.06)	$-1.42$ 0.04
GL20:DTG-30 <sup>d</sup> (2)	CDTG-13	( $-45.29$ , $-10.53$ , 15.73) (198.01, 19.10, 79.35)	(0.72, $-0.10$ , 0.13) (0.07, 0.14, 0.04)	$-1.69$ 0.01
IR18:Group A (2)	CDTG-11,23	( $-23.57$ , 84.56, 10.25) (90.30, 20.95, 61.77)	(0.43, $+0.73$ , 0.07) (0.14, 0.14, 0.04)	$-1.71$ 0.05
IR18:Group B (1)	CDTG-13	( $-45.29$ , $-10.53$ , 15.73) (198.01, 19.10, 79.35)	(0.72, $-0.10$ , 0.13) (0.07, 0.14, 0.04)	$-1.69$ 0.01
IR18:Group C (2)	CDTG-16	(53.27, 127.04, $-33.27$ ) (76.88, 23.75, 77.77)	(0.20, $+0.98$ , 0.16) (0.02, 0.05, 0.02)	$-1.68$ 0.02
IR18:Group D (1)	CDTG-10	( $-204.81$ , $-8.90$ , 18.44) (19.37, 11.98, 21.57)	(1.02, $-0.07$ , 0.00) (0.04, 0.10, 0.00)	$-1.61$ 0.02
IR18:Group E (2)	CDTG-1	(27.81, 15.37, 6.98) (41.86, 4.04, 46.33)	(0.59, $+0.12$ , 0.03) (0.03, 0.03, 0.01)	$-1.84$ 0.03
IR18:Group F (1)	CDTG-22	( $-113.36$ , 49.73, 8.26) (69.95, 8.02, 62.15)	(0.53, $+0.38$ , 0.05) (0.03, 0.04, 0.02)	$-1.76$ 0.02
IR18:Group H (1)	CDTG-19	(9.73, $-24.40$ , 39.72) (82.12, 10.27, 76.64)	(0.40, $-0.16$ , 0.19) (0.02, 0.08, 0.02)	$-1.85$ 0.02

<sup>a</sup>Tentative associations with Sequoia (Myeong et al. 2019) and Thamnos (Koppelman et al. 2019a) substructures.

<sup>b</sup>Metal-Weak Thick Disk; originally identified by Morrison et al. (1990), and recently shown to be an independent structure from the canonical thick disk by Carollo et al. (2019) and An & Beers (2020).

<sup>c</sup>These DTGs have been attributed to the Helmi et al. (1999) Stream by Yuan et al. (2020) and Limberg et al. (2020).

<sup>d</sup>These DTGs have been attributed to the *Gaia*-Sausage by Yuan et al. (2020) and Limberg et al. (2020).

NOTE—In the first column, the number in parenthesis indicates the number of RPE stars from our study associated with the listed substructure, DTG, or group.

**Table 2.** RPA Classes, Temperatures, and Elemental Abundances for the Initial Sample

Name	RPA Class	$T_{\text{eff}}$	[Fe/H]	[C/Fe]	[C/Fe] <sub>c</sub>	[Sr/Fe]	[Ba/Fe]	[Eu/Fe]	Reference	RPA
		(K)								
2MASS J00002259-1302275	r-I	4576	-2.90	-0.65	-0.65	-1.20	-0.38	+0.58	a	1
2MASS J00002416-1107454	r-I	4693	-2.43	-0.27	+0.30	-0.04	-0.24	+0.51	b	1
SMSS J000113.96-363337.9	limited-r	4810	-2.32	-0.33	+0.09	-0.04	-1.21	-0.55	c	0
HD 224930	r-I	5275	-1.00	...	...	...	-0.19	+0.34	d	0
2MASS J00021668-2453494	r-I	5020	-1.81	-0.88	-0.57	+0.59	+0.10	+0.52	a	1
BPS CS 22957-0036	r-I	5970	-2.28	+0.04	+0.04	+0.20	-0.22	+0.55	e	0
HD 20	r-II	5445	-1.58	-0.34	-0.32	+0.13	+0.32	+0.80	f	0
2MASS J00073817-0345509	r-II	4663	-2.09	-0.32	+0.17	+0.41	+0.11	+0.73	g	1
BPS CS 31070-0073	r-II / CEMP-r	6190	-2.55	+1.34	+1.34	-0.04	+2.42	+2.83	h	0
2MASS J00093394-1857008	r-I	4815	-1.88	-0.17	+0.06	+0.13	+0.23	+0.46	b	1
2MASS J00101758-1735387	r-II	5229	-2.41	0.00	+0.01	+0.09	+0.43	+1.35	i	1
HE 0010-3422	r-II / CEMP-r	5400	-2.78	+1.92	+1.94	+0.85	+1.54	+1.72	j	0
2MASS J00154806-6253207	r-I	4725	-2.30	-0.55	-0.33	+0.30	+0.08	+0.40	b	1
2MASS J00172430-3333151	r-I	4764	-2.29	-0.07	+0.23	+0.35	+0.05	+0.59	b	1
2MASS J00182832-3900338	r-I	4639	-1.80	-0.35	+0.15	+0.28	+0.07	+0.57	b	1
BPS CS 22882-0001	r-II	5930	-2.62	+0.68	+0.77	+0.16	+0.06	+0.81	e	0
2MASS J00223225-4839449	r-I	4648	-1.75	-0.25	+0.20	-0.05	+0.10	+0.65	b	1
BPS CS 30339-0052	r-I	5580	-2.69	+0.67	+0.68	+0.61	-0.53	+0.55	e	0
BPS CS 29497-0004	r-II	5090	-2.63	+0.10	+0.11	+0.55	+1.01	+1.68	k	0
2MASS J00305267-1007042	limited-r	4831	-2.35	0.00	+0.50	+0.50	-0.71	0.00	g	1
2MASS J00400685-4325183	r-I	4630	-2.55	-0.85	-0.13	-1.52	-1.56	+0.55	a	1
2MASS J00405260-5122491	r-II	5689	-2.11	-0.04	-0.04	+0.09	-0.04	+0.86	a	1
2MASS J00413026-4058547	r-I	4605	-2.58	-0.49	+0.20	+0.04	-0.27	+0.38	b	1
2MASS J00442897-1017497	r-I	4672	-2.41	-0.25	+0.36	-0.08	-0.07	+0.47	b	1
2MASS J00452379-2112161	r-I	4783	-2.63	-0.15	+0.50	-0.10	-0.25	+0.40	i	1
2MASS J00452879-5846450	r-I	4754	-2.22	-0.25	+0.37	+0.28	+0.12	+0.57	b	1
2MASS J00453930-7457294	r-I / CEMP-r	4947	-2.00	+0.93	+0.98	+0.83	+0.37	+0.55	a	1
HE 0045-2430	r-I	5377	-1.77	-0.09	-0.08	-0.75	-0.34	+0.33	f	0
2MASS J00482431-1041309	r-I	4764	-2.50	-0.25	+0.47	+0.25	+0.09	+0.45	b	1
2MASS J00512646-1053170	r-II	6340	-2.38	-1.75	-1.75	+0.49	+0.50	+1.21	i	1
2MASS J00524174-0902235	r-II	5170	-1.46	-1.37	-1.04	-1.41	-0.72	+0.94	i	1
2MASS J00532781-0253169	r-I	4370	-2.16	-0.30	+0.40	-0.05	-0.24	+0.39	g	1
2MASS J00541965-0611555	r-I	4707	-2.32	-0.20	+0.50	+0.26	-0.21	+0.59	g	1
HE 0057-4541	r-I	5144	-2.40	+0.44	+0.45	+0.21	-0.06	+0.55	l	0
BPS CS 22953-0003	r-II	4860	-3.13	+0.10	+0.35	+0.32	+0.29	+0.79	e	0
BPS CS 22183-0031	r-II	4850	-3.57	+0.30	+0.56	-0.22	+0.13	+0.84	e	0
2MASS J01094330-5907230	limited-r	4714	-2.49	-0.17	+0.51	+0.08	-0.49	+0.01	b	1
2MASS J01165010-6307441	r-I	5112	-1.64	+0.15	+0.18	-0.23	0.00	+0.37	i	1
2MASS J01202234-5425582	r-I	5125	-2.11	-0.09	-0.08	+0.50	+0.16	+0.30	a	1
2MASS J01213447-2528002	r-I	4551	-2.61	-0.50	+0.24	+0.13	-0.30	+0.30	b	1
2MASS J01293113-1600454	r-II	4876	-2.81	+0.35	+0.51	+0.88	+0.95	+1.76	a	1
2MASS J01311599-4016510	r-I	4824	-2.17	-0.10	+0.27	+0.18	-0.12	+0.53	b	1
2MASS J01321981-3040512	r-I	5175	-2.13	-0.15	-0.14	+0.07	+0.03	+0.42	b	1
2MASS J01371888-1729037	r-I	4381	-2.55	-0.85	-0.07	-0.18	-0.31	+0.33	b	1
2MASS J01373857-2618131	r-I	4579	-2.80	-0.15	+0.57	0.00	+0.03	+0.62	b	1
2MASS J01425422-5032488	r-I	5132	-2.09	+0.07	+0.08	+0.13	-0.13	+0.38	a	1
2MASS J01425445-0904162	r-II	4662	-1.73	-0.55	-0.15	+0.30	+0.35	+0.83	b	1
2MASS J01493760-4551222	r-I	4965	-2.73	-0.10	+0.36	-0.40	-0.05	+0.30	b	1
2MASS J01530024-3417360	r-II	5323	-1.50	+0.01	+0.02	+0.40	+0.09	+0.71	a	1
2MASS J01553180-4919420	r-II	5004	-3.01	+0.40	+0.41	+0.06	+0.15	+0.72	i	1
2MASS J01555066-6400155	r-II	4779	-2.71	-0.20	+0.26	-0.14	+0.10	+0.80	i	1
2MASS J01565634-1402108	r-II	4622	-2.08	-0.27	+0.37	+0.10	-0.11	+0.76	g	1
BPS CS 22958-0037	r-I	5770	-2.51	+0.33	+0.35	-0.09	-0.36	+0.51	e	0
2MASS J02031860-7930291	r-I	4720	-3.03	-0.52	+0.21	-0.23	+0.07	+0.36	c	0
2MASS J02070641-5009166	r-I	4526	-2.15	-0.80	-0.20	+0.13	+0.20	+0.65	b	1
BPS CS 22958-0052	r-II	6090	-2.62	+0.32	+0.32	+0.13	0.00	+1.00	e	0
HD 13979	limited-r	4830	-2.97	-1.17	-0.81	-0.18	-0.78	-0.29	e	0
2MASS J02165716-7547064	r-II	4543	-2.50	-0.33	+0.42	+0.25	+0.25	+1.12	a	1
2MASS J02230804-3129531	r-I	4757	-1.82	-0.30	+0.12	+0.15	+0.10	+0.45	b	1
2MASS J02265832-0749596	r-I	5088	-1.94	-0.05	-0.04	+0.23	+0.08	+0.56	b	1
2MASS J02274104-0519230	r-I	4498	-2.38	-0.70	+0.08	+0.72	-0.18	+0.42	g	1
2MASS J02355867-6745520	r-I / CEMP-r	4653	-1.55	+0.97	+1.10	+0.10	+0.49	+0.50	a	1
2MASS J02413897-0427349	r-I	4539	-2.48	-0.35	+0.40	+0.24	-0.26	+0.48	g	1
HE 0240-0807	r-II	4740	-2.88	-0.43	+0.02	-0.13	+0.20	+0.78	l	0

**Table 2** continued

Table 2 (continued)

Name	RPA Class	$T_{\text{eff}}$	[Fe/H]	[C/Fe]	[C/Fe] <sub>c</sub>	[Sr/Fe]	[Ba/Fe]	[Eu/Fe]	Reference	RPA
		(K)								
BD+42:621	$r$ -I	4725	-2.48	...	...	-0.18	-0.55	+0.54	m	0
2MASS J02462013-1518419	$r$ -II	4879	-2.71	+0.04	+0.12	+0.58	+0.60	+1.45	a	1
SMSS J024858.41-684306.4	$r$ -II / CEMP- $r$	4977	-3.71	+0.66	+0.91	-0.16	+0.59	+1.00	c	0
2MASS J02500719-5145148	$r$ -I / CEMP- $r$	4707	-2.20	+1.04	+1.28	-0.05	+0.48	+0.62	a	1
2MASS J02515281-3717316	$r$ -I	4660	-2.33	-0.40	+0.34	-0.33	-0.22	+0.33	b	1
2MASS J02570028-3024374	$r$ -I	4833	-2.05	+0.15	+0.33	-0.03	+0.03	+0.55	b	1
BPS CS 31078-0018	$r$ -II	5257	-2.85	+0.35	+0.36	+0.24	+0.72	+1.23	n	0
HE 0300-0751	$r$ -II	5280	-2.27	+0.10	+0.11	+0.13	+0.02	+0.77	f	0
2MASS J03071478-0534554	$r$ -I	4568	-2.23	-0.21	+0.44	+0.38	+0.17	+0.50	g	1
2MASS J03073894-0502491	$r$ -II	4450	-2.22	-0.57	+0.01	+1.25	+0.14	+1.27	i	1
2MASS J03084611-4747083	$r$ -I	5071	-1.56	+0.20	+0.22	+0.09	+0.18	+0.55	c	0
2MASS J03133726-1020553	$r$ -I	4757	-2.05	-0.31	+0.17	-0.17	-0.12	+0.42	g	1
2MASS J03154102-7626329	$r$ -I	4657	-2.71	-0.10	+0.55	-0.22	-0.01	+0.50	i	1
HE 0315+0000	$r$ -I	5013	-2.73	+0.18	+0.19	-0.01	+0.34	+0.65	f	0
BPS CS 22968-0026	$r$ -I	5850	-2.57	-0.09	-0.09	+0.23	-0.51	+0.58	e	0
2MASS J03210882-3944213	$r$ -I	4671	-1.91	-0.60	+0.03	+0.20	+0.13	+0.55	b	1
2MASS J03270229+0132322	$r$ -II	5170	-2.39	+0.35	+0.36	-0.05	+0.50	+1.07	i	1
BPS CS 29526-0110	$r$ -II / CEMP- $r$	6650	-2.19	+2.38	+2.38	+0.27	+2.27	+2.28	h	0
HE 0328-1047	$r$ -I	5301	-2.25	+0.15	+0.16	+0.01	-0.07	+0.42	f	0
CD-24:1782	limited- $r$	4950	-3.05	+0.10	+0.15	-0.15	-0.91	-0.24	e	0
HE 0337-5127	$r$ -I	5247	-2.62	+0.16	+0.17	-0.01	-0.02	+0.60	f	0
2MASS J03422816-6500355	$r$ -II	4976	-2.16	+0.05	+0.06	+0.33	+0.40	+1.05	b	1
SMSS J034249.53-284216.0	$r$ -I	4828	-2.33	-0.50	-0.08	-0.52	-0.78	+0.31	c	0
HE 0341-4024	$r$ -I	6108	-1.82	+0.27	+0.27	-0.09	-0.08	+0.69	f	0
2MASS J03434624-0924169	$r$ -I	4380	-1.92	-0.40	+0.24	-0.02	-0.07	+0.38	g	1
2MASS J03550926-0637108	limited- $r$	5076	-2.38	-0.80	-0.29	+0.50	-0.28	+0.25	g	1
2MASS J03563703-5838281	limited- $r$	4450	-2.87	-0.78	-0.02	+0.55	-0.50	+0.11	a	1
BPS CS 30494-0003	limited- $r$	4930	-2.97	+0.14	+0.24	+0.12	-0.65	+0.02	e	0
BPS CS 29529-0054	$r$ -II	5710	-2.55	+0.58	+0.58	-0.10	-0.02	+0.90	e	0
2MASS J04012191-2635058	$r$ -I	4856	-2.20	+0.03	+0.13	+0.13	+0.15	+0.38	b	1
RAVE J040618.2-030525	$r$ -II	5100	-1.46	+0.54	+0.56	...	+0.98	+1.17	o	0
2MASS J04121388-1205050	$r$ -I	4658	-2.73	-0.12	+0.60	+0.42	-0.43	+0.52	a	1
BPS CS 22186-0005	$r$ -II	6250	-2.72	...	...	-1.02	-0.62	+0.71	p	0
BPS CS 22186-0002	$r$ -I	5500	-2.72	+0.15	+0.15	-0.14	-0.30	+0.44	e	0
2MASS J04182158-2323391	$r$ -I	4633	-1.82	-0.44	+0.07	+0.19	+0.13	+0.48	b	1
2MASS J04192966-0517491	$r$ -I	4568	-2.02	-0.36	+0.20	+0.23	0.00	+0.40	g	1
BPS CS 22186-0023	limited- $r$	4820	-3.04	+0.06	+0.41	-0.27	-1.18	-0.70	e	0
BPS CS 22182-0033	$r$ -I	5810	-2.65	+0.13	+0.13	+0.04	-0.47	+0.40	e	0
HE 0420+0123a	$r$ -II / CEMP- $r$	4800	-3.03	+0.33	+0.78	-0.25	+0.15	+0.79	q	0
BPS CS 22186-0025	$r$ -I	4900	-3.00	-0.62	-0.19	-0.12	+0.02	+0.54	r	0
2MASS J04245677-6500173	$r$ -I	4608	-2.37	-0.52	+0.20	-0.30	+0.19	+0.30	i	1
2MASS J04263084-4058516	$r$ -I	4612	-2.43	-0.60	-0.01	+0.02	+0.07	+0.40	b	1
HE 0430-4901	$r$ -I	5296	-2.72	+0.09	+0.10	-0.58	-0.07	+1.16	f	0
2MASS J04315411-0632100	$r$ -I	5274	-2.18	-0.05	-0.05	+0.05	-0.10	+0.30	b	1
HE 0432-0923	$r$ -II	5131	-3.19	+0.24	+0.25	+0.47	+0.72	+1.25	f	0
HE 0442-1234	$r$ -I	4604	-2.41	-0.61	0.00	-0.32	-0.13	+0.52	f	0
BPS CS 22191-0029	$r$ -I	5810	-2.94	+0.96	+1.28	+0.29	-0.37	+0.37	e	0
2MASS J04520910-6209121	$r$ -I	4623	-2.79	-0.19	+0.49	-0.14	-0.14	+0.46	b	1
2MASS J04530168-2437144	$r$ -I	4672	-2.44	-0.80	-0.04	-0.21	-0.04	+0.59	g	1
2MASS J04565146-3115427	$r$ -I	4190	-2.19	-0.25	+0.45	+0.02	-0.33	+0.34	g	1
2MASS J05030025-7601462	$r$ -I	4725	-2.17	-0.20	+0.40	0.00	-0.21	+0.40	i	1
SMSS J051008.62-372019.8	$r$ -II	5170	-3.20	+0.56	+0.57	+0.41	+0.75	+0.95	c	0
HE 0512-3835	$r$ -I	4948	-2.40	-0.22	-0.18	+0.03	-0.11	+0.37	f	0
HE 0516-3820	$r$ -I	5269	-2.51	+0.35	+0.36	+0.23	+0.06	+0.64	l	0
2MASS J05241392-0336543	$r$ -II	4513	-2.50	-0.40	+0.09	-0.27	+0.47	+1.50	i	1
HE 0524-2055	$r$ -I	4749	-2.76	+0.10	+0.51	-0.01	-0.04	+0.50	l	0
2MASS J05311779-5810048	$r$ -I	5141	-2.40	+0.17	+0.18	-0.13	-0.11	+0.65	b	1
HE 0534-4615	$r$ -I	5506	-2.01	+0.13	+0.13	+0.04	-0.01	+0.49	f	0
2MASS J05381700-7516207	$r$ -I	4968	-1.84	+0.01	+0.04	+0.46	+0.23	+0.53	b	1
2MASS J05383296-5904280	$r$ -II	5824	-2.54	...	...	+1.11	+0.76	+1.28	b	1
2MASS J05384334-5147228	limited- $r$	4918	-2.92	+0.59	+0.97	-0.10	-0.66	-0.20	i	1
HE 0538-4515	$r$ -I	5896	-1.52	+0.15	+0.15	+0.16	-0.10	+0.51	f	0
2MASS J05521578-3953184	$r$ -I	4705	-2.37	-0.22	+0.23	+0.23	-0.04	+0.41	b	1
2MASS J05564771-6639054	$r$ -I	4711	-2.06	-0.45	-0.11	+0.10	+0.08	+0.45	b	1
2MASS J06090353-7122260	$r$ -I	4878	-2.75	-0.08	+0.38	-0.16	-0.45	+0.32	b	1
2MASS J06195001-5312114	$r$ -II	5212	-2.04	+0.30	+0.31	+1.00	-0.03	+0.73	b	1

Table 2 continued

Table 2 (continued)

Name	RPA Class	$T_{\text{eff}}$	[Fe/H]	[C/Fe]	[C/Fe] <sub>c</sub>	[Sr/Fe]	[Ba/Fe]	[Eu/Fe]	Reference	RPA
		(K)								
SMSS J062609.83-590503.2	r-II	4960	-2.77	+0.27	+0.47	-0.02	+0.84	+1.06	c	0
2MASS J06290787-6709523	r-I	4616	-2.79	-0.44	+0.30	-0.44	-0.17	+0.46	b	1
2MASS J06320130-2026538	r-I	5067	-1.56	-0.05	-0.03	+1.44	+0.15	+0.70	b	1
2MASS J06332771-3519240	r-I	5224	-1.86	+0.02	+0.03	+0.12	+0.02	+0.45	b	1
SMSS J063447.15-622355.0	r-II / CEMP-r	4432	-3.41	+0.08	+0.83	-0.56	+0.41	+0.89	c	0
2MASS J06392518-7414056	r-I	5089	-2.51	+0.35	+0.36	+0.07	-0.28	+0.40	i	1
2MASS J06401317-3540444	r-I	4942	-2.38	-0.10	-0.09	+0.24	+0.05	+0.38	b	1
2MASS J07052028-3343242	r-I	4757	-2.24	-0.36	+0.27	+0.03	-0.17	+0.62	g	1
2MASS J07150266-0154092	r-II	4855	-2.60	+0.07	+0.08	< -2.42	+0.52	+0.88	i	1
2MASS J07161594-5135248	r-I	4575	-1.85	-0.47	+0.13	+0.21	+0.28	+0.46	b	1
2MASS J07202253-3358518	r-II	5040	-1.61	+0.11	+0.13	+0.49	+0.68	+1.44	b	1
2MASS J07250021-7022038	r-I / CEMP-r	4837	-2.65	+0.30	+0.77	-0.14	-0.30	+0.33	i	1
2MASS J07352232-4425010	r-II	5245	-1.62	-0.01	0.00	+0.24	+0.39	+0.79	b	1
2MASS J07393021-5548171	r-I	4426	-1.74	-0.95	-0.40	+0.35	+0.50	+0.63	b	1
BD-01:1792	r-I	4850	-1.26	...	...	...	-0.02	+0.38	d	0
2MASS J07411443-4339360	r-I	4974	-1.74	+0.05	+0.07	+0.02	+0.13	+0.50	b	1
RAVE J074824.3-483141	r-I	5305	-2.13	0.00	+0.32	+0.66	-0.20	+0.45	o	0
2MASS J07501424-4123454	r-I	5021	-1.89	+0.17	+0.18	+0.15	+0.27	+0.59	b	1
2MASS J08015897-5752032	r-I	4622	-1.75	-0.35	+0.17	+0.20	+0.15	+0.55	b	1
2MASS J08025449-5224304	limited-r	4486	-2.68	-0.55	+0.21	+0.75	-0.21	+0.10	i	1
2MASS J08032084-5856521	r-I	5158	-1.74	+0.01	+0.03	+0.24	+0.26	+0.49	b	1
2MASS J08134364-2332528	r-I	4836	-1.72	-0.40	+0.10	+0.10	+0.28	+0.32	b	1
2MASS J08155667-2204105	r-I	4877	-1.85	-0.13	-0.03	+0.11	+0.21	+0.57	b	1
2MASS J08393460-2122069	r-I	4779	-1.94	-0.20	+0.14	+0.15	+0.13	+0.42	b	1
2MASS J08580584-0809174	r-I / CEMP-r	4530	-3.16	+0.01	+0.76	+0.01	-0.34	+0.27	s	1
2MASS J08594093-1415151	r-I	4876	-1.46	-0.27	-0.20	+0.13	+0.35	+0.52	b	1
2MASS J09185890-2311511	r-II	4662	-2.05	-0.35	+0.32	-0.51	-0.06	+0.71	g	1
2MASS J09255655-3450373	r-I	4619	-1.82	-0.46	-0.04	+0.39	+0.22	+0.62	b	1
2MASS J09261133-1526232	r-I	5004	-1.70	+0.01	+0.03	+0.06	+0.28	+0.43	b	1
2MASS J09284944-0738585	r-I	4760	-1.22	0.00	+0.07	+0.45	+0.32	+0.60	b	1
2MASS J09364069-2038386	r-I	4778	-1.78	-0.35	-0.05	+0.15	+0.12	+0.48	b	1
2MASS J09463483-0626532	r-I	4370	-1.99	-0.46	+0.21	+0.03	-0.07	+0.35	g	1
2MASS J09531322+0744515	r-I	4702	-4.04	-0.40	-0.21	+0.01	+0.30	+0.50	i	1
2MASS J09544277+5246414	r-II	4340	-2.99	-0.50	+0.24	+0.30	+0.35	+1.28	t	1
2MASS J09574607-3923072	r-I	4903	-1.73	-0.06	+0.25	+0.22	+0.21	+0.55	b	1
2MASS J09580181-1446137	r-I	4756	-2.33	-0.50	+0.03	+0.59	+0.20	+0.59	g	1
2MASS J10025125-4331098	r-I	4788	-2.90	...	...	-0.36	-0.71	+0.42	b	1
2MASS J10044858-2706500	r-I	4831	-2.40	+0.04	+0.55	0.00	-0.38	+0.41	g	1
2MASS J10063414-7030212	r-I	4963	-2.20	+0.19	+0.33	-0.21	+0.03	+0.39	i	1
2MASS J10082492-2314124	r-I	4898	-1.97	0.00	+0.02	+0.15	+0.23	+0.40	b	1
BPS BS 15621-0047	r-II / CEMP-r	4750	-2.29	+1.06	+1.30	+0.24	+0.35	+0.84	h	0
2MASS J10121964-3221347	r-I	4595	-2.68	-0.55	+0.20	-0.20	-0.07	+0.55	b	1
2MASS J10191573-1924464	r-II	4564	-1.19	-0.32	-0.23	+0.63	+0.73	+0.75	b	1
2MASS J10194932-4900584	r-I	5013	-1.50	-0.05	-0.02	+0.20	+0.22	+0.45	b	1
2MASS J10223779-3400209	r-I	4831	-2.14	-0.15	+0.15	+0.35	-0.29	+0.37	g	1
2MASS J10302845-7543299	r-I	4684	-2.21	-0.52	+0.22	-0.07	+0.08	+0.53	b	1
2MASS J10344785-4823544	limited-r	4927	-2.08	0.00	+0.20	+0.18	-0.35	-0.08	b	1
2MASS J10345348-1117221	r-I	4548	-1.89	-0.65	-0.04	+0.05	-0.32	+0.35	b	1
2MASS J10362687-3746174	r-I	4597	-1.83	-0.51	+0.08	+0.22	+0.32	+0.60	b	1
2MASS J10401894-4106124	r-II	4958	-1.55	0.00	+0.02	+0.13	+0.35	+0.82	b	1
HE 1044-2509	r-II	5227	-2.89	+0.52	+0.53	+0.23	+0.24	+0.94	f	0
2MASS J10492192-1154173	r-I	4915	-2.18	-0.42	-0.41	-0.06	-0.16	+0.33	g	1
2MASS J10513692-2115466	r-I	4430	-1.73	-0.30	+0.27	+0.03	-0.27	+0.32	g	1
SMSS J105320.99-435300.1	r-I	5022	-1.86	+0.09	+0.13	-0.16	-0.09	+0.37	c	0
J1054+0528	r-I / CEMP-r	5030	-3.30	+0.82	+0.86	-0.30	-0.52	+0.44	u	0
2MASS J10550658+1931580	r-I	4851	-2.32	+0.30	+0.68	-0.22	-0.50	+0.50	i	1
2MASS J10594136-2052253	r-I	4370	-2.16	-0.42	+0.28	+0.26	-0.07	+0.35	g	1
2MASS J11014865-3749526	r-I	4452	-2.20	-0.70	+0.06	+0.10	-0.12	+0.50	b	1
LAMOST J110901+075441	r-II	4440	-3.41	-0.57	+0.15	+0.29	+0.31	+1.16	v	0
2MASS J11165400-7250160	r-I	4369	-2.88	-0.90	-0.14	+0.17	-0.30	+0.30	i	1
LAMOST J112456.61+453531.	r-II	5180	-1.27	-0.42	-0.40	-0.36	+0.24	+1.10	w	0
HE 1127-1143	r-II	5224	-2.73	+0.54	+0.55	+0.24	+0.63	+1.08	f	0
2MASS J11301705-1449325	r-I	4985	-2.45	-0.10	-0.09	+0.08	-0.12	+0.50	g	1
2MASS J11303693+0224037	r-I	4702	-1.86	-0.20	+0.36	-0.40	-0.40	+0.35	i	1
HE 1131+0141	r-II	5236	-2.49	+0.12	+0.13	+0.15	+0.52	+0.87	f	0
2MASS J11370170-5401298	r-I	4466	-1.80	-0.80	-0.19	+0.05	+0.10	+0.63	b	1

Table 2 continued

Table 2 (*continued*)

Name	RPA Class	$T_{\text{eff}}$	[Fe/H]	[C/Fe]	[C/Fe] <sub>c</sub>	[Sr/Fe]	[Ba/Fe]	[Eu/Fe]	Reference	RPA
		(K)								
2MASS J11404726-0833030	$r$ -I	5118	-1.55	+0.03	+0.05	+0.11	+0.36	+0.55	b	1
2MASS J11404944-1615396	$r$ -II	4697	-1.68	-0.40	+0.02	+0.20	+0.27	+0.88	b	1
BD+26:2251	$r$ -I	5875	-1.10	...	...	...	+0.01	+0.48	d	0
2MASS J11444086-0409511	$r$ -I	4614	-2.52	-0.40	+0.33	-0.01	-0.26	+0.58	g	1
2MASS J11444480-1128167	$r$ -I	5006	-2.42	-0.35	-0.34	+0.03	-0.29	+0.35	g	1
2MASS J11463882-0422395	$r$ -I / CEMP- $r$	4235	-2.05	+0.25	+0.74	-0.28	+0.32	+0.62	g	1
2MASS J11471027+0341265	$r$ -I	4819	-2.47	+0.10	+0.61	-0.84	-0.05	+0.40	i	1
2MASS J11472988-0521444	$r$ -I	4707	-2.00	-0.25	+0.34	0.00	-0.22	+0.31	g	1
2MASS J11510227-6940416	$r$ -I	4630	-2.53	-0.52	+0.17	-0.01	-0.17	+0.48	i	1
HD 103095	$r$ -II	4950	-1.46	...	...	...	-0.03	+0.72	d	0
2MASS J11543613-0133450	$r$ -II	5230	-1.89	+0.30	+0.31	+0.10	+0.50	+0.80	x	0
RAVE J115941.7-382043	$r$ -I	5120	-1.10	+0.18	+0.19	...	-0.01	+0.70	o	0
2MASS J12044314-2911051	$r$ -II	4465	-2.35	-0.67	+0.11	+0.28	+0.33	+0.71	b	1
2MASS J12045624-0759232	$r$ -I	4530	-2.72	-0.24	+0.50	-0.29	-0.11	+0.33	g	1
2MASS J12070990-3653243	$r$ -I	4604	-1.76	-0.50	-0.05	+0.10	-0.10	+0.40	b	1
2MASS J12091322-1415313	$r$ -II	4370	-2.11	-0.50	+0.20	-0.01	+0.11	+0.81	g	1
2MASS J12102259-4902190	$r$ -I	4822	-1.69	-0.05	+0.33	+0.15	+0.23	+0.58	b	1
HD 106373	$r$ -I	6040	-2.61	+0.92	+1.05	+0.34	-0.39	+0.42	e	0
HE 1212-0127	$r$ -I	4915	-2.15	-0.39	-0.21	-0.20	-0.32	+0.35	f	0
HE 1214-1819	$r$ -I	4916	-3.01	+0.35	+0.42	+0.27	-0.04	+0.49	f	0
2MASS J12170829+0415146	$r$ -II	4630	-2.22	-0.40	+0.31	-0.44	+0.15	+1.10	i	1
2MASS J12203297+0257138	$r$ -I	4707	-2.63	-0.55	+0.14	0.00	0.00	+0.45	i	1
HE 1219-0312	$r$ -II	5060	-2.96	+0.03	+0.04	+0.35	+0.65	+1.38	y	0
HD 107752	$r$ -I	4826	-2.83	...	...	-0.04	-0.25	+0.36	z	0
2MASS J12233047-4216365	$r$ -I	4797	-2.33	-0.40	+0.34	-0.28	-0.32	+0.30	i	1
2MASS J12255123-2351074	$r$ -I	4990	-3.04	+0.30	+0.32	-0.09	-0.34	+0.52	i	1
HD 108317	$r$ -I	5030	-2.62	-0.02	-0.01	+0.15	-0.16	+0.30	e	0
HD 108577	$r$ -I	4900	-2.36	...	...	...	-0.17	+0.36	aa	0
2MASS J12292696-0442325	$r$ -I	4523	-2.23	-0.40	+0.28	0.00	-0.22	+0.46	g	1
HE 1226-1149	$r$ -II	5120	-2.91	+0.42	+0.43	+0.35	+0.90	+1.55	ab	0
2MASS J12341308-3149577	$r$ -I	4772	-1.34	-0.20	-0.13	+0.35	+0.18	+0.35	b	1
2MASS J12351734+0945333	$r$ -I	4630	-2.39	-0.40	+0.28	-0.50	+0.05	+0.30	i	1
RAVE J123550.1-313111	$r$ -I / CEMP- $r$	4655	-2.46	+0.61	+1.11	...	+0.27	+0.59	o	0
2MASS J12405721-4051430	$r$ -I	5163	-1.48	+0.05	+0.07	+0.20	+0.22	+0.45	b	1
HE 1247-2114	limited- $r$	5012	-2.61	+0.32	+0.34	+0.37	-0.43	+0.22	f	0
2MASS J12503987-0307485	$r$ -I	5060	-2.15	-0.27	-0.26	-0.57	+0.10	+0.45	g	1
2MASS J12535742-3801355	$r$ -I	4773	-2.37	-0.01	+0.55	-0.06	-0.14	+0.53	b	1
2MASS J12563137-0834098	$r$ -I	4210	-2.34	-0.44	+0.31	+0.32	-0.28	+0.45	g	1
2MASS J12571667-4335318	$r$ -I	4845	-1.96	-0.05	+0.05	+0.05	+0.15	+0.30	b	1
HE 1256-0228	$r$ -I	4860	-2.07	-0.04	+0.15	0.00	+0.12	+0.51	f	0
2MASS J12591462-7049592	$r$ -I	4468	-2.45	-0.60	+0.16	+0.25	+0.25	+0.50	i	1
BPS BS 16929-0005	$r$ -II / CEMP- $r$	5250	-3.15	+1.50	+1.51	+0.52	+0.27	+1.01	h	0
2MASS J13052137-1137220	$r$ -II	4711	-2.07	-0.30	+0.35	-0.43	+0.20	+1.09	i	1
RAVE J130524.5-393126	$r$ -II	4820	-2.25	+0.17	+0.54	+0.43	+0.12	+0.76	o	0
2MASS J13085850-2712188	limited- $r$	4487	-2.38	-0.60	+0.15	+0.25	-0.30	+0.20	b	1
2MASS J13101305-3342369	$r$ -I	4594	-2.01	-0.60	+0.01	+0.40	+0.08	+0.53	b	1
HE 1311-1412	$r$ -I	4796	-2.91	-0.15	+0.28	-0.06	-0.06	+0.53	f	0
BPS CS 22877-0015	$r$ -II	6150	-2.12	+0.15	+0.15	+0.39	+0.30	+0.72	e	0
HD 115444	$r$ -II	4650	-2.99	-0.11	+0.32	+0.32	+0.18	+0.85	ac	0
2MASS J13164824-2743351	$r$ -I	4990	-1.61	-0.05	-0.03	+0.26	+0.01	+0.54	a	1
BPS BS 16033-0081	$r$ -I / CEMP- $r$	5020	-2.20	+0.77	+0.92	-1.99	-0.93	+0.38	h	0
2MASS J13214178-4320055	$r$ -I	4892	-2.17	-0.30	+0.26	-0.05	+0.15	+0.58	b	1
HE 1320-1339	limited- $r$	4690	-3.18	-0.97	-0.28	+0.20	-0.68	-0.21	e	0
2MASS J13254554-1747547	$r$ -I	4588	-2.32	-0.58	+0.18	-0.02	-0.44	+0.40	g	1
2MASS J13260450-1525020	limited- $r$	4798	-2.38	-0.12	+0.48	-0.10	-0.67	-0.28	g	1
2MASS J13261792-0945176	$r$ -I	4815	-2.88	+0.10	+0.52	-0.07	-0.25	+0.40	i	1
2MASS J13315746-1929446	$r$ -I	5077	-1.19	+0.09	+0.11	+0.29	+0.44	+0.51	b	1
2MASS J13330890-4654079	$r$ -I / CEMP- $r$	4591	-3.02	+0.05	+0.78	0.00	-0.17	+0.49	b	1
HD 118055	$r$ -I	4400	-1.91	...	...	...	+0.04	+0.54	d	0
2MASS J13351401-0110524	$r$ -I	4568	-2.45	-0.52	+0.21	-0.39	-0.22	+0.53	g	1
SMSS J133532.32-210632.9	$r$ -I	4734	-2.73	-0.50	+0.23	+0.29	-0.02	+0.31	c	0
2MASS J13374885-0826176	$r$ -II	4265	-2.62	-0.40	+0.34	+0.17	+0.02	+0.93	g	1
2MASS J13425404-0717005	$r$ -I	4568	-2.51	-0.62	+0.14	+0.04	-0.26	+0.44	g	1
HD 119516	$r$ -I	5290	-2.26	-0.42	+0.28	+0.26	-0.02	+0.34	ad	0
BPS BS 16089-0013	$r$ -I	4900	-2.70	+0.40	+0.66	+0.16	-0.13	+0.46	ae	0
2MASS J13494713-7423395	$r$ -I	4788	-2.85	+0.10	+0.60	+0.10	+0.05	+0.70	i	1

Table 2 *continued*

Table 2 (continued)

Name	RPA Class	$T_{\text{eff}}$	[Fe/H]	[C/Fe]	[C/Fe] <sub>c</sub>	[Sr/Fe]	[Ba/Fe]	[Eu/Fe]	Reference	RPA
		(K)								
2MASS J13511539-7340363	r-I	5044	-2.49	0.00	+0.01	-0.20	+0.17	+0.50	i	1
2MASS J13524835+1254216	r-I	4815	-1.96	-0.20	+0.39	-0.20	-0.30	+0.30	i	1
2MASS J14004919+4551581	r-II	4699	-1.93	...	...	+0.10	-0.02	+0.77	af	0
HD 122563	limited-r	4500	-2.97	-0.45	+0.30	-0.19	-1.17	-0.84	e	0
2MASS J14032900-5250429	r-I	5121	-1.86	-0.05	-0.04	+0.15	+0.10	+0.38	b	1
2MASS J14043762+0011117	r-I / CEMP-r	4370	-1.87	+0.65	+0.96	+0.43	+0.38	+0.58	g	1
HD 122956	r-I	4600	-1.70	...	...	+0.18	+0.15	+0.55	ag	0
2MASS J14100568-0701443	r-I	4698	-1.98	-0.30	+0.29	+0.10	+0.10	+0.68	i	1
2MASS J14101587-0343553	r-I	4931	-2.06	-0.15	-0.09	-0.15	-0.12	+0.67	g	1
2MASS J14155955-3219255	r-I	4486	-2.62	-0.81	-0.04	-0.11	-0.26	+0.47	b	1
2MASS J14164084-2422000	limited-r	4540	-2.73	-0.86	-0.09	+0.48	-0.44	+0.02	a	1
2MASS J14180866-2842077	r-I	4672	-2.32	-0.35	+0.30	-0.41	-0.11	+0.43	g	1
2MASS J14191395-0844410	r-I	4831	-2.08	-0.07	+0.22	+0.34	-0.15	+0.34	g	1
BD+01:2916	r-I	4150	-1.80	...	...	...	+0.07	+0.65	ag	0
2MASS J14232679-2834200	r-I	5200	-1.90	+0.43	+0.44	+0.44	-0.07	+0.61	a	1
2MASS J14234371-4025526	r-I	4833	-2.74	-0.40	+0.28	-0.47	+0.10	+0.30	i	1
BD+08:2856	r-I	4550	-2.10	...	...	...	-0.15	+0.42	aa	0
BPS CS 22883-0037	r-I	5900	-1.91	-0.09	+0.04	+0.31	+0.08	+0.41	p	0
2MASS J14301385-2317388	r-I	4490	-1.40	-0.70	-0.17	+0.40	+0.34	+0.62	a	1
BD+18:2890	r-I	4900	-1.71	...	...	...	+0.16	+0.39	aa	0
HE 1429-0347	r-I	5000	-2.71	+0.31	+0.41	+0.10	-0.34	+0.47	j	0
2MASS J14325334-4125494	r-II	5020	-2.79	-0.14	-0.13	+0.32	+0.71	+1.61	a	1
HE 1430+0053	r-II	5201	-3.03	+0.29	+0.30	-0.78	-0.10	+0.72	f	0
2MASS J14354680-1124122	r-II	5079	-1.35	-0.05	-0.03	+0.38	+0.42	+0.72	b	1
2MASS J14435196-2106283	limited-r	4486	-1.93	-0.95	-0.23	+0.18	-0.45	-0.30	b	1
BPS BS 16083-0172	r-I	5300	-2.50	+0.34	+0.35	+0.14	-0.37	+0.63	ae	0
2MASS J14533307-4428301	limited-r	4701	-2.46	-0.80	-0.02	-0.15	-0.78	-0.26	b	1
2MASS J14534137+0040467	r-II	4630	-3.09	-0.41	+0.32	+0.44	+1.05	+1.80	i	1
2MASS J14543792+0830379	r-II / CEMP-r	4891	-2.31	+0.30	+0.73	0.00	+0.35	+1.10	i	1
2MASS J14590234-0916105	r-I	4684	-2.38	-0.30	+0.32	-0.22	-0.10	+0.45	i	1
2MASS J14592981-3852558	r-II	4484	-2.48	-0.95	-0.17	+0.23	+0.13	+0.93	b	1
2MASS J15002498-0613374	r-I	4460	-2.05	-0.36	+0.33	+0.12	-0.10	+0.39	g	1
2MASS J15042611-2231523	r-I	4990	-2.91	-0.04	-0.03	-0.08	+0.16	+0.54	i	1
2MASS J15062866-1428038	r-I	5278	-2.25	-0.08	-0.08	+0.17	-0.01	+0.65	b	1
BD+30:2611	r-I	4275	-1.40	...	...	...	+0.08	+0.45	ag	0
2MASS J15075699-0659593	r-I	4300	-2.07	-0.20	+0.44	+0.12	-0.10	+0.36	g	1
2MASS J15083385-1459166	r-I	4543	-2.29	-0.65	+0.08	0.00	-0.10	+0.49	g	1
HD 134440	r-I	4750	-1.51	...	...	...	-0.31	+0.40	d	0
2MASS J15111672+0025252	r-I	4568	-2.46	-0.90	-0.12	+0.02	-0.18	+0.41	g	1
HD 135148	r-I	4275	-1.70	...	...	...	+0.30	+0.58	ag	0
2MASS J15133549-1244339	r-I / CEMP-r	4855	-2.04	+0.45	+0.75	-2.87	-0.10	+0.55	i	1
BPS CS 30306-0132	r-II	5110	-2.42	+0.34	+0.35	+0.14	+0.22	+0.85	ah	0
2MASS J15155734-1054220	r-I	4856	-1.75	+0.02	+0.30	+0.44	+0.52	+0.66	b	1
RAVE J151558.3-203821	r-I	4525	-2.74	-0.15	+0.58	+0.27	-0.39	+0.36	o	0
2MASS J15204531-1742486	r-I	4887	-2.81	+0.30	+0.54	-2.85	-0.30	+0.35	i	1
2MASS J15211026-0607566	r-II	4707	-2.00	-0.20	+0.34	-0.18	+0.10	+0.93	g	1
2MASS J15213995-3538094	r-II	5850	-2.80	+0.56	+0.57	+1.16	+1.35	+2.23	ai	0
2MASS J15260106-0911388	r-II	4499	-2.83	-0.82	-0.06	+0.90	+0.69	+1.70	a	1
2MASS J15271353-2336177	r-I	5882	-2.15	+0.33	+0.33	+0.35	-0.03	+0.70	a	1
2MASS J15293404-3906241	r-I	4492	-2.74	...	...	-0.36	-0.16	+0.34	b	1
2MASS J15383085-1804242	r-II	4752	-2.09	-0.10	+0.26	+0.44	+0.62	+1.27	g	1
2MASS J15475517-0837102	limited-r	4285	-2.48	-0.60	+0.16	+0.78	-0.50	-0.10	g	1
SMSS J155430.57-263904.8	r-II	4783	-2.61	-0.26	+0.41	+0.14	+0.80	+1.14	c	0
2MASS J15582962-1224344	r-II	5125	-2.54	-0.14	+0.31	+0.53	+0.04	+0.89	a	1
2MASS J16024498-1521016	r-I	5240	-1.80	-0.05	-0.05	+0.35	+0.08	+0.55	a	1
BD+42:2667	r-I	5950	-1.48	...	...	...	+0.09	+0.44	d	0
SMSS J160447.75-293146.7	r-I / CEMP-r	4675	-2.66	+0.26	+0.88	+0.27	+0.01	+0.31	c	0
2MASS J16064231-1632461	limited-r	4285	-2.28	-0.30	+0.43	+0.01	-0.57	-0.27	g	1
2MASS J16095117-0941174	r-I	4634	-2.66	-0.50	+0.25	-0.06	-0.30	+0.41	g	1
2MASS J16122832-0848083	r-I	4350	-2.11	-0.50	+0.20	+0.29	+0.04	+0.58	g	1
2MASS J16163560-0401148	r-I	4370	-1.97	-0.40	+0.25	+0.08	-0.19	+0.52	g	1
2MASS J16285613-1014576	r-I	4955	-2.00	-0.30	+0.24	-0.26	-0.02	+0.36	g	1
BD+09:3223	r-I	5350	-2.20	...	...	+0.16	+0.41	+0.42	ag	0
HD 149414	r-I	5175	-1.26	...	...	...	+0.06	+0.50	d	0
BPS BS 16080-0054	limited-r	4800	-3.00	-0.10	+0.62	+0.25	-0.76	-0.12	ae	0
2MASS J16393106-0522517	limited-r	4370	-2.07	-0.42	+0.26	+0.36	-0.26	-0.07	g	1

Table 2 continued

Table 2 (continued)

Name	RPA Class	$T_{\text{eff}}$	[Fe/H]	[C/Fe]	[C/Fe] <sub>c</sub>	[Sr/Fe]	[Ba/Fe]	[Eu/Fe]	Reference	RPA
		(K)								
2MASS J16455116-0429474	limited-r	4310	-2.15	-0.35	+0.36	+0.38	-0.37	-0.15	g	1
BPS CS 22878-0121	r-I	5450	-2.40	-0.50	-0.40	+0.17	-0.01	+0.49	p	0
SMSS J165023.82-252948.7	r-I	4833	-2.48	-0.45	+0.17	+0.22	+0.47	+0.56	c	0
RAVE J165300.5-005507	r-I	4480	-1.72	-0.36	+0.23	-0.39	-0.43	+0.68	o	0
2MASS J16592172-6827199	r-I	4621	-2.80	-0.60	-0.05	-0.30	-0.20	+0.40	i	1
2MASS J17043634-6219457	r-I	4882	-1.99	-0.10	+0.49	-0.16	-0.25	+0.55	i	1
2MASS J17060555+0412354	r-I	4653	-2.71	-0.10	+0.60	-0.57	+0.05	+0.50	i	1
2MASS J17093199-6027271	r-I	4547	-2.47	-0.45	+0.30	+0.28	-0.15	+0.60	a	1
2MASS J17124284-5211479	r-I	4750	-2.78	-0.42	+0.27	-0.03	-0.58	+0.48	a	1
2MASS J17131974-7113010	r-I	4819	-2.63	-0.20	+0.52	-0.10	0.00	+0.50	i	1
2MASS J17163340-7009028	r-II	4684	-2.39	-0.35	+0.32	-0.07	+0.05	+0.89	i	1
2MASS J17225742-7123000	r-II	5080	-2.42	-0.33	-0.32	+0.31	+0.70	+1.07	a	1
BD+17:3248	r-II	5200	-2.09	-0.47	-0.24	+0.29	+0.40	+0.91	aj	0
2MASS J17285930-7427532	limited-r	4900	-2.04	-0.42	-0.02	+0.74	-0.53	+0.23	a	1
2MASS J17360008-5145303	r-I	4882	-2.60	0.00	+0.19	-0.53	-0.15	+0.50	i	1
2MASS J17383643-5358288	r-I	4671	-2.30	-0.73	+0.05	-0.03	-0.01	+0.55	b	1
2MASS J17400682-6102129	r-I	4880	-2.24	-0.26	-0.03	+0.16	-0.31	+0.31	a	1
2MASS J17414840-5340354	r-I	4580	-2.19	-0.55	+0.13	+0.25	0.00	+0.63	b	1
2MASS J17435113-5359333	r-II	5080	-2.24	-0.35	+0.02	0.00	-0.07	+0.73	a	1
SMSS J175046.30-425506.9	r-II	4752	-2.17	-0.12	+0.31	+0.40	+0.85	+1.75	c	0
RAVE J175159.8-475131	r-I	4495	-2.02	-0.27	+0.37	+0.38	-0.14	+0.68	o	0
2MASS J17541561-5148268	r-I	4810	-2.14	-0.60	-0.11	-0.20	-0.05	+0.50	i	1
G 154-34	r-I	5599	-2.24	...	...	+0.28	-0.10	+0.50	z	0
SMSS J175738.37-454823.5	r-II	4617	-2.46	-0.43	+0.25	+0.21	-1.99	+1.02	c	0
2MASS J18024226-4404426	r-II	4701	-1.55	+0.35	+0.56	+0.68	+0.95	+1.05	a	1
2MASS J18050641-4907579	r-II	4430	-2.58	-0.70	+0.06	+0.10	+0.15	+0.73	b	1
2MASS J18121045-4934495	limited-r	4436	-3.02	-0.33	+0.41	+0.25	-0.50	-0.07	a	1
SMSS J181505.16-385514.9	r-II	4962	-3.29	+0.23	+0.23	-0.19	+0.04	+0.96	ak	0
2MASS J18174532-3353235	r-II	4500	-1.67	...	...	...	+0.49	+0.99	al	0
2MASS J18272347-5133001	r-I	4583	-1.86	-0.47	-0.02	+0.43	+0.18	+0.56	b	1
2MASS J18285086-3434203	r-I	4630	-2.46	-0.58	+0.14	+0.22	-0.29	+0.53	a	1
2MASS J18294122-4504000	r-I	4700	-2.48	-0.46	+0.19	+0.47	-0.06	+0.70	a	1
2MASS J18294359-4924253	r-II	4621	-1.22	-0.61	-0.22	-0.11	+0.29	+0.89	i	1
RAVE J183013.5-455510	r-I / CEMP-r	4765	-3.57	+1.90	+2.34	-0.56	+0.35	+0.69	am	1
SMSS J183128.71-341018.4	r-II	4940	-1.83	+0.01	+0.03	+0.97	+0.53	+1.25	an	0
SMSS J183225.29-334938.4	r-II	5293	-1.74	-0.22	-0.20	+0.26	+0.50	+1.08	an	0
2MASS J18332056-3802590	r-I	4756	-1.79	-0.38	+0.01	-0.10	-0.20	+0.30	i	1
2MASS J18362318-6428124	r-I	4896	-2.57	+0.10	+0.30	-0.63	+0.18	+0.57	a	1
2MASS J18363613-7136597	r-I	4650	-2.52	-0.75	+0.03	+0.01	-0.37	+0.56	a	1
SMSS J183647.89-274333.1	r-II	4649	-2.48	-0.47	+0.22	+0.18	+0.13	+0.82	ak	0
HD 175305	r-I	5100	-1.50	...	...	+0.13	+0.12	+0.44	ag	0
2MASS J18562774-7251331	r-I	4709	-2.26	-0.48	+0.24	0.00	-0.01	+0.32	a	1
HD 175606	limited-r	5920	-2.39	+0.09	+0.09	+0.25	-0.27	+0.14	e	0
2MASS J19014952-4844359	r-II	4820	-1.87	+0.02	+0.20	+0.37	-0.24	+0.93	a	1
2MASS J19050116-1949280	r-I	4687	-1.89	-0.43	+0.21	-0.01	-0.08	+0.36	g	1
SMSS J190911.03-213207.5	r-I	4626	-2.40	-0.56	+0.20	-0.04	+0.04	+0.43	c	0
2MASS J19092677-5140208	r-I	4729	-2.50	-0.40	+0.09	-0.04	+0.25	+0.60	i	1
SMSS J190931.13-214053.9	r-I	4500	-3.33	-0.35	+0.39	-0.72	+0.04	+0.66	c	0
HD 178443	r-I	5180	-2.07	-0.39	-0.03	+0.24	+0.35	+0.37	ao	0
HD 179626	r-I	5625	-1.26	...	...	...	-0.02	+0.47	d	0
2MASS J19161821-5544454	r-II	4450	-2.35	-0.80	-0.01	+0.48	-0.12	+1.08	a	1
2MASS J19192768-5959140	r-I	4549	-2.62	-0.60	+0.13	-0.05	+0.25	+0.60	i	1
2MASS J19202070-6627202	limited-r	4690	-2.10	-0.28	+0.09	+0.73	-0.11	+0.29	a	1
2MASS J19215077-4452545	r-II	4450	-2.56	-0.77	+0.01	-0.05	-0.31	+0.74	a	1
2MASS J19232518-5833410	r-II	5035	-2.08	+0.27	+0.28	+0.56	+0.11	+0.76	a	1
2MASS J19232941-4425432	r-I	4437	-2.06	-0.95	-0.20	+0.05	0.00	+0.38	b	1
RAVE J192632.8-584657	r-II	4355	-2.48	-0.22	+0.51	+0.38	-0.35	+0.76	o	0
RAVE J192819.9-633935	r-I / CEMP-r	4730	-2.38	+0.17	+0.74	...	+0.09	+0.45	o	0
2MASS J19291910-52528181	r-I	4594	-2.52	-0.59	+0.11	-0.56	+0.01	+0.56	i	1
BPS CS 22896-0055	r-I	5970	-2.52	+0.89	+1.03	+0.16	-0.24	+0.47	e	0
2MASS J19310426-3707397	r-I	4720	-2.21	-0.45	+0.05	-0.70	-0.40	+0.40	i	1
2MASS J19324858-5908019	r-II	4540	-1.93	-0.51	-0.38	+0.90	+0.65	+0.90	a	1
2MASS J19345326-3236567	r-I	4634	-2.17	-0.40	+0.26	+0.15	+0.07	+0.63	b	1
2MASS J19345497-5751400	limited-r	4580	-2.46	-0.70	-0.45	+0.25	-0.71	+0.17	a	1
SMSS J193617.38-790231.4	r-I	5260	-1.29	+0.33	+0.35	+0.05	-0.08	+0.42	c	0
BPS CS 22891-0209	limited-r	4620	-3.49	-0.65	+0.06	+0.41	-0.57	-0.13	e	0

Table 2 continued

Table 2 (continued)

Name	RPA Class	$T_{\text{eff}}$	[Fe/H]	[C/Fe]	[C/Fe] <sub>c</sub>	[Sr/Fe]	[Ba/Fe]	[Eu/Fe]	Reference	RPA
(K)										
BPS CS 22896-0154	r-II	5250	-2.69	+0.27	+0.28	+0.54	+0.51	+0.86	r	0
2MASS J19445483-4039459	r-I	4500	-1.98	-0.27	+0.33	+0.21	+0.13	+0.33	b	1
2MASS J19451414-1729269	r-I	4631	-2.63	-0.25	+0.41	+0.25	-0.03	+0.55	b	1
RAVE J194550.6-392631	r-II / CEMP-r	4650	-2.94	+0.17	+0.87	+0.20	+0.40	+0.90	o	0
2MASS J19494025-5424113	limited-r	4486	-2.81	-0.55	+0.20	-0.05	-1.01	-0.39	a	1
2MASS J19534978-5940001	limited-r	4614	-2.79	-0.44	+0.31	+0.25	-0.52	+0.04	a	1
2MASS J19552158-4613569	r-I	4756	-2.70	-0.25	+0.21	-0.25	-0.25	+0.37	i	1
2MASS J19563822-4054235	r-I	5395	-2.45	0.00	+0.53	+0.15	-0.20	+0.30	i	1
Gaia DR2 2233912206910720000	r-II	5070	-1.72	...	...	...	-0.15	+1.11	af	0
2MASS J19584033+0430396	r-I	4718	-1.82	...	...	+0.22	+0.02	+0.70	af	0
SMSS J195931.70-643529.3	r-II	4639	-2.58	-0.45	+0.25	+0.20	-0.01	+0.74	c	0
2MASS J19594558-2549075	limited-r	4540	-2.44	-0.70	+0.07	+0.10	-0.50	+0.04	a	1
2MASS J20000364-3301351	r-II	4474	-1.94	-0.85	-0.17	+0.20	+0.02	+0.90	b	1
2MASS J20005766-2541488	r-I	4731	-2.05	-0.05	+0.27	+0.60	+0.35	+0.40	b	1
2MASS J20050670-3057445	r-II	4624	-2.74	-0.30	+0.44	-0.16	+0.36	+0.86	g	1
2MASS J20080083-2759265	r-I	4481	-2.17	-0.75	+0.01	+0.25	0.00	+0.35	b	1
2MASS J20093393-3410273	r-II	4690	-1.99	-0.86	-0.47	+0.59	+0.23	+1.32	a	1
2MASS J20102782-0826556	r-I	4195	-2.02	-0.45	+0.23	+0.04	-0.39	+0.42	g	1
2MASS J20103193-3558546	r-I	4931	-2.56	-0.20	+0.52	+0.18	-0.03	+0.38	b	1
2MASS J20194310-3158163	r-I	4927	-2.19	-0.02	-0.01	+0.31	+0.16	+0.46	b	1
BPS CS 22943-0132	r-II	5850	-2.63	+0.69	+0.69	+0.27	-0.05	+0.86	e	0
2MASS J20233743-1659533	r-I	4635	-2.60	-0.57	-0.03	+0.23	-0.07	+0.50	b	1
2MASS J20303339-2519500	r-I	4315	-2.21	-0.65	+0.10	+0.41	-0.29	+0.41	a	1
2MASS J20362262-0714197	r-I / CEMP-r	4283	-2.41	+0.30	+0.88	+0.02	-0.57	+0.48	g	1
2MASS J20374042-5520500	r-I	4801	-2.98	0.00	+0.51	-0.10	-0.17	+0.40	i	1
2MASS J20384318-0023327	r-II	4630	-2.91	-0.44	+0.59	+0.54	+0.83	+1.64	ap	1
2MASS J20385893-0252115	r-I	4280	-2.16	-0.50	+0.22	+0.39	-0.26	+0.59	g	1
2MASS J20411424-4654315	r-II	4647	-2.30	-0.30	+0.32	+0.02	-0.02	+0.88	b	1
BPS CS 22955-0174	r-I	5520	-3.10	+0.05	+0.59	+0.40	-0.23	+0.34	e	0
2MASS J20435776-4408037	r-II	4410	-1.93	-0.70	0.00	+0.20	+0.15	+0.78	b	1
2MASS J20453454-1431151	r-I	4582	-2.84	-0.22	+0.51	+0.13	-0.12	+0.31	b	1
BPS CS 22879-0103	limited-r	5720	-2.16	+0.10	+0.48	+0.86	+0.06	+0.29	e	0
BPS CS 22879-0097	limited-r	5800	-2.45	+0.25	+0.26	+0.25	-0.40	+0.24	p	0
2MASS J20492765-5124440	r-I	4250	-2.47	-0.77	-0.02	+0.13	-0.25	+0.58	a	1
2MASS J20504869-3355289	r-I	4549	-2.64	-0.34	+0.38	+0.24	-0.06	+0.62	b	1
2MASS J20514971-6158008	r-I	5285	-1.87	+0.10	+0.11	+0.28	-0.18	+0.43	a	1
BPS CS 22940-0121	r-I	5400	-2.91	+0.01	+0.04	+0.36	+0.21	+0.61	p	0
2MASS J20554594-3155159	r-I	4581	-2.67	-0.45	+0.30	+0.02	-0.05	+0.67	b	1
2MASS J20560913-1331176	limited-r	4780	-2.30	0.00	+0.42	+0.13	-0.56	0.00	a	1
2MASS J20584918-0354340	r-I	4831	-2.36	0.00	+0.40	-0.24	-0.09	+0.36	g	1
2MASS J21003824-0539171	r-I	4872	-2.28	-0.15	+0.50	+0.20	-0.13	+0.38	b	1
BPS CS 22897-0008	limited-r	4550	-3.83	+0.50	+1.22	+0.56	-1.27	-0.13	e	0
2MASS J21055865-4919336	r-I	4633	-2.27	-0.50	+0.13	-0.05	+0.12	+0.67	b	1
2MASS J21063474-4957500	r-I	5238	-2.91	+0.52	+0.53	-0.48	-0.20	+0.54	a	1
2MASS J21064294-6828266	r-II	5186	-2.76	+0.53	+0.54	+0.90	+0.52	+1.32	a	1
2MASS J21091825-1310062	r-II	4855	-2.40	-0.28	+0.27	+0.14	+0.12	+1.25	a	1
2MASS J21095804-0945400	r-II	4492	-2.73	-0.45	+0.30	+0.60	-0.12	+0.77	a	1
BPS CS 22937-0072	limited-r	5500	-2.72	-0.05	+0.16	+0.30	-0.41	-0.19	e	0
2MASS J21162185-0213420	r-I	4248	-2.58	-0.95	-0.17	-0.41	-0.31	+0.60	g	1
2MASS J21220020-0820333	r-I	4720	-3.42	-0.30	+0.09	-0.19	+0.20	+0.40	i	1
2MASS J21224590-4641030	r-II	4652	-2.96	-0.18	+0.32	+0.25	+0.01	+0.90	a	1
2MASS J21262525-2144243	r-I	4450	-2.81	-0.88	-0.14	+0.37	-0.02	+0.58	a	1
BD-03:5215	r-I	5700	-1.20	...	...	...	+0.46	+0.56	ag	0
2MASS J21370807-0927347	limited-r	4470	-2.46	-0.50	+0.25	+0.63	-0.61	+0.11	a	1
HE 2134+0001	r-I	5257	-2.22	+0.20	+0.21	-0.08	-0.42	+0.47	f	0
BPS CS 22944-0039	limited-r	5350	-2.43	-0.47	+0.03	+0.46	-0.12	+0.21	p	0
2MASS J21462219-0512324	r-I	4723	-1.72	-0.47	+0.09	+0.21	+0.33	+0.45	b	1
G 214-1	r-I	5370	-2.29	-0.12	-0.12	+0.46	+0.27	+0.56	e	0
BPS CS 22951-0059	r-I	5120	-2.84	+0.17	+0.18	+0.12	-0.73	+0.33	e	0
RAVE J215118.3-135937	r-I	4830	-2.10	+0.34	+0.69	+0.56	-0.85	+0.37	o	0
BPS CS 29493-0062	r-I	5520	-2.76	+0.10	+0.10	+0.18	-0.51	+0.31	e	0
BPS CS 22965-0016	limited-r	4770	-3.13	-0.68	-0.16	+0.32	-0.88	-0.24	e	0
HE 2155+0136	r-I	5331	-2.07	0.00	0.00	-0.13	+0.13	+0.68	f	0
HE 2154-2838	r-I	5303	-1.85	+0.05	+0.05	+0.03	-0.03	+0.45	f	0
HE 2159-0551	limited-r	4800	-2.81	-0.24	+0.20	+0.16	-1.58	-0.20	j	0
BPS BS 17569-0049	r-II	4700	-2.88	-0.22	+0.44	+0.31	+0.20	+0.72	r	0

Table 2 continued



Table 2 (continued)

Name	RPA Class	$T_{\text{eff}}$	[Fe/H]	[C/Fe]	[C/Fe] <sub>c</sub>	[Sr/Fe]	[Ba/Fe]	[Eu/Fe]	Reference	RPA
		(K)								
HE 2206-2245	$r$ -I	5100	-2.73	+0.21	+0.22	-0.05	-0.11	+0.62	f	0
BPS CS 22886-0012	$r$ -II	5650	-2.88	-0.16	-0.16	+0.31	+0.14	+0.85	e	0
SMSS J221448.33-453949.9	$r$ -II	4522	-2.56	-0.67	+0.05	+0.17	+0.57	+0.94	c	0
2MASS J22161170-5319492	$r$ -I	5112	-2.51	-0.15	+0.31	+0.20	+0.31	+0.59	b	1
2MASS J22163596+0246171	$r$ -I	4900	-2.37	-0.10	0.00	+0.17	-0.27	+0.45	a	1
BPS CS 22892-0052	$r$ -II / CEMP- $r$	4800	-3.10	+0.88	+1.26	+0.93	+1.23	+1.64	aq	0
2MASS J22182082-3827554	$r$ -II	5089	-2.57	+0.30	+0.31	+0.08	+0.50	+1.10	i	1
2MASS J22190836-2333467	$r$ -II	4743	-2.56	-0.13	+0.39	+0.27	+0.24	+0.87	b	1
HE 2216-1548	$r$ -I	5154	-1.70	-0.38	-0.10	+0.05	+0.29	+0.58	f	0
2MASS J22220344-8024592	$r$ -I / CEMP- $r$	4684	-2.50	+0.20	+0.83	-0.80	-0.30	+0.37	i	1
BPS CS 22886-0043	$r$ -II	6000	-2.16	+0.46	+0.66	+0.74	+0.35	+0.81	p	0
BPS CS 22960-0064	$r$ -I	5060	-2.77	+0.14	+0.15	+0.25	-0.20	+0.35	e	0
BPS CS 22956-0114	limited- $r$	4900	-3.19	-1.05	-0.88	-0.07	-0.65	-0.12	e	0
HE 2224+0143	$r$ -II	5198	-2.58	+0.35	+0.36	+0.23	+0.59	+1.05	f	0
BPS CS 22875-0029	$r$ -II	5990	-2.71	+0.96	+1.08	+0.85	+0.30	+0.92	e	0
2MASS J22302641-1949527	$r$ -I	4657	-2.28	-0.20	+0.48	-0.28	-0.10	+0.40	i	1
BPS CS 29491-0069	$r$ -II	5300	-2.51	+0.23	+0.24	+0.15	+0.24	+0.96	y	0
HE 2229-4153	$r$ -I	5156	-2.62	+0.53	+0.54	+0.28	-0.19	+0.39	l	0
2MASS J22345447-6605172	$r$ -I	4873	-2.49	-0.30	+0.31	-0.03	-0.20	+0.40	i	1
BPS CS 29491-0053	limited- $r$	4700	-3.04	-0.28	+0.32	-0.24	-0.89	-0.42	r	0
2MASS J22373316-4341181	$r$ -I	4707	-2.51	-0.21	+0.06	+0.14	-0.06	+0.40	b	1
2MASS J22394827-0803536	$r$ -I	4540	-2.79	-0.90	-0.36	+0.04	-0.10	+0.60	i	1
HE 2242-1930	$r$ -I	5281	-2.21	+0.09	+0.10	-0.04	-0.10	+0.56	f	0
HE 2244-1503	$r$ -II	5122	-2.88	+0.15	+0.16	-0.20	+0.45	+0.95	f	0
2MASS J22492756-2238289	$r$ -I	4930	-1.82	-0.08	+0.12	+0.39	-0.43	+0.48	a	1
HE 2252-4225	$r$ -II	4710	-2.63	-0.61	-0.29	-0.13	+0.29	+0.81	ar	0
HE 2252-4157	$r$ -II	5090	-1.93	-0.15	-0.14	-0.20	+0.45	+0.95	f	0
2MASS J22562536-0719562	$r$ -II	4558	-2.26	-0.50	+0.18	+0.08	+0.26	+1.10	g	1
2MASS J23022289-6833233	$r$ -I	5063	-2.64	+0.30	+0.31	+0.15	-0.29	+0.61	a	1
HE 2301-4024	$r$ -II	5743	-2.11	+0.30	+0.30	0.00	+0.49	+0.98	f	0
2MASS J23060975-6107368	$r$ -I	4669	-2.32	-0.36	+0.25	+0.09	-0.14	+0.31	b	1
2MASS J23100319-7702165	$r$ -I	4756	-1.81	-0.10	+0.39	-0.23	-0.10	+0.65	i	1
BPS CS 29513-0003	$r$ -I	5480	-2.47	-0.05	+0.06	+0.24	-0.08	+0.49	e	0
BPS CS 22888-0047	$r$ -II	5950	-2.54	+0.90	+1.00	+0.60	+0.04	+0.86	e	0
BPS CS 22945-0017	$r$ -II / CEMP- $r$	6080	-2.89	+1.78	+1.78	+0.39	+0.49	+1.13	e	0
2MASS J23242766-2728055	$r$ -I	4743	-2.40	+0.07	+0.49	+0.27	+0.32	+0.55	b	1
2MASS J23251897-0815539	$r$ -I	4995	-2.30	-0.70	-0.24	-0.42	-0.33	+0.55	g	1
2MASS J23265258-0159248	$r$ -I	4360	-3.13	-0.63	+0.12	+0.07	+0.31	+0.69	a	1
2MASS J23285061-0432368	$r$ -I	4792	-1.99	+0.05	+0.41	-0.10	0.00	+0.53	b	1
HD 221170	$r$ -II	4510	-2.18	-0.71	+0.04	+0.02	+0.26	+0.80	as	0
HE 2327-5642	$r$ -II	5050	-2.78	+0.13	+0.14	-0.15	+0.31	+0.98	ar	0
BPS CS 22941-0017	$r$ -I	5070	-3.11	+0.14	+0.15	-0.05	-0.49	+0.36	e	0
2MASS J23342332-2748003	$r$ -II	4617	-2.46	-0.24	+0.48	+0.39	-0.06	+0.71	b	1
BPS CS 30315-0029	$r$ -I / CEMP- $r$	4570	-3.40	+0.06	+0.81	-0.32	+0.17	+0.68	l	0
2MASS J23362202-5607498	$r$ -II	4630	-2.06	-0.05	+0.47	+1.00	+0.24	+1.14	a	1
BPS CS 22952-0015	$r$ -I	4850	-3.26	...	...	-0.87	-1.45	+0.39	at	0
BPS CS 29499-0003	$r$ -I	6080	-2.51	+0.10	+0.10	+0.17	-0.33	+0.63	e	0
2MASS J23411581-6406440	$r$ -I	4824	-2.78	-0.45	+0.27	-0.16	-0.10	+0.35	i	1
2MASS J23425814-4327352	$r$ -I	4867	-2.17	-0.24	-0.18	+0.19	-0.01	+0.36	b	1
HD 222925	$r$ -II	5636	-1.47	-0.20	-0.18	+0.58	+0.55	+1.33	au	0
2MASS J23475942-5701184	$r$ -I	4668	-2.24	-0.55	+0.20	-0.08	-0.07	+0.45	b	1
BPS CS 22966-0057	$r$ -I	5300	-2.62	+0.06	+0.07	-0.10	-0.24	+0.41	r	0
2MASS J23490902-2447176	$r$ -I	5248	-2.20	+0.17	+0.18	-0.03	-0.16	+0.65	b	1
HE 2347-1334	limited- $r$	4453	-2.55	-0.50	+0.25	-0.22	-0.79	-0.26	f	0
BPS CS 29499-0058	$r$ -I	6060	-2.81	+0.39	+0.39	+0.07	-0.50	+0.44	e	0
BPS CS 22945-0058	$r$ -II	5990	-2.98	+0.68	+0.68	+0.35	+0.29	+1.14	e	0
BPS CS 22945-0056	$r$ -I	6000	-2.82	+1.60	+1.75	-0.09	-0.40	+0.68	e	0
BPS CS 29517-0025	$r$ -I / CEMP- $r$	5300	-2.57	+0.14	+0.73	...	-0.21	+0.55	av	0
SDSS J235718.91-005247.8	$r$ -II	5000	-3.36	+0.43	+0.43	+0.78	+1.12	+1.92	aw	0

Table 2 continued

Table 2 (continued)

Name	RPA Class	$T_{\text{eff}}$	[Fe/H]	[C/Fe]	[C/Fe] <sub>c</sub>	[Sr/Fe]	[Ba/Fe]	[Eu/Fe]	Reference	RPA
(K)										

NOTE—Sources for chemical-abundance information:

NOTE—<sup>a</sup> Hansen et al. (2018), <sup>b</sup> Holmbeck et al. (2020), <sup>c</sup> Jacobson et al. (2015), <sup>d</sup> Fulbright (2000), <sup>e</sup> Roederer et al. (2014), <sup>f</sup> Barklem et al. (2005), <sup>g</sup> Sakari et al. (2018), <sup>h</sup> Allen et al. (2012), <sup>i</sup> Ezzeddine et al. (2020), <sup>j</sup> Hansen et al. (2015), <sup>k</sup> Christlieb et al. (2004), <sup>l</sup> Siqueira Mello et al. (2014), <sup>m</sup> Hansen et al. (2012), <sup>n</sup> Lai et al. (2008), <sup>o</sup> Rasmussen et al. (2020), <sup>p</sup> Preston et al. (2006), <sup>q</sup> Hollek et al. (2011), <sup>r</sup> Cayrel et al. (2004), <sup>s</sup> Cain et al. (2018), <sup>t</sup> Holmbeck et al. (2018), <sup>u</sup> Mardini et al. (2019), <sup>v</sup> Li et al. (2015), <sup>w</sup> Xing et al. (2019), <sup>x</sup> Valentini et al. (2019), <sup>y</sup> Hayek, W. et al. (2009), <sup>z</sup> Ishigaki et al. (2013), <sup>aa</sup> Johnson & Bolte (2002), <sup>ab</sup> Cohen et al. (2013), <sup>ac</sup> Westin et al. (2000), <sup>ad</sup> Roederer et al. (2010), <sup>ae</sup> Aoki et al. (2005), <sup>af</sup> Hawkins & Wyse (2018), <sup>ag</sup> Burris et al. (2000), <sup>ah</sup> Honda et al. (2004), <sup>ai</sup> Cain et al. (2020), <sup>aj</sup> Cowan et al. (2002), <sup>ak</sup> Howes et al. (2015), <sup>al</sup> Johnson et al. (2013), <sup>am</sup> Placco et al. (2020), <sup>an</sup> Howes et al. (2016), <sup>ao</sup> McWilliam et al. (1995), <sup>ap</sup> Placco et al. (2017), <sup>aq</sup> Sneden et al. (2003), <sup>ar</sup> Mashonkina et al. (2014), <sup>as</sup> Ivans et al. (2006), <sup>at</sup> Ryan et al. (1996), <sup>au</sup> Roederer et al. (2018b), <sup>av</sup> Masseron et al. (2012), <sup>aw</sup> Aoki et al. (2010)

NOTE—The code in the column RPA indicates if the reported information is drawn from papers from the RPA (1) or other sources (0).

Table 3. Derived Dynamical Parameters for the RPE Sample

Name	Energy	Ecc	$J_r$	$J_\phi$	$J_z$	$r_{\text{peri}}$	$r_{\text{apo}}$	$Z_{\text{max}}$
	$\times 10^5$		$\times 10^3$	$\times 10^3$	$\times 10^3$			
	( $\text{km}^2 \text{s}^{-2}$ )		( $\text{kpc km s}^{-1}$ )	( $\text{kpc km s}^{-1}$ )	( $\text{kpc km s}^{-1}$ )	(kpc)	(kpc)	(kpc)
2MASS J00002259-1302275*	-1.50	0.79	0.74	+0.57	0.34	1.68	14.46	9.65
2MASS J00002416-1107454*	-1.39	0.73	0.85	-0.87	0.46	2.85	18.29	12.07
HD 224930	-1.68	0.25	0.07	+1.41	0.01	4.86	8.13	0.42
2MASS J00021668-2453494*	-1.42	0.40	0.25	+0.92	1.07	6.18	14.51	12.61
BPS CS 22957-0036	-1.72	0.84	0.58	-0.32	0.10	0.82	9.44	4.26
HD 20	-1.57	0.98	1.15	+0.06	0.01	0.15	13.44	5.68
2MASS J00073817-0345509*	-1.71	0.86	0.75	+0.04	0.10	0.73	10.08	3.45
2MASS J00093394-1857008	-1.74	0.64	0.37	-0.74	0.04	1.96	8.96	1.37
2MASS J00101758-1735387	-1.54	0.04	0.00	+0.68	1.14	7.97	8.64	7.95
2MASS J00154806-6253207	-1.69	0.85	0.52	-0.16	0.40	0.79	9.53	8.25
2MASS J00172430-3333151	-1.58	0.43	0.23	+1.31	0.12	4.28	10.83	3.32
2MASS J00182832-3900338	-1.19	0.53	0.74	+0.80	1.93	7.74	25.26	24.08
BPS CS 22882-0001	-1.32	0.45	0.39	-1.21	1.13	6.99	18.52	15.55
2MASS J00223225-4839449	-1.31	0.63	0.79	-1.53	0.34	4.69	20.70	10.91
BPS CS 29497-0004*	-1.45	0.56	0.49	+1.29	0.25	4.15	14.90	6.90
2MASS J00400685-4325183	-1.59	0.57	0.31	-0.69	0.50	3.07	10.99	8.20
2MASS J00405260-5122491	-1.82	0.93	0.59	+0.14	0.03	0.31	8.32	4.01
2MASS J00413026-4058547	-1.20	0.50	0.63	+0.71	2.06	8.09	24.11	23.24
2MASS J00442897-1017497	-1.70	0.79	0.47	-0.30	0.31	1.10	9.33	6.78
2MASS J00452379-2112161	-1.68	0.48	0.21	+0.94	0.17	3.19	9.02	3.78
2MASS J00452879-5846450	-1.24	0.96	1.78	+0.20	0.36	0.53	25.43	20.46
2MASS J00453930-7457294	-1.34	0.51	0.48	+0.17	1.88	5.83	18.08	17.99
HE 0045-2430	-1.25	0.86	1.68	-0.73	0.17	1.86	24.65	13.72
2MASS J00482431-1041309	-1.59	0.93	0.93	+0.23	0.08	0.49	12.79	5.14
2MASS J00512646-1053170	-1.60	0.63	0.41	+0.80	0.22	2.54	11.22	5.41
2MASS J00524174-0902235	-1.29	0.76	1.16	+0.95	0.41	2.96	22.19	14.75
2MASS J00532781-0253169*	-1.56	0.19	0.05	-1.46	0.27	6.55	9.45	4.59
2MASS J00541965-0611555*	-1.63	0.75	0.48	-0.12	0.68	1.54	10.58	10.09
HE 0057-4541*	-1.21	0.71	1.24	-1.29	0.65	4.47	26.51	18.70
BPS CS 22953-0003	-1.41	0.79	0.91	-0.72	0.39	2.04	17.78	11.08
BPS CS 22183-0031	-1.63	0.93	0.91	-0.11	0.08	0.46	11.88	4.64
2MASS J01165010-6307441	-1.74	0.91	0.70	-0.22	0.03	0.47	9.70	4.27
2MASS J01202234-5425582	-1.62	0.66	0.50	+0.89	0.04	2.27	11.26	1.83
2MASS J01213447-2528002	-1.56	0.33	0.13	-1.33	0.30	5.42	10.58	5.45
2MASS J01293113-1600454	-1.49	0.26	0.09	-0.91	1.01	6.81	11.52	9.97
2MASS J01311599-4016510	-1.63	0.87	0.62	-0.15	0.42	0.75	10.83	9.48
2MASS J01321981-3040512	-1.71	0.58	0.28	+0.59	0.31	2.35	8.86	5.87
2MASS J01371888-1729037	-1.46	0.82	0.83	-0.20	0.69	1.59	15.67	14.70
2MASS J01373857-2618131	-1.66	0.55	0.28	+0.83	0.24	2.86	9.73	4.91
2MASS J01425422-5032488	-1.68	0.39	0.17	-1.27	0.01	3.94	8.98	0.82
2MASS J01425445-0904162	-1.69	0.58	0.34	+0.93	0.04	2.57	9.62	1.59
2MASS J01493760-4551222	-1.56	0.98	1.07	-0.04	0.10	0.14	13.24	6.16
2MASS J01530024-3417360	-1.65	0.97	0.95	-0.08	0.01	0.18	11.40	5.08
2MASS J01553180-4919420	-1.21	0.70	1.23	+1.76	0.15	4.56	25.98	8.78

Table 3 continued

Table 3 (continued)

Name	Energy	Ecc	$J_r$	$J_\phi$	$J_z$	$r_{\text{peri}}$	$r_{\text{apo}}$	$Z_{\text{max}}$
	$\times 10^5$		$\times 10^3$	$\times 10^3$	$\times 10^3$			
	( $\text{km}^2 \text{s}^{-2}$ )		( $\text{kpc km s}^{-1}$ )	( $\text{kpc km s}^{-1}$ )	( $\text{kpc km s}^{-1}$ )	(kpc)	(kpc)	(kpc)
2MASS J01555066-6400155	-1.64	0.22	0.05	-1.29	0.20	5.39	8.38	3.57
2MASS J01565634-1402108*	-1.49	0.95	1.14	+0.11	0.16	0.40	15.28	6.71
BPS CS 22958-0037	-1.01	0.74	2.06	+1.85	0.77	5.97	40.91	27.99
2MASS J02031860-7930291*	-1.56	0.27	0.08	+1.32	0.36	5.82	10.11	5.71
2MASS J02070641-5009166	-1.46	0.58	0.49	+1.27	0.23	3.92	14.69	6.22
BPS CS 22958-0052	-1.67	0.66	0.46	+0.83	0.03	2.11	10.38	1.35
2MASS J02165716-7547064	-1.34	0.48	0.44	+1.93	0.28	6.39	18.01	7.91
2MASS J02230804-3129531	-1.64	0.62	0.39	+0.80	0.18	2.47	10.52	4.59
2MASS J02265832-0749596	-1.69	0.44	0.18	+1.03	0.12	3.42	8.77	2.91
2MASS J02274104-0519230*	-1.21	0.64	0.98	+0.44	1.78	5.67	25.45	24.84
2MASS J02355867-6745520	-1.77	0.73	0.38	+0.50	0.12	1.34	8.49	3.40
2MASS J02413897-0427349	-1.38	0.68	0.83	-1.39	0.08	3.52	18.29	3.86
2MASS J02462013-1518419*	-1.12	0.76	1.71	-1.85	0.14	4.42	32.09	9.50
SMSS J024858.41-684306.4	-0.68	0.87	5.82	+2.85	0.34	6.32	92.45	40.60
2MASS J02500719-5145148	-1.27	0.32	0.23	+0.62	2.23	9.67	18.89	18.41
2MASS J02515281-3717316	-1.72	0.70	0.45	+0.57	0.09	1.65	9.45	2.91
2MASS J02570028-3024374	-1.79	0.80	0.51	+0.39	0.02	0.93	8.50	1.16
BPS CS 31078-0018	-1.65	0.55	0.34	+1.09	0.03	3.01	10.29	1.35
HE 0300-0751*	-0.55	0.74	9.25	-6.02	1.48	18.03	193.43	117.46
2MASS J03071478-0534554*	-1.59	0.88	0.74	+0.23	0.33	0.77	12.10	9.31
2MASS J03073894-0502491	-1.28	0.60	0.73	+1.37	0.71	5.37	21.41	15.28
2MASS J03084611-4747083*	-1.22	0.87	1.59	-0.57	0.64	1.92	26.24	21.17
2MASS J03133726-1020553	-1.49	0.81	0.94	-0.65	0.07	1.55	15.15	3.82
2MASS J03154102-7626329	-1.38	0.61	0.61	+0.61	1.03	4.17	17.37	15.84
BPS CS 22968-0026	-1.59	0.98	0.99	-0.04	0.11	0.14	12.89	5.58
2MASS J03210882-3944213	-1.60	0.49	0.28	-1.14	0.14	3.66	10.72	3.80
2MASS J03270229+0132322	-1.27	0.37	0.32	+1.28	1.50	8.98	19.75	17.39
BPS CS 29526-0110	-1.59	0.38	0.14	-0.89	0.55	4.52	9.99	7.39
HE 0328-1047	-1.45	0.54	0.46	-1.46	0.15	4.44	14.82	5.21
HE 0337-5127*	-1.57	0.45	0.22	+0.96	0.48	4.18	11.04	7.44
2MASS J03422816-6500355	-1.78	0.64	0.36	+0.69	0.02	1.82	8.36	0.84
SMSS J034249.53-284216.0*	-1.39	0.60	0.58	+1.29	0.39	4.27	17.05	10.27
HE 0341-4024	-1.74	0.94	0.76	-0.14	0.01	0.30	9.77	4.51
2MASS J03434624-0924169	-1.37	0.88	1.36	+0.58	0.08	1.25	19.39	5.40
BPS CS 29529-0054	-1.76	0.83	0.57	+0.32	0.05	0.85	9.03	3.59
2MASS J04012191-2635058	-1.67	0.95	0.78	-0.13	0.11	0.29	10.99	4.90
RAVE J040618.2-030525	-1.27	0.98	1.85	-0.07	0.11	0.22	24.35	11.99
2MASS J04121388-1205050*	-1.58	0.69	0.51	+0.68	0.28	2.20	11.90	6.85
BPS CS 22186-0005	-1.53	0.88	0.81	+0.14	0.51	0.84	13.56	12.13
BPS CS 22186-0002	-1.53	0.74	0.70	-0.85	0.06	2.07	13.60	3.01
2MASS J04182158-2323391	-1.69	0.94	0.83	+0.14	0.03	0.31	10.69	4.76
2MASS J04192966-0517491	-1.61	0.89	0.82	-0.30	0.10	0.71	11.99	5.02
BPS CS 22182-0033	-1.61	0.70	0.53	-0.78	0.10	2.07	11.55	3.59
HE 0420+0123a	-1.68	0.68	0.40	+0.52	0.27	1.83	9.64	5.94
BPS CS 22186-0025*	-1.16	0.74	1.45	+1.62	0.33	4.26	29.08	14.96
2MASS J04245677-6500173	-1.68	0.70	0.44	+0.62	0.16	1.78	9.97	4.21
2MASS J04263084-4058516	-1.64	0.66	0.43	+0.76	0.14	2.19	10.53	4.00
HE 0430-4901	-1.67	0.68	0.44	+0.71	0.11	1.96	10.15	3.49
2MASS J04315411-0632100	-1.62	0.26	0.07	-1.18	0.31	5.23	8.93	4.90
HE 0432-0923*	-1.37	0.51	0.45	+1.63	0.35	5.58	17.01	8.65
HE 0442-1234*	-1.32	0.19	0.07	-2.69	0.20	10.80	15.75	5.31
BPS CS 22191-0029	-1.31	0.16	0.05	+0.88	2.00	11.31	15.51	14.73
2MASS J04520910-6209121	-1.71	0.71	0.38	-0.34	0.40	1.51	9.02	7.21
2MASS J04530168-2437144	-0.74	0.72	3.88	-3.86	1.09	11.74	80.74	50.03
2MASS J04565146-3115427	-1.71	0.91	0.67	-0.17	0.13	0.44	9.74	4.91
2MASS J05030025-7601462	-1.60	0.66	0.39	-0.11	0.96	2.34	11.08	10.90
SMSS J051008.62-372019.8	-1.59	0.30	0.09	-0.84	0.68	5.14	9.54	7.63
HE 0512-3835*	-1.36	0.87	1.24	-0.49	0.36	1.45	19.86	13.44
HE 0516-3820	-1.66	0.54	0.31	+1.03	0.06	2.96	9.89	2.18
2MASS J05241392-0336543*	-1.23	0.39	0.36	+2.53	0.46	9.36	21.42	10.94
HE 0524-2055*	-1.35	0.65	0.79	+1.44	0.17	4.02	18.89	6.85
2MASS J05311779-5810048	-1.69	0.70	0.46	+0.69	0.06	1.80	10.02	2.35
HE 0534-4615	-1.52	0.84	0.97	+0.52	0.04	1.25	14.44	3.91
2MASS J05381700-7516207	-1.69	0.43	0.19	+1.11	0.06	3.48	8.77	1.95

Table 3 continued

Table 3 (continued)

Name	Energy	Ecc	$J_r$	$J_\phi$	$J_z$	$r_{\text{peri}}$	$r_{\text{apo}}$	$Z_{\text{max}}$
	$\times 10^5$		$\times 10^3$	$\times 10^3$	$\times 10^3$			
	( $\text{km}^2 \text{s}^{-2}$ )		( $\text{kpc km s}^{-1}$ )	( $\text{kpc km s}^{-1}$ )	( $\text{kpc km s}^{-1}$ )	(kpc)	(kpc)	(kpc)
2MASS J05383296-5904280	-1.68	0.47	0.20	+0.86	0.26	3.23	9.04	4.81
HE 0538-4515	-1.63	0.24	0.07	+1.49	0.05	5.33	8.77	1.73
2MASS J05521578-3953184	-1.68	0.62	0.40	+0.88	0.03	2.32	10.00	1.44
2MASS J05564771-6639054	-1.65	0.91	0.86	+0.27	0.01	0.55	11.49	4.30
2MASS J06090353-7122260	-1.69	0.58	0.26	-0.35	0.60	2.32	8.82	7.86
2MASS J06195001-5312114	-1.61	0.26	0.07	+1.27	0.27	5.35	9.21	4.56
SMSS J062609.83-590503.2	-1.17	0.54	0.77	+2.76	0.15	7.97	26.40	7.50
2MASS J06290787-6709523	-1.60	0.27	0.08	+1.26	0.30	5.37	9.42	4.96
2MASS J06320130-2026538	-1.65	0.37	0.14	+1.28	0.07	4.20	9.16	1.98
2MASS J06332771-3519240	-1.53	0.78	0.83	-0.78	0.00	1.73	14.09	0.46
SMSS J063447.15-622355.0*	-0.54	0.89	8.58	+3.75	0.30	7.94	137.86	50.36
2MASS J06392518-7414056	-1.78	0.54	0.25	+0.84	0.02	2.38	7.94	0.90
2MASS J06401317-3540444	-1.73	0.90	0.61	+0.13	0.19	0.51	9.22	6.20
2MASS J07052028-3343242	-1.34	0.99	1.85	-0.04	0.01	0.13	21.21	7.17
2MASS J07150266-0154092	-1.42	0.12	0.02	+2.46	0.00	9.51	12.00	0.36
2MASS J07161594-5135248	-1.77	0.80	0.47	-0.41	0.08	1.00	8.82	3.49
2MASS J07202253-3358518	-0.84	0.78	3.24	-0.05	3.25	7.27	60.38	60.36
2MASS J07250021-7022038	-1.68	0.73	0.52	-0.63	0.06	1.60	10.32	1.82
2MASS J07352232-4425010	-1.60	0.98	1.04	-0.06	0.03	0.13	12.58	5.48
2MASS J07393021-5548171	-1.69	0.84	0.60	-0.35	0.13	0.89	10.04	4.57
BD-01:1792	-1.69	0.96	0.81	+0.10	0.04	0.22	10.56	4.86
2MASS J07411443-4339360	-1.22	0.69	1.07	-1.68	0.33	4.66	25.06	13.40
RAVE J074824.3-483141	-1.49	0.97	1.18	-0.09	0.12	0.23	15.20	6.59
2MASS J07501424-4123454	-1.37	0.91	1.49	-0.46	0.01	0.90	19.69	1.38
2MASS J08015897-5752032	-1.35	0.77	1.07	+1.14	0.07	2.61	19.84	3.81
2MASS J08032084-5856521	-1.74	0.45	0.19	+1.03	0.03	3.14	8.23	1.16
2MASS J08134364-2332528	-1.66	0.47	0.21	+0.98	0.20	3.39	9.48	4.22
2MASS J08155667-2204105	-1.64	0.70	0.37	-0.18	0.76	1.79	10.35	9.86
2MASS J08393460-2122069	-1.63	0.90	0.77	-0.24	0.13	0.57	11.35	5.30
2MASS J08580584-0809174	-1.48	0.36	0.20	+1.74	0.15	6.01	12.78	4.23
2MASS J08594093-1415151	-1.49	0.90	1.01	-0.32	0.19	0.80	15.07	7.16
2MASS J09185890-2311511	-0.97	0.83	2.83	+1.86	0.13	4.08	45.66	18.36
2MASS J09255655-3450373	-1.65	0.83	0.72	-0.43	0.04	1.01	11.12	4.06
2MASS J09261133-1526232	-1.35	0.92	1.60	-0.42	0.01	0.81	20.56	0.87
2MASS J09284944-0738585	-1.63	0.42	0.20	+1.33	0.02	4.04	9.85	1.05
2MASS J09364069-2038386	-1.61	0.57	0.38	-1.12	0.03	3.04	11.00	1.46
2MASS J09463483-0626532*	-1.50	0.91	0.90	+0.14	0.47	0.71	14.44	12.75
2MASS J09544277+5246414	-1.29	0.41	0.36	-2.09	0.53	8.06	19.45	11.26
2MASS J09574607-3923072	-1.69	0.51	0.25	+1.01	0.05	2.98	9.16	1.83
2MASS J09580181-1446137	-1.43	0.54	0.41	-0.02	1.65	4.57	15.23	15.21
2MASS J10025125-4331098	-1.73	0.90	0.61	-0.14	0.18	0.51	9.16	5.66
2MASS J10044858-2706500*	-1.68	0.75	0.46	-0.11	0.61	1.33	9.46	9.19
2MASS J10063414-7030212	-1.71	0.45	0.18	+0.91	0.18	3.21	8.50	3.74
2MASS J10082492-2314124	-1.63	0.46	0.24	+1.27	0.02	3.72	10.09	1.16
BPS BS 15621-0047	-1.55	0.24	0.07	+1.76	0.04	6.26	10.14	1.65
2MASS J10121964-3221347	-1.47	0.93	1.30	-0.19	0.04	0.55	16.07	5.47
2MASS J10191573-1924464	-1.66	0.34	0.13	+1.34	0.04	4.41	9.00	1.48
2MASS J10194932-4900584	-1.42	0.99	1.59	+0.01	0.00	0.11	18.01	6.71
2MASS J10223779-3400209	-1.79	0.80	0.50	-0.40	0.02	0.94	8.57	0.94
2MASS J10302845-7543299	-1.78	0.90	0.62	-0.22	0.03	0.48	8.88	3.97
2MASS J10345348-1117221	-1.71	0.83	0.62	+0.39	0.05	0.93	9.94	3.89
2MASS J10362687-3746174	-1.74	0.79	0.55	+0.47	0.02	1.11	9.32	1.36
2MASS J10401894-4106124	-1.36	0.32	0.19	+1.71	0.69	8.00	15.68	10.65
HE 1044-2509*	-1.48	0.18	0.04	-1.64	0.41	7.74	11.07	6.25
2MASS J10492192-1154173	-1.80	0.94	0.66	+0.11	0.02	0.26	8.70	4.23
2MASS J10513692-2115466	-1.72	0.62	0.35	+0.74	0.08	2.11	9.09	2.81
SMSS J105320.99-435300.1	-0.08	0.99	84.85	+3.92	0.02	7.28	2056.99	156.47
J1054+0528*	-1.62	0.48	0.26	+1.13	0.13	3.60	10.30	3.33
2MASS J10550658+1931580*	-1.49	0.57	0.40	+0.99	0.48	3.75	13.68	9.23
2MASS J10594136-2052253	-1.71	0.83	0.55	+0.30	0.20	0.91	9.50	5.76
2MASS J11014865-3749526	-1.62	0.74	0.61	-0.71	0.04	1.72	11.51	1.71
LAMOST J110901+075441*	-1.24	0.94	2.05	+0.04	0.20	0.80	25.57	14.32
2MASS J11165400-7250160	-1.77	0.79	0.39	+0.17	0.38	0.95	7.91	6.93
LAMOST J112456.61+453531.*	-1.39	0.40	0.26	-0.54	1.58	6.70	15.44	14.83

Table 3 continued

Table 3 (continued)

Name	Energy	Ecc	$J_r$	$J_\phi$	$J_z$	$r_{\text{peri}}$	$r_{\text{apo}}$	$Z_{\text{max}}$
	$\times 10^5$		$\times 10^3$	$\times 10^3$	$\times 10^3$			
	( $\text{km}^2 \text{s}^{-2}$ )		( $\text{kpc km s}^{-1}$ )	( $\text{kpc km s}^{-1}$ )	( $\text{kpc km s}^{-1}$ )	(kpc)	(kpc)	(kpc)
2MASS J11301705-1449325	-1.58	0.30	0.10	+1.27	0.31	5.31	9.96	5.32
2MASS J11303693+0224037*	-1.65	0.94	0.80	+0.12	0.14	0.37	11.49	4.81
2MASS J11370170-5401298	-1.71	0.57	0.30	+0.86	0.07	2.49	9.08	2.37
2MASS J11404726-0833030	-1.83	0.93	0.61	+0.14	0.02	0.31	8.23	3.97
2MASS J11404944-1615396*	-1.65	0.97	0.89	-0.04	0.09	0.15	11.35	5.44
BD+26:2251	-1.23	0.94	1.83	+0.35	0.21	0.84	26.25	18.56
2MASS J11444086-0409511	-0.94	0.69	2.27	-3.20	0.29	8.37	49.04	19.41
2MASS J11444480-1128167	-1.59	0.93	1.01	-0.23	0.00	0.47	12.76	4.62
2MASS J11463882-0422395*	-1.70	0.95	0.65	+0.08	0.23	0.26	9.92	5.86
2MASS J11471027+0341265*	-1.04	0.71	1.90	-2.21	0.44	6.17	39.09	21.10
2MASS J11472988-0521444	-1.22	0.91	2.01	+0.65	0.06	1.30	27.09	5.90
2MASS J11510227-6940416	-1.89	0.96	0.58	-0.07	0.01	0.17	7.38	3.82
HD 103095	-1.38	0.86	1.35	+0.71	0.00	1.41	19.39	0.17
2MASS J11543613-0133450*	-1.08	0.96	2.63	+0.18	0.68	0.68	37.26	34.16
RAVE J115941.7-382043	-1.66	0.21	0.05	+1.49	0.01	5.36	8.12	0.47
2MASS J12044314-2911051	-1.56	0.68	0.53	+0.78	0.24	2.42	12.57	6.21
2MASS J12045624-0759232*	-1.12	0.79	1.81	-1.14	0.65	3.68	32.23	23.37
2MASS J12070990-3653243	-1.71	0.53	0.21	-0.13	0.85	2.56	8.16	8.04
2MASS J12091322-1415313*	-1.62	0.68	0.42	-0.40	0.55	2.06	10.80	9.16
2MASS J12102259-4902190	-1.50	0.96	1.16	+0.13	0.11	0.28	15.28	5.99
HD 106373	-1.40	0.89	1.32	+0.53	0.03	1.10	18.57	3.08
HD 107752	-1.57	0.49	0.29	-1.16	0.22	3.93	11.46	5.10
2MASS J12233047-4216365*	-1.55	0.70	0.61	+0.91	0.08	2.29	12.96	2.42
2MASS J12255123-2351074*	-1.55	0.23	0.06	+1.22	0.51	6.22	9.93	6.59
HD 108317	-1.67	0.46	0.24	+1.21	0.00	3.51	9.60	0.26
HD 108577	-1.50	0.60	0.40	-0.34	1.04	3.42	13.49	12.88
2MASS J12292696-0442325	-1.45	0.81	0.87	-0.49	0.47	1.76	16.34	12.16
HE 1226-1149*	-1.15	0.48	0.65	+1.89	1.28	9.32	26.57	21.10
2MASS J12341308-3149577	-1.63	0.54	0.27	-0.72	0.42	3.03	10.10	7.16
2MASS J12351734+0945333*	-1.45	0.34	0.17	+1.07	0.89	6.44	13.18	10.79
RAVE J123550.1-313111	-1.67	0.70	0.47	+0.65	0.11	1.75	10.10	3.55
2MASS J12405721-4051430	-1.73	0.95	0.80	+0.11	0.01	0.24	9.90	4.64
2MASS J12503987-0307485	-1.26	0.47	0.50	-2.03	0.58	7.69	21.19	12.89
2MASS J12535742-3801355	-0.91	0.75	2.71	-1.58	1.57	7.20	52.69	45.23
2MASS J12563137-0834098	-1.75	0.76	0.40	-0.32	0.28	1.17	8.53	5.86
2MASS J12571667-4335318	-1.78	0.54	0.24	+0.81	0.04	2.36	7.93	1.37
HE 1256-0228*	-1.69	0.48	0.20	+0.81	0.27	3.07	8.78	4.86
2MASS J12591462-7049592	-1.86	0.89	0.56	+0.13	0.03	0.45	7.59	3.38
BPS BS 16929-0005	-1.68	0.55	0.28	+0.85	0.17	2.76	9.38	3.93
2MASS J13052137-1137220*	-1.55	0.64	0.41	-0.39	0.79	2.77	12.20	11.17
RAVE J130524.5-393126	-1.85	0.62	0.27	-0.58	0.05	1.69	7.18	1.56
2MASS J13101305-3342369	-1.79	0.41	0.14	+0.96	0.04	3.10	7.33	1.20
BPS CS 22877-0015	-1.83	0.79	0.46	+0.39	0.02	0.93	7.91	1.12
HD 115444	-1.67	0.78	0.62	+0.56	0.03	1.30	10.68	1.18
2MASS J13164824-2743351	-1.42	0.94	1.46	-0.18	0.03	0.55	17.84	5.71
BPS BS 16033-0081	-1.61	0.35	0.12	-0.79	0.62	4.60	9.36	7.42
2MASS J13214178-4320055	-1.86	0.97	0.52	+0.03	0.10	0.11	7.68	4.01
2MASS J13254554-1747547	-1.35	0.72	0.87	-0.77	0.71	3.22	19.64	15.76
2MASS J13261792-0945176	-1.76	0.64	0.29	-0.54	0.22	1.81	8.09	4.36
2MASS J13315746-1929446	-1.73	0.40	0.16	+1.14	0.01	3.50	8.27	0.53
2MASS J13330890-4654079*	-1.76	0.18	0.03	+1.07	0.12	4.50	6.45	2.28
HD 118055	-1.64	0.44	0.20	+1.01	0.24	3.71	9.60	4.71
SMSS J133532.32-210632.9*	-1.80	0.60	0.23	-0.53	0.22	1.87	7.46	4.06
2MASS J13374885-0826176	-1.72	0.48	0.17	+0.65	0.38	2.90	8.26	5.64
2MASS J13425404-0717005	-1.14	0.57	0.94	+1.13	1.71	7.69	28.54	26.02
HD 119516	-1.32	0.48	0.44	+1.17	1.07	6.58	18.55	15.51
BPS BS 16089-0013	-1.47	0.74	0.71	-0.53	0.54	2.22	14.98	12.10
2MASS J13494713-7423395	-1.84	0.84	0.36	+0.13	0.29	0.61	6.86	5.62
2MASS J13511539-7340363	-1.38	0.90	1.43	-0.53	0.00	1.03	19.22	0.84
2MASS J13524835+1254216*	-1.53	0.93	0.92	+0.11	0.33	0.48	13.87	10.84
2MASS J14004919+4551581	-0.84	0.97	5.09	+0.43	0.19	0.95	63.79	45.86
2MASS J14032900-5250429	-1.84	0.80	0.48	+0.37	0.00	0.86	7.91	0.19
2MASS J14043762+0011117*	-1.63	0.83	0.57	+0.27	0.37	1.03	10.89	8.47
HD 122956	-1.78	0.84	0.43	+0.17	0.29	0.71	7.98	6.27

Table 3 continued

Table 3 (continued)

Name	Energy	Ecc	$J_r$	$J_\phi$	$J_z$	$r_{\text{peri}}$	$r_{\text{apo}}$	$Z_{\text{max}}$
	$\times 10^5$		$\times 10^3$	$\times 10^3$	$\times 10^3$			
	( $\text{km}^2 \text{s}^{-2}$ )		( $\text{kpc km s}^{-1}$ )	( $\text{kpc km s}^{-1}$ )	( $\text{kpc km s}^{-1}$ )	(kpc)	(kpc)	(kpc)
2MASS J14101587-0343553	-1.72	0.65	0.40	+0.77	0.03	2.01	9.39	1.20
2MASS J14155955-3219255	-1.48	0.49	0.32	+1.05	0.57	4.62	13.41	9.64
2MASS J14180866-2842077	-1.75	0.86	0.62	-0.17	0.11	0.71	9.36	3.59
2MASS J14191395-0844410	-1.66	0.44	0.20	+1.16	0.07	3.65	9.41	2.32
BD+01:2916	-1.80	0.77	0.46	-0.36	0.08	1.08	8.28	3.11
2MASS J14232679-2834200	-1.77	0.26	0.05	-0.98	0.14	3.94	6.67	2.58
2MASS J14234371-4025526*	-1.18	0.79	1.66	+1.32	0.18	3.26	28.44	12.96
BD+08:2856	-1.55	0.63	0.51	+1.11	0.06	2.92	12.73	1.99
BPS CS 22883-0037*	-1.16	0.82	1.78	+0.54	0.93	2.98	30.02	27.38
2MASS J14301385-2317388	-1.21	0.68	1.11	-1.44	0.60	4.89	25.86	17.26
BD+18:2890	-1.61	0.81	0.77	-0.48	0.06	1.28	12.12	3.61
HE 1429-0347	-1.48	0.55	0.38	+1.12	0.42	4.05	13.93	8.54
2MASS J14325334-4125494	-1.12	0.89	2.22	+0.87	0.24	1.93	33.30	18.72
HE 1430+0053*	-1.63	0.54	0.29	-0.85	0.29	3.11	10.19	5.69
2MASS J14354680-1124122	-1.67	0.13	0.02	+1.51	0.01	5.80	7.60	0.60
BPS BS 16083-0172	-1.68	0.74	0.51	+0.59	0.10	1.55	10.33	3.35
2MASS J14543792+0830379*	-1.87	0.82	0.36	+0.24	0.17	0.70	7.05	3.51
2MASS J14590234-0916105*	-1.35	0.85	1.12	-0.39	0.70	1.65	20.22	17.34
2MASS J14592981-3852558*	-1.79	0.12	0.01	-1.00	0.15	4.61	5.83	2.38
2MASS J15002498-0613374	-1.49	0.43	0.28	+1.73	0.04	5.21	13.08	2.44
2MASS J15042611-2231523	-1.63	0.53	0.29	+0.88	0.27	3.17	10.30	5.49
2MASS J15062866-1428038	-1.72	0.32	0.10	+1.25	0.02	4.15	7.97	0.81
BD+30:2611	-1.29	0.43	0.40	+1.32	1.17	7.62	19.33	16.16
2MASS J15075699-0659593	-1.60	0.68	0.38	-0.08	0.96	2.12	11.24	11.12
2MASS J15083385-1459166	-1.77	0.78	0.38	+0.31	0.26	1.01	8.15	5.03
HD 134440	-0.96	0.82	2.75	-2.19	0.04	4.62	46.07	7.36
2MASS J15111672+0025252*	-1.63	0.33	0.10	-0.85	0.55	4.60	9.06	6.81
HD 135148	-1.50	0.95	1.21	+0.04	0.12	0.36	15.34	5.74
2MASS J15133549-1244339	-1.83	0.36	0.09	-0.84	0.10	3.06	6.45	2.19
BPS CS 30306-0132	-1.69	0.49	0.23	+0.93	0.15	3.07	9.05	3.47
2MASS J15155734-1054220	-1.65	0.73	0.57	+0.71	0.03	1.71	10.91	1.35
RAVE J151558.3-203821	-1.84	0.31	0.07	-0.89	0.08	3.30	6.22	1.90
2MASS J15204531-1742486	-1.82	0.71	0.30	+0.29	0.29	1.20	7.11	5.26
2MASS J15211026-0607566	-1.64	0.48	0.23	-0.87	0.31	3.39	9.74	5.62
2MASS J15213995-3538094	-0.99	0.75	2.19	+2.13	0.53	5.99	42.50	24.38
2MASS J15260106-0911388	-1.13	0.70	1.48	-1.85	0.45	5.42	31.71	17.83
2MASS J15271353-2336177	-1.78	0.61	0.32	+0.73	0.03	1.98	8.31	1.03
2MASS J15293404-3906241	-1.86	0.24	0.04	-0.90	0.07	3.52	5.71	1.57
2MASS J15383085-1804242	-1.81	0.64	0.28	-0.52	0.15	1.63	7.48	3.54
SMSS J155430.57-263904.8*	-1.24	0.82	1.42	+0.78	0.52	2.41	24.99	17.92
2MASS J15582962-1224344	-1.73	0.17	0.02	+1.11	0.16	4.82	6.80	2.78
2MASS J16024498-1521016	-1.63	0.35	0.14	+1.42	0.03	4.59	9.48	1.26
BD+42:2667	-1.77	0.96	0.74	-0.08	0.00	0.18	9.09	4.45
SMSS J160447.75-293146.7*	-1.82	0.92	0.36	-0.06	0.38	0.31	7.43	5.84
2MASS J16095117-0941174	-1.74	0.52	0.19	-0.57	0.38	2.52	8.02	5.66
2MASS J16122832-0848083	-1.86	0.43	0.14	+0.78	0.06	2.60	6.49	1.74
2MASS J16163560-0401148	-1.73	0.63	0.36	+0.76	0.05	2.07	9.04	1.65
2MASS J16285613-1014576	-1.70	0.33	0.11	+1.30	0.01	4.22	8.32	0.54
BD+09:3223	-1.62	0.98	1.06	+0.02	0.00	0.10	12.18	5.42
HD 149414	-1.70	0.55	0.26	+0.72	0.26	2.57	8.98	4.94
BPS CS 22878-0121	-1.41	0.59	0.54	-0.85	0.74	4.17	16.09	13.12
SMSS J165023.82-252948.7*	-1.56	0.59	0.43	+1.11	0.11	3.19	12.20	3.56
RAVE J165300.5-005507	-2.01	0.72	0.28	+0.20	0.09	0.90	5.47	1.95
2MASS J16592172-6827199*	-1.09	0.73	1.72	-1.62	0.61	5.10	34.20	22.71
2MASS J17043634-6219457*	-1.82	0.64	0.26	-0.52	0.16	1.64	7.44	3.30
2MASS J17060555+0412354*	-1.40	0.76	0.85	-0.65	0.59	2.49	17.76	13.89
2MASS J17093199-6027271*	-1.19	0.84	1.95	-1.00	0.09	2.21	29.17	10.30
2MASS J17124284-5211479*	-1.60	0.49	0.27	+1.07	0.23	3.72	10.76	5.05
2MASS J17131974-7113010	-1.80	0.27	0.06	+0.97	0.09	3.69	6.38	1.95
2MASS J17163340-7009028*	-1.76	0.19	0.03	+0.93	0.24	4.37	6.47	3.47
2MASS J17225742-7123000	-1.40	0.49	0.41	-1.32	0.58	5.46	16.06	11.04
BD+17:3248	-1.84	0.96	0.59	+0.06	0.05	0.16	8.03	4.09
2MASS J17360008-5145303	-1.69	0.59	0.33	+0.85	0.10	2.44	9.51	2.89
2MASS J17383643-5358288	-1.84	0.41	0.11	+0.71	0.16	2.67	6.36	2.92

Table 3 continued

Table 3 (continued)

Name	Energy	Ecc	$J_r$	$J_\phi$	$J_z$	$r_{\text{peri}}$	$r_{\text{apo}}$	$Z_{\text{max}}$
	$\times 10^5$		$\times 10^3$	$\times 10^3$	$\times 10^3$			
	( $\text{km}^2 \text{s}^{-2}$ )		( $\text{kpc km s}^{-1}$ )	( $\text{kpc km s}^{-1}$ )	( $\text{kpc km s}^{-1}$ )	(kpc)	(kpc)	(kpc)
2MASS J17400682-6102129	-1.70	0.44	0.14	-0.54	0.57	3.22	8.20	6.78
2MASS J17414840-5340354*	-1.85	0.55	0.16	+0.36	0.35	1.81	6.30	4.79
2MASS J17435113-5359333	-1.85	0.45	0.12	+0.58	0.23	2.39	6.28	3.65
SMSS J175046.30-425506.9*	-1.56	0.75	0.65	-0.64	0.20	1.87	12.76	6.44
RAVE J175159.8-475131	-2.04	0.72	0.18	-0.24	0.13	0.80	4.78	2.62
2MASS J17541561-5148268*	-1.96	0.80	0.22	-0.07	0.31	0.58	5.23	4.67
G 154-34	-1.65	0.80	0.46	-0.21	0.55	1.18	10.38	9.49
SMSS J175738.37-454823.5*	-2.18	0.22	0.01	+0.25	0.19	1.69	2.66	1.96
2MASS J18024226-4404426*	-1.27	0.93	1.73	-0.34	0.46	0.67	25.28	18.49
2MASS J18050641-4907579	-2.01	0.85	0.31	+0.19	0.06	0.47	5.77	2.72
SMSS J181505.16-385514.9	-1.95	0.64	0.15	-0.15	0.38	1.12	5.26	4.69
2MASS J18174532-3353235*	-2.42	0.46	0.01	+0.00	0.16	0.61	1.63	1.46
2MASS J18272347-5133001	-1.80	0.83	0.60	+0.11	0.09	0.77	8.44	3.01
2MASS J18285086-3434203*	-2.34	0.85	0.11	-0.04	0.09	0.19	2.60	1.46
2MASS J18294122-4504000*	-1.99	0.55	0.12	+0.42	0.14	1.48	5.09	2.40
2MASS J18294359-4924253	-2.14	0.79	0.10	+0.06	0.26	0.42	3.48	3.05
RAVE J183013.5-455510	-1.73	0.12	0.01	+1.05	0.22	5.07	6.39	3.15
SMSS J183128.71-341018.4*	-2.11	0.52	0.06	+0.21	0.23	1.15	3.56	2.72
SMSS J183225.29-334938.4*	-2.04	0.79	0.14	+0.11	0.29	0.57	4.49	3.63
2MASS J18362318-6428124	-1.77	0.16	0.02	+1.13	0.07	4.58	6.36	1.65
2MASS J18363613-7136597	-1.72	0.27	0.07	+1.21	0.06	4.33	7.59	1.75
SMSS J183647.89-274333.1*	-1.68	0.90	0.68	-0.22	0.15	0.53	10.53	4.77
HD 175305	-1.30	0.41	0.35	+1.31	1.21	7.91	18.75	15.82
2MASS J18562774-7251331	-1.69	0.97	0.77	+0.06	0.11	0.18	10.39	5.05
2MASS J19014952-4844359*	-1.98	0.91	0.38	-0.13	0.06	0.31	6.20	3.12
2MASS J19050116-1949280	-1.75	0.79	0.50	+0.42	0.08	1.10	9.12	3.48
SMSS J190911.03-213207.5*	-2.00	0.87	0.25	+0.05	0.21	0.36	5.00	3.80
2MASS J19092677-5140208*	-1.55	0.72	0.58	-0.47	0.50	1.95	12.94	10.22
SMSS J190931.13-214053.9*	-1.94	0.34	0.05	+0.54	0.21	2.41	4.94	2.83
HD 178443	-1.36	0.96	1.28	-0.13	0.45	0.43	20.09	17.45
HD 179626	-1.77	0.98	0.75	-0.01	0.03	0.08	9.14	4.60
2MASS J19161821-5544454*	-1.95	0.41	0.08	+0.53	0.16	2.11	5.08	2.55
2MASS J19192768-5959140	-1.32	0.89	1.55	-0.59	0.06	1.25	21.65	4.37
2MASS J19215077-4452545*	-1.76	0.34	0.09	+0.94	0.16	3.57	7.19	2.97
2MASS J19232518-5833410	-1.77	0.87	0.49	-0.18	0.23	0.60	8.40	5.47
2MASS J19232941-4425432	-1.53	0.70	0.64	-0.92	0.11	2.40	13.66	3.93
RAVE J192632.8-584657*	-1.97	0.51	0.09	-0.35	0.25	1.59	4.85	3.33
RAVE J192819.9-633935*	-1.66	0.46	0.22	+1.06	0.14	3.51	9.51	3.36
2MASS J19291910-5528181*	-1.78	0.34	0.06	+0.43	0.58	3.27	6.54	5.70
BPS CS 22896-0055	-1.41	0.95	1.39	-0.20	0.14	0.47	18.08	8.85
2MASS J19310426-3707397*	-1.92	0.62	0.13	-0.26	0.35	1.32	5.58	4.32
2MASS J19324858-5908019*	-1.41	0.56	0.46	-0.41	1.32	4.58	16.13	15.53
2MASS J19345326-3236567	-1.70	0.95	0.72	-0.11	0.14	0.28	10.03	5.24
SMSS J193617.38-790231.4	-1.22	0.71	1.25	-1.85	0.02	4.29	25.61	3.15
BPS CS 22896-0154	-1.84	0.26	0.06	-0.93	0.07	3.54	6.07	1.56
2MASS J19445483-4039459	-1.76	0.44	0.17	-0.95	0.06	3.05	7.82	1.76
2MASS J19451414-1729269	-1.66	0.68	0.48	-0.78	0.05	1.99	10.53	1.91
RAVE J194550.6-392631*	-1.89	0.20	0.02	-0.69	0.21	3.35	5.05	2.75
2MASS J19552158-4613569	-1.89	0.75	0.33	-0.34	0.10	0.94	6.74	3.12
2MASS J19563822-4054235	-1.28	0.61	0.77	+0.67	1.39	5.31	21.64	20.28
Gaia DR2 2233912206910720000	-0.55	0.88	8.14	-0.31	3.90	8.45	133.70	133.25
2MASS J19584033+0430396	-0.87	0.82	3.43	-0.50	2.09	5.50	57.62	56.42
SMSS J195931.70-643529.3*	-1.55	0.34	0.11	-0.27	1.32	5.21	10.48	10.28
2MASS J20000364-3301351	-1.91	0.75	0.27	-0.29	0.16	0.92	6.38	3.21
2MASS J20005766-2541488	-1.69	0.82	0.61	+0.41	0.08	0.99	10.31	3.90
2MASS J20050670-3057445	-1.62	0.59	0.39	-1.02	0.08	2.79	10.94	2.15
2MASS J20080083-2759265	-1.98	0.58	0.13	-0.38	0.17	1.39	5.14	2.70
2MASS J20093393-3410273*	-1.38	0.76	0.94	-0.62	0.63	2.42	19.03	15.18
2MASS J20102782-0826556	-1.61	0.84	0.78	-0.47	0.04	1.06	12.04	1.63
2MASS J20103193-3558546	-1.81	0.83	0.39	+0.15	0.30	0.67	7.37	6.00
2MASS J20194310-3158163	-1.77	0.92	0.68	+0.18	0.01	0.40	9.08	4.16
BPS CS 22943-0132	-1.60	0.29	0.09	+1.34	0.20	5.24	9.45	3.99
2MASS J20233743-1659533	-1.88	0.84	0.38	-0.18	0.16	0.57	6.72	4.15
2MASS J20303339-2519500	-1.83	0.24	0.04	-0.79	0.20	3.57	5.81	2.95

Table 3 continued

Table 3 (continued)

Name	Energy	Ecc	$J_r$	$J_\phi$	$J_z$	$r_{\text{peri}}$	$r_{\text{apo}}$	$Z_{\text{max}}$
	$\times 10^5$		$\times 10^3$	$\times 10^3$	$\times 10^3$			
	( $\text{km}^2 \text{s}^{-2}$ )		( $\text{kpc km s}^{-1}$ )	( $\text{kpc km s}^{-1}$ )	( $\text{kpc km s}^{-1}$ )	(kpc)	(kpc)	(kpc)
2MASS J20362262-0714197	-1.71	0.11	0.01	-0.46	0.79	5.12	6.39	5.85
2MASS J20374042-5520500	-1.83	0.82	0.30	+0.14	0.39	0.71	7.01	6.03
2MASS J20384318-0023327*	-1.33	0.54	0.63	-1.38	0.63	5.47	19.49	13.65
2MASS J20385893-0252115	-1.82	0.93	0.51	-0.09	0.16	0.30	7.71	4.56
2MASS J20411424-4654315*	-1.88	0.81	0.30	+0.18	0.25	0.67	6.47	4.53
BPS CS 22955-0174*	-1.80	0.64	0.23	+0.38	0.33	1.62	7.31	5.29
2MASS J20435776-4408037	-1.85	0.35	0.07	+0.68	0.20	2.83	5.94	3.09
2MASS J20453454-1431151	-1.88	0.69	0.34	+0.48	0.02	1.28	7.06	1.01
2MASS J20492765-5124440	-1.91	0.76	0.24	+0.26	0.22	0.84	6.12	3.63
2MASS J20504869-3355289*	-1.87	0.87	0.41	-0.07	0.20	0.47	6.78	4.72
2MASS J20514971-6158008	-1.66	0.30	0.09	+1.22	0.15	4.62	8.51	3.14
BPS CS 22940-0121*	-1.64	0.65	0.33	-0.33	0.67	2.17	10.21	9.21
2MASS J20554594-3155159	-1.80	0.73	0.37	-0.45	0.12	1.26	7.99	3.43
2MASS J20584918-0354340	-1.87	0.96	0.57	-0.05	0.04	0.15	7.60	3.91
2MASS J21003824-0539171	-1.86	0.69	0.34	+0.49	0.04	1.32	7.33	1.20
2MASS J21055865-4919336	-1.59	0.30	0.08	-0.60	0.92	5.18	9.55	8.59
2MASS J21063474-4957500	-1.45	0.77	0.82	-0.78	0.21	2.10	15.99	6.98
2MASS J21064294-6828266	-1.72	0.29	0.07	+0.80	0.38	4.05	7.32	4.88
2MASS J21091825-1310062	-1.83	0.85	0.42	-0.14	0.22	0.58	7.18	5.16
2MASS J21095804-0945400*	-1.80	0.37	0.10	+0.86	0.14	3.15	6.84	2.66
2MASS J21162185-0213420	-1.70	0.19	0.04	+1.31	0.06	5.00	7.40	1.65
2MASS J21220020-0820333*	-1.84	0.65	0.24	+0.42	0.22	1.45	6.90	3.98
2MASS J21224590-4641030	-1.72	0.52	0.18	+0.36	0.63	2.57	8.10	7.26
2MASS J21262525-2144243*	-1.74	0.92	0.50	-0.02	0.32	0.35	8.86	6.90
BD-03:5215	-1.70	0.93	0.68	-0.11	0.18	0.37	9.86	6.60
HE 2134+0001	-1.54	0.15	0.03	+1.79	0.09	7.12	9.69	2.44
2MASS J21462219-0512324	-1.65	0.74	0.48	-0.45	0.32	1.59	10.44	7.20
G 214-1	-1.68	0.59	0.35	+0.89	0.07	2.56	9.84	2.63
BPS CS 22951-0059*	-1.49	0.37	0.20	+1.49	0.33	5.74	12.61	6.48
RAVE J215118.3-135937	-1.85	0.85	0.50	-0.26	0.03	0.63	7.75	3.46
BPS CS 29493-0062	-1.61	0.05	0.00	+1.72	0.02	7.18	7.87	0.77
HE 2155+0136	-1.79	0.80	0.45	-0.34	0.11	0.91	8.13	3.77
HE 2154-2838*	-1.74	0.50	0.17	-0.58	0.38	2.66	7.95	5.49
HE 2206-2245*	-1.74	0.34	0.08	-0.66	0.45	3.55	7.24	5.39
BPS CS 22886-0012*	-1.78	0.43	0.16	+0.95	0.04	3.00	7.56	1.36
2MASS J22161170-5319492	-1.77	0.77	0.54	+0.38	0.05	1.13	8.86	3.15
2MASS J22163596+0246171*	-1.79	0.90	0.51	+0.17	0.17	0.45	8.33	4.51
BPS CS 22892-0052*	-1.59	0.81	0.65	+0.37	0.34	1.23	12.13	8.80
2MASS J22182082-3827554	-1.37	0.43	0.32	+0.79	1.33	6.54	16.21	14.91
2MASS J22190836-2333467	-1.70	0.46	0.19	+0.96	0.15	3.25	8.74	3.44
2MASS J22220344-8024592	-1.68	0.20	0.03	+0.20	1.11	4.87	7.36	7.25
BPS CS 22886-0043	-1.70	0.68	0.31	+0.45	0.38	1.75	9.17	6.51
BPS CS 22960-0064	-1.71	0.47	0.20	+0.98	0.10	3.16	8.65	2.65
HE 2224+0143*	-1.82	0.73	0.42	+0.38	0.08	1.25	7.93	2.62
BPS CS 22875-0029*	-1.43	0.93	1.20	+0.19	0.33	0.56	17.30	13.65
2MASS J22302641-1949527*	-1.35	0.35	0.22	+1.37	1.05	7.92	16.44	13.28
BPS CS 29491-0069	-1.09	0.65	1.32	-1.63	1.13	6.98	32.68	25.87
HE 2229-4153	-1.66	0.37	0.11	-0.47	0.79	3.93	8.55	7.73
2MASS J22345447-6605172	-1.72	0.38	0.13	+1.02	0.13	3.61	8.06	2.83
2MASS J22373316-4341181	-1.82	0.80	0.45	-0.30	0.08	0.87	8.01	3.25
HE 2242-1930	-1.39	0.50	0.43	+1.70	0.25	5.52	16.52	6.98
HE 2244-1503*	-1.01	0.68	1.70	+2.64	0.42	7.40	39.16	19.01
2MASS J22492756-2238289	-1.70	0.89	0.57	-0.20	0.25	0.61	9.69	5.79
2MASS J22562536-0719562	-1.65	0.79	0.55	+0.39	0.27	1.25	10.66	6.82
2MASS J23022289-6833233	-1.79	0.76	0.40	+0.37	0.14	1.07	7.96	3.91
HE 2301-4024*	-1.16	0.66	1.19	-1.38	0.93	5.80	28.23	22.27
2MASS J23060975-6107368	-1.67	0.76	0.54	-0.51	0.13	1.37	10.22	4.27
2MASS J23100319-7702165	-1.54	0.61	0.47	+1.01	0.21	3.13	12.83	5.59
BPS CS 29513-0003	-1.53	0.36	0.15	-1.07	0.59	5.32	11.24	8.16
BPS CS 22945-0017	-1.67	0.43	0.18	+1.02	0.17	3.59	9.00	3.70
2MASS J23242766-2728055	-1.75	0.75	0.39	-0.34	0.28	1.24	8.49	5.85
2MASS J23251897-0815539	-1.67	0.37	0.11	-0.63	0.61	3.91	8.40	6.91
2MASS J23265258-0159248	-1.54	0.75	0.70	-0.72	0.16	1.94	13.49	5.35
2MASS J23285061-0432368	-1.68	0.48	0.23	+1.06	0.07	3.24	9.20	2.00

Table 3 continued



Table 3 (continued)

Name	Energy	Ecc	$J_r$	$J_\phi$	$J_z$	$r_{\text{peri}}$	$r_{\text{apo}}$	$Z_{\text{max}}$
	$\times 10^5$		$\times 10^3$	$\times 10^3$	$\times 10^3$			
	( $\text{km}^2 \text{s}^{-2}$ )		( $\text{kpc km s}^{-1}$ )	( $\text{kpc km s}^{-1}$ )	( $\text{kpc km s}^{-1}$ )	(kpc)	(kpc)	(kpc)
HD 221170	-1.68	0.60	0.37	+0.95	0.01	2.51	9.96	0.86
HE 2327-5642	-1.45	0.66	0.60	-0.65	0.66	3.08	15.19	12.47
BPS CS 22941-0017*	-1.49	0.20	0.05	+1.36	0.61	7.32	10.96	7.63
2MASS J23342332-2748003*	-1.78	0.91	0.48	+0.14	0.23	0.40	8.40	4.91
2MASS J23362202-5607498*	-1.52	0.68	0.48	+0.19	1.01	2.51	13.33	12.97
BPS CS 22952-0015*	-1.57	0.38	0.15	+0.83	0.66	4.67	10.41	8.26
BPS CS 29499-0003	-1.57	0.87	0.86	+0.37	0.11	0.88	13.13	4.57
2MASS J23411581-6406440	-1.67	0.96	0.66	+0.05	0.33	0.23	10.31	8.56
2MASS J23425814-4327352	-1.56	0.44	0.26	+1.47	0.05	4.42	11.48	2.47
HD 222925	-1.53	0.92	1.04	-0.28	0.09	0.57	14.47	5.25
2MASS J23475942-5701184	-1.82	0.80	0.38	-0.28	0.18	0.85	7.47	4.23
BPS CS 22966-0057	-1.67	0.69	0.39	-0.46	0.38	1.80	9.77	7.15
2MASS J23490902-2447176	-1.00	0.88	2.84	+1.13	0.39	2.75	43.07	24.86
BPS CS 29499-0058	-1.55	0.75	0.58	+0.19	0.73	1.81	12.76	12.19
BPS CS 22945-0058	-1.74	0.96	0.70	+0.09	0.09	0.22	9.58	4.72
BPS CS 22945-0056	-1.21	0.72	1.23	-1.25	0.65	4.24	26.34	18.29
BPS CS 29517-0025	-1.45	0.25	0.09	-1.22	0.87	7.43	12.50	9.91
SDSS J235718.91-005247.8	-1.40	0.39	0.25	-1.29	0.82	6.66	15.06	11.55

NOTE—Single (\*) mark indicates the 16 stars with relative distance errors in the range  $20\% < \epsilon < 30\%$ . See text for details.

Table 4. CDTGs Identified from the HDBSCAN Algorithm

Name	Class	[Fe/H]	[C/Fe]	[C/Fe] <sub>c</sub>	[Sr/Fe]	[Ba/Fe]	[Eu/Fe]	[Eu/H]
<i>CDTG-1</i> ( $N = 6$ , $\text{CL} = 99.8\%$ )								
2MASS J10492192-1154173	$r$ -I	-2.18	-0.42	-0.41	-0.06	-0.16	+0.33	-1.85
2MASS J20584918-0354340	$r$ -I	-2.36	0.00	+0.40	-0.24	-0.09	+0.36	-2.00
2MASS J12591462-7049592	$r$ -I	-2.45	-0.60	+0.16	+0.25	+0.25	+0.50	-1.95
2MASS J11404726-0833030	$r$ -I	-1.55	+0.03	+0.05	+0.11	+0.36	+0.55	-1.00
2MASS J00405260-5122491	$r$ -II	-2.11	-0.04	-0.04	+0.09	-0.04	+0.86	-1.25
BD+17:3248	$r$ -II	-2.09	-0.47	-0.24	+0.29	+0.40	+0.91	-1.18
$\mu \pm \sigma$ ([X/Y])		$-2.19 \pm 0.28$	$-0.25 \pm 0.27$	$-0.01 \pm 0.28$	$+0.08 \pm 0.19$	$+0.12 \pm 0.23$	$+0.57 \pm 0.24$	$-1.54 \pm 0.43$
Cumulative fraction value		0.20		0.70	0.32	0.44	0.68	
<i>CDTG-2</i> ( $N = 8$ , $\text{CL} = 99.1\%$ )								
2MASS J19445483-4039459	$r$ -I	-1.98	-0.27	+0.33	+0.21	+0.13	+0.33	-1.65
2MASS J15293404-3906241	$r$ -I	-2.74	...	...	-0.36	-0.16	+0.34	-2.40
RAVE J151558.3-203821	$r$ -I	-2.74	-0.15	+0.58	+0.27	-0.39	+0.36	-2.38
2MASS J20303339-2519500	$r$ -I	-2.21	-0.65	+0.10	+0.41	-0.29	+0.41	-1.80
2MASS J15133549-1244339	$r$ -I / CEMP- $r$	-2.04	+0.45	+0.75	-2.87	-0.10	+0.55	-1.49
2MASS J14232679-2834200	$r$ -I	-1.90	+0.43	+0.44	+0.44	-0.07	+0.61	-1.29
BPS CS 22896-0154	$r$ -II	-2.69	+0.27	+0.28	+0.54	+0.51	+0.86	-1.83
2MASS J14592981-3852558*	$r$ -II	-2.48	-0.95	-0.17	+0.23	+0.13	+0.93	-1.55
$\mu \pm \sigma$ ([X/Y])		$-2.35 \pm 0.35$	$-0.12 \pm 0.52$	$+0.34 \pm 0.29$	$+0.29 \pm 0.28$	$-0.05 \pm 0.27$	$+0.51 \pm 0.24$	$-1.73 \pm 0.40$
Cumulative fraction value		0.26		0.72	0.58	0.51	0.64	
<i>CDTG-3</i> ( $N = 3$ , $\text{CL} = 97.4\%$ )								
2MASS J16024498-1521016	$r$ -I	-1.80	-0.05	-0.05	+0.35	+0.08	+0.55	-1.25
2MASS J09284944-0738585	$r$ -I	-1.22	0.00	+0.07	+0.45	+0.32	+0.60	-0.62
2MASS J10191573-1924464	$r$ -II	-1.19	-0.32	-0.23	+0.63	+0.73	+0.75	-0.44
$\mu \pm \sigma$ ([X/Y])		$-1.40 \pm 0.28$	$-0.12 \pm 0.14$	$-0.07 \pm 0.12$	$+0.48 \pm 0.12$	$+0.38 \pm 0.27$	$+0.63 \pm 0.08$	$-0.77 \pm 0.35$
Cumulative fraction value		0.40		0.28	0.23	0.67	0.22	
<i>CDTG-4</i> ( $N = 4$ , $\text{CL} = 93.7\%$ )								
2MASS J00413026-4058547	$r$ -I	-2.58	-0.49	+0.20	+0.04	-0.27	+0.38	-2.20
2MASS J02274104-0519230*	$r$ -I	-2.38	-0.70	+0.08	+0.72	-0.18	+0.42	-1.96
2MASS J00453930-7457294	$r$ -I / CEMP- $r$	-2.00	+0.93	+0.98	+0.83	+0.37	+0.55	-1.45

Table 4 continued

Table 4 (continued)

Name	Class	[Fe/H]	[C/Fe]	[C/Fe] <sub>c</sub>	[Sr/Fe]	[Ba/Fe]	[Eu/Fe]	[Eu/H]
2MASS J00182832-3900338	r-I	-1.80	-0.35	+0.15	+0.28	+0.07	+0.57	-1.23
$\mu \pm \sigma$ ([X/Y])		-2.19±0.32	-0.50±0.28	+0.15±0.07	+0.48±0.34	-0.03±0.27	+0.48±0.09	-1.71±0.41
Cumulative fraction value		0.43		0.10	0.79	0.64	0.24	
<i>CDTG-5 (N = 3, CL = 92.8%)</i>								
HD 224930	r-I	-1.00	...	...	...	-0.19	+0.34	-0.66
2MASS J16285613-1014576	r-I	-2.00	-0.30	+0.24	-0.26	-0.02	+0.36	-1.64
2MASS J15062866-1428038	r-I	-2.25	-0.08	-0.08	+0.17	-0.01	+0.65	-1.60
$\mu \pm \sigma$ ([X/Y])		-1.75±0.54	...	...	...	-0.07±0.08	+0.45±0.14	-1.30±0.45
Cumulative fraction value		0.85		...	...	0.11	0.43	
<i>CDTG-6 (N = 3, CL = 91.1%)</i>								
HD 149414	r-I	-1.26	...	...	...	+0.06	+0.50	-0.76
2MASS J01373857-2618131	r-I	-2.80	-0.15	+0.57	0.00	+0.03	+0.62	-2.18
2MASS J05383296-5904280	r-II	-2.54	...	...	+1.11	+0.76	+1.28	-1.26
$\mu \pm \sigma$ ([X/Y])		-2.20±0.67	...	...	...	+0.28±0.34	+0.80±0.34	-1.40±0.59
Cumulative fraction value		0.95		...	...	0.80	0.85	
<i>CDTG-7 (N = 7, CL = 90.6%)</i>								
2MASS J15204531-1742486	r-I	-2.81	+0.30	+0.54	-2.85	-0.30	+0.35	-2.46
2MASS J20103193-3558546	r-I	-2.56	-0.20	+0.52	+0.18	-0.03	+0.38	-2.18
2MASS J15083385-1459166	r-I	-2.29	-0.65	+0.08	0.00	-0.10	+0.49	-1.80
HD 122956	r-I	-1.70	...	...	+0.18	+0.15	+0.55	-1.15
2MASS J13494713-7423395	r-I	-2.85	+0.10	+0.60	+0.10	+0.05	+0.70	-2.15
2MASS J23342332-2748003*	r-II	-2.46	-0.24	+0.48	+0.39	-0.06	+0.71	-1.75
2MASS J20411424-4654315*	r-II	-2.30	-0.30	+0.32	+0.02	-0.02	+0.88	-1.42
$\mu \pm \sigma$ ([X/Y])		-2.49±0.36	-0.18±0.32	+0.50±0.15	+0.12±0.14	-0.03±0.13	+0.57±0.19	-1.84±0.44
Cumulative fraction value		0.34		0.21	0.14	0.08	0.47	
<i>CDTG-8 (N = 3, CL = 89.9%)</i>								
2MASS J06290787-6709523	r-I	-2.79	-0.44	+0.30	-0.44	-0.17	+0.46	-2.33
2MASS J11301705-1449325	r-I	-2.45	-0.10	-0.09	+0.08	-0.12	+0.50	-1.95
2MASS J06195001-5312114	r-II	-2.04	+0.30	+0.31	+1.00	-0.03	+0.73	-1.31
$\mu \pm \sigma$ ([X/Y])		-2.43±0.31	-0.08±0.30	+0.17±0.19	+0.21±0.60	-0.11±0.06	+0.56±0.12	-1.86±0.42
Cumulative fraction value		0.46		0.51	0.95	0.06	0.35	
<i>CDTG-9 (N = 5, CL = 89.8%)</i>								
BD+42:2667	r-I	-1.48	...	...	...	+0.09	+0.44	-1.04
2MASS J12405721-4051430	r-I	-1.48	+0.05	+0.07	+0.20	+0.22	+0.45	-1.03
HD 179626	r-I	-1.26	...	...	...	-0.02	+0.47	-0.79
2MASS J04182158-2323391	r-I	-1.82	-0.44	+0.07	+0.19	+0.13	+0.48	-1.34
HE 0341-4024	r-I	-1.82	+0.27	+0.27	-0.09	-0.08	+0.69	-1.13
$\mu \pm \sigma$ ([X/Y])		-1.56±0.24	-0.04±0.30	+0.14±0.09	+0.10±0.13	+0.07±0.11	+0.46±0.02	-1.06±0.19
Cumulative fraction value		0.21		0.18	0.29	0.13	0.02	
<i>CDTG-10 (N = 4, CL = 87.9%)</i>								
2MASS J11444480-1128167	r-I	-2.42	-0.35	-0.34	+0.03	-0.29	+0.35	-2.07
BD+09:3223	r-I	-2.20	...	...	+0.16	+0.41	+0.42	-1.78
2MASS J01530024-3417360	r-II	-1.50	+0.01	+0.02	+0.40	+0.09	+0.71	-0.79
2MASS J07352232-4425010	r-II	-1.62	-0.01	0.00	+0.24	+0.39	+0.79	-0.83
$\mu \pm \sigma$ ([X/Y])		-1.93±0.41	-0.12±0.17	-0.11±0.17	+0.20±0.14	+0.21±0.31	+0.57±0.20	-1.35±0.61
Cumulative fraction value		0.61		0.44	0.29	0.74	0.61	
<i>CDTG-11 (N = 6, CL = 87.1%)</i>								
2MASS J02515281-3717316	r-I	-2.33	-0.40	+0.34	-0.33	-0.22	+0.33	-2.00
2MASS J04263084-4058516	r-I	-2.43	-0.60	-0.01	+0.02	+0.07	+0.40	-2.03

Table 4 continued

Table 4 (continued)

Name	Class	[Fe/H]	[C/Fe]	[C/Fe] <sub>c</sub>	[Sr/Fe]	[Ba/Fe]	[Eu/Fe]	[Eu/H]
HE 0430-4901	$r$ -I	-2.72	+0.09	+0.10	-0.58	-0.07	+1.16	-2.13
RAVE J123550.1-313111	$r$ -I / CEMP- $r$	-2.46	+0.61	+1.11	...	+0.27	+0.59	-1.87
BPS BS 16083-0172	$r$ -I	-2.50	+0.34	+0.35	+0.14	-0.37	+0.63	-1.87
2MASS J05311779-5810048	$r$ -I	-2.40	+0.17	+0.18	-0.13	-0.11	+0.65	-1.75
$\mu \pm \sigma$ ([X/Y])		-2.43 $\pm$ 0.10	+0.06 $\pm$ 0.44	+0.20 $\pm$ 0.24	-0.16 $\pm$ 0.27	-0.08 $\pm$ 0.21	+0.59 $\pm$ 0.13	-1.94 $\pm$ 0.13
Cumulative fraction value		0.02		0.56	0.62	0.36	0.72	
<i>CDTG-12</i> ( $N = 6$ , CL = 86.2%)								
2MASS J10223779-3400209	$r$ -I	-2.14	-0.15	+0.15	+0.35	-0.29	+0.37	-1.77
RAVE J215118.3-135937	$r$ -I	-2.10	+0.34	+0.69	+0.56	-0.85	+0.37	-1.73
2MASS J22373316-4341181	$r$ -I	-2.51	-0.21	+0.06	+0.14	-0.06	+0.40	-2.11
2MASS J07161594-5135248	$r$ -I	-1.85	-0.47	+0.13	+0.21	+0.28	+0.46	-1.39
BD+01:2916	$r$ -I	-1.80	...	...	...	+0.07	+0.65	-1.15
HE 2155+0136	$r$ -I	-2.07	0.00	0.00	-0.13	+0.13	+0.68	-1.39
$\mu \pm \sigma$ ([X/Y])		-2.06 $\pm$ 0.24	-0.13 $\pm$ 0.28	+0.09 $\pm$ 0.10	+0.22 $\pm$ 0.24	-0.01 $\pm$ 0.35	+0.44 $\pm$ 0.15	-1.57 $\pm$ 0.34
Cumulative fraction value		0.13		0.14	0.56	0.80	0.36	
<i>CDTG-13</i> ( $N = 9$ , CL = 84.8%)								
2MASS J18562774-7251331	$r$ -I	-2.26	-0.48	+0.24	0.00	-0.01	+0.32	-1.94
2MASS J04565146-3115427	$r$ -I	-2.19	-0.25	+0.45	+0.02	-0.33	+0.34	-1.85
2MASS J04012191-2635058	$r$ -I	-2.20	+0.03	+0.13	+0.13	+0.15	+0.38	-1.82
BD-01:1792	$r$ -I	-1.26	...	...	...	-0.02	+0.38	-0.88
BD-03:5215	$r$ -I	-1.20	...	...	...	+0.46	+0.56	-0.64
2MASS J07393021-5548171	$r$ -I	-1.74	-0.95	-0.40	+0.35	+0.50	+0.63	-1.11
2MASS J19345326-3236567	$r$ -I	-2.17	-0.40	+0.26	+0.15	+0.07	+0.63	-1.54
2MASS J00073817-0345509*	$r$ -II	-2.09	-0.32	+0.17	+0.41	+0.11	+0.73	-1.36
SMSS J183647.89-274333.1*	$r$ -II	-2.48	-0.47	+0.22	+0.18	+0.13	+0.82	-1.66
$\mu \pm \sigma$ ([X/Y])		-2.20 $\pm$ 0.21	-0.38 $\pm$ 0.23	+0.22 $\pm$ 0.10	+0.17 $\pm$ 0.15	+0.11 $\pm$ 0.24	+0.53 $\pm$ 0.18	-1.47 $\pm$ 0.46
Cumulative fraction value		0.03		0.05	0.16	0.37	0.40	
<i>CDTG-14</i> ( $N = 12$ , CL = 84.1%)								
2MASS J17400682-6102129	$r$ -I	-2.24	-0.26	-0.03	+0.16	-0.31	+0.31	-1.93
2MASS J06090353-7122260	$r$ -I	-2.75	-0.08	+0.38	-0.16	-0.45	+0.32	-2.43
2MASS J10044858-2706500*	$r$ -I	-2.40	+0.04	+0.55	0.00	-0.38	+0.41	-1.99
2MASS J15111672+0025252*	$r$ -I	-2.46	-0.90	-0.12	+0.02	-0.18	+0.41	-2.05
G 154-34	$r$ -I	-2.24	...	...	+0.28	-0.10	+0.50	-1.74
2MASS J23251897-0815539	$r$ -I	-2.30	-0.70	-0.24	-0.42	-0.33	+0.55	-1.75
2MASS J08155667-2204105	$r$ -I	-1.85	-0.13	-0.03	+0.11	+0.21	+0.57	-1.28
2MASS J00541965-0611555*	$r$ -I	-2.32	-0.20	+0.50	+0.26	-0.21	+0.59	-1.73
BPS CS 22940-0121*	$r$ -I	-2.91	< +0.01	< +0.04	+0.36	+0.21	+0.61	-2.30
HE 2206-2245*	$r$ -I	-2.73	+0.21	+0.22	-0.05	-0.11	+0.62	-2.11
2MASS J12091322-1415313*	$r$ -II	-2.11	-0.50	+0.20	-0.01	+0.11	+0.81	-1.30
SMSS J051008.62-372019.8	$r$ -II	-3.20	+0.56	+0.57	+0.41	+0.75	+0.95	-2.25
$\mu \pm \sigma$ ([X/Y])		-2.39 $\pm$ 0.38	-0.19 $\pm$ 0.42	+0.20 $\pm$ 0.29	+0.09 $\pm$ 0.23	-0.13 $\pm$ 0.30	+0.54 $\pm$ 0.18	-1.94 $\pm$ 0.36
Cumulative fraction value		0.24		0.72	0.32	0.61	0.36	
<i>CDTG-15</i> ( $N = 6$ , CL = 83.2%)								
HD 119516	$r$ -I	-2.26	< -0.42	< +0.28	+0.26	-0.02	+0.34	-1.92
2MASS J22302641-1949527*	$r$ -I	-2.28	-0.20	+0.48	-0.28	-0.10	+0.40	-1.88
HD 175305	$r$ -I	-1.50	...	...	+0.13	+0.12	+0.44	-1.06
BD+30:2611	$r$ -I	-1.40	...	...	...	+0.08	+0.45	-0.95
2MASS J03154102-7626329	$r$ -I	-2.71	-0.10	+0.55	-0.22	-0.01	+0.50	-2.21
2MASS J00021668-2453494*	$r$ -I	-1.81	-0.88	-0.57	+0.59	+0.10	+0.52	-1.29
$\mu \pm \sigma$ ([X/Y])		-2.00 $\pm$ 0.49	-0.39 $\pm$ 0.35	+0.15 $\pm$ 0.51	+0.10 $\pm$ 0.33	+0.03 $\pm$ 0.08	+0.44 $\pm$ 0.06	-1.56 $\pm$ 0.50
Cumulative fraction value		0.71		0.96	0.76	0.04	0.06	
<i>CDTG-16</i> ( $N = 8$ , CL = 82.7%)								
2MASS J08134364-2332528	$r$ -I	-1.72	-0.40	+0.10	+0.10	+0.28	+0.32	-1.40
2MASS J10063414-7030212	$r$ -I	-2.20	+0.19	+0.33	-0.21	+0.03	+0.39	-1.81
2MASS J00452379-2112161	$r$ -I	-2.63	-0.15	+0.50	-0.10	-0.25	+0.40	-2.23
RAVE J192819.9-633935*	$r$ -I / CEMP- $r$	-2.38	+0.17	+0.74	...	+0.09	+0.45	-1.93

Table 4 continued

Table 4 (continued)

Name	Class	[Fe/H]	[C/Fe]	[C/Fe] <sub>c</sub>	[Sr/Fe]	[Ba/Fe]	[Eu/Fe]	[Eu/H]
2MASS J02265832-0749596	r-I	-1.94	-0.05	-0.04	+0.23	+0.08	+0.56	-1.38
BPS CS 30306-0132	r-II	-2.42	+0.34	+0.35	+0.14	+0.22	+0.85	-1.57
2MASS J22190836-2333467	r-II	-2.56	-0.13	+0.39	+0.27	+0.24	+0.87	-1.69
BPS CS 22945-0017	r-II / CEMP-r	-2.89	+1.78	+1.78	+0.39	+0.49	+1.13	-1.76
$\mu \pm \sigma$ ([X/Y])		-2.38±0.38	+0.01±0.28	+0.34±0.32	+0.13±0.21	+0.16±0.20	+0.55±0.30	-1.71±0.27
Cumulative fraction value		0.35		0.81	0.35	0.24	0.82	
<i>CDTG-17 (N = 3, CL = 79.4%)</i>								
BD+26:2251	r-I	-1.10	...	...	...	+0.01	+0.48	-0.62
2MASS J07052028-3343242	r-I	-2.24	-0.36	+0.27	+0.03	-0.17	+0.62	-1.62
RAVE J040618.2-030525	r-II	-1.46	+0.54	+0.56	...	+0.98	+1.17	-0.29
$\mu \pm \sigma$ ([X/Y])		-1.60±0.48	...	...	...	+0.27±0.51	+0.76±0.30	-0.84±0.57
Cumulative fraction value		0.77		...	...	0.94	0.79	
<i>CDTG-18 (N = 4, CL = 79.3%)</i>								
HD 108577	r-I	-2.36	...	...	...	-0.17	+0.36	-2.00
2MASS J15075699-0659593	r-I	-2.07	-0.20	+0.44	+0.12	-0.10	+0.36	-1.71
2MASS J05030025-7601462	r-I	-2.17	-0.20	+0.40	0.00	-0.21	+0.40	-1.77
2MASS J23362202-5607498*	r-II	-2.06	-0.05	+0.47	> +1.00	+0.24	+1.14	-0.92
$\mu \pm \sigma$ ([X/Y])		-2.12±0.13	-0.15±0.07	+0.44±0.03	...	-0.16±0.11	+0.37±0.02	-1.81±0.36
Cumulative fraction value		0.10		0.02	...	0.17	0.04	
<i>CDTG-19 (N = 4, CL = 78.0%)</i>								
2MASS J23475942-5701184	r-I	-2.24	-0.55	+0.20	-0.08	-0.07	+0.45	-1.79
2MASS J20233743-1659533	r-I	-2.60	-0.57	-0.03	+0.23	-0.07	+0.50	-2.10
2MASS J20504869-3355289*	r-I	-2.64	-0.34	+0.38	+0.24	-0.06	+0.62	-2.02
2MASS J21091825-1310062	r-II	-2.40	-0.28	+0.27	+0.14	+0.12	+1.25	-1.15
$\mu \pm \sigma$ ([X/Y])		-2.48±0.17	-0.44±0.14	+0.23±0.16	+0.20±0.12	-0.07±0.01	+0.52±0.12	-1.94±0.36
Cumulative fraction value		0.16		0.37	0.23	0.00	0.38	
<i>CDTG-20 (N = 5, CL = 77.3%)</i>								
2MASS J09261133-1526232	r-I	-1.70	+0.01	+0.03	+0.06	+0.28	+0.43	-1.27
2MASS J13511539-7340363	r-I	-2.49	0.00	+0.01	-0.20	+0.17	+0.50	-1.99
2MASS J13164824-2743351	r-I	-1.61	-0.05	-0.03	+0.26	+0.01	+0.54	-1.07
2MASS J07501424-4123454	r-I	-1.89	+0.17	+0.18	+0.15	+0.27	+0.59	-1.30
2MASS J19192768-5959140	r-I	-2.62	-0.60	+0.13	-0.05	+0.25	+0.60	-2.02
$\mu \pm \sigma$ ([X/Y])		-2.00±0.48	+0.01±0.09	+0.05±0.09	+0.05±0.17	+0.25±0.06	+0.54±0.07	-1.43±0.49
Cumulative fraction value		0.70		0.11	0.33	0.06	0.12	
<i>CDTG-21 (N = 4, CL = 76.2%)</i>								
RAVE J074824.3-483141	r-I	-2.13	0.00	+0.32	+0.66	-0.20	+0.45	-1.68
2MASS J12102259-4902190	r-I	-1.69	-0.05	+0.33	+0.15	+0.23	+0.58	-1.11
HD 135148	r-I	-1.70	...	...	...	+0.30	+0.58	-1.12
2MASS J01565634-1402108*	r-II	-2.08	-0.27	+0.37	+0.10	-0.11	+0.76	-1.32
$\mu \pm \sigma$ ([X/Y])		-1.90±0.22	-0.11±0.12	+0.34±0.02	+0.30±0.25	+0.06±0.23	+0.58±0.12	-1.22±0.24
Cumulative fraction value		0.22		0.01	0.63	0.51	0.36	
<i>CDTG-22 (N = 4, CL = 75.7%)</i>								
2MASS J19050116-1949280	r-I	-1.89	-0.43	+0.21	-0.01	-0.08	+0.36	-1.53
2MASS J02570028-3024374	r-I	-2.05	+0.15	+0.33	-0.03	+0.03	+0.55	-1.50
2MASS J22161170-5319492	r-I	-2.51	-0.15	+0.31	+0.20	+0.31	+0.59	-1.92
BPS CS 29529-0054	r-II	-2.55	+0.58	+0.58	-0.10	-0.02	+0.90	-1.65
$\mu \pm \sigma$ ([X/Y])		-2.26±0.31	+0.02±0.40	+0.31±0.14	-0.03±0.11	-0.02±0.13	+0.58±0.21	-1.59±0.17
Cumulative fraction value		0.39		0.30	0.20	0.22	0.64	

Table 4 continued

Table 4 (continued)

Name	Class	[Fe/H]	[C/Fe]	[C/Fe] <sub>c</sub>	[Sr/Fe]	[Ba/Fe]	[Eu/Fe]	[Eu/H]
<i>CDTG-23</i> ( $N = 4$ , CL = 75.4%)								
2MASS J12571667–4335318	$r$ -I	-1.96	-0.05	+0.05	+0.05	+0.15	+0.30	-1.66
2MASS J08032084–5856521	$r$ -I	-1.74	+0.01	+0.03	+0.24	+0.26	+0.49	-1.25
2MASS J15271353–2336177	$r$ -I	-2.15	+0.33	+0.33	+0.35	-0.03	+0.70	-1.45
BPS CS 22886–0012*	$r$ -II	-2.88	-0.16	-0.16	+0.31	+0.14	+0.85	-2.03
$\mu \pm \sigma$ ([X/Y])		-2.05±0.44	-0.03±0.19	+0.05±0.19	+0.28±0.12	+0.14±0.11	+0.59±0.22	-1.58±0.31
Cumulative fraction value		0.67		0.47	0.23	0.17	0.67	
<i>CDTG-24</i> ( $N = 4$ , CL = 61.4%)								
2MASS J05521578–3953184	$r$ -I	-2.37	-0.22	+0.23	+0.23	-0.04	+0.41	-1.96
G 214–1	$r$ -I	-2.29	-0.12	-0.12	+0.46	+0.27	+0.56	-1.73
HE 0516–3820	$r$ -I	-2.51	+0.35	+0.36	+0.23	+0.06	+0.64	-1.87
2MASS J01425445–0904162	$r$ -II	-1.73	-0.55	-0.15	+0.30	+0.35	+0.83	-0.90
$\mu \pm \sigma$ ([X/Y])		-2.38±0.26	-0.16±0.34	+0.07±0.24	+0.25±0.09	+0.16±0.16	+0.61±0.16	-1.85±0.18
Cumulative fraction value		0.31		0.63	0.14	0.32	0.50	
<i>CDTG-25</i> ( $N = 3$ , CL = 61.2%)								
2MASS J14191395–0844410	$r$ -I	-2.08	-0.07	+0.22	+0.34	-0.15	+0.34	-1.74
2MASS J23285061–0432368	$r$ -I	-1.99	+0.05	+0.41	-0.10	0.00	+0.53	-1.46
2MASS J09574607–3923072	$r$ -I	-1.73	-0.06	+0.25	+0.22	+0.21	+0.55	-1.18
$\mu \pm \sigma$ ([X/Y])		-1.93±0.15	-0.03±0.05	+0.29±0.08	+0.15±0.19	+0.02±0.15	+0.47±0.09	-1.46±0.23
Cumulative fraction value		0.13		0.14	0.46	0.31	0.26	
<i>CDTG-26</i> ( $N = 3$ , CL = 54.4%)								
HE 0057–4541*	$r$ -I	-2.40	+0.44	+0.45	+0.21	-0.06	+0.55	-1.85
2MASS J03084611–4747083*	$r$ -I	-1.56	+0.20	+0.22	+0.09	+0.18	+0.55	-1.01
BPS CS 22945–0056	$r$ -I	-2.82	< +1.60	< +1.75	-0.09	-0.40	+0.68	-2.14
$\mu \pm \sigma$ ([X/Y])		-2.26±0.52	...	...	+0.07±0.12	-0.09±0.24	+0.59±0.06	-1.67±0.48
Cumulative fraction value		0.83		...	0.26	0.59	0.12	
<i>CDTG-27</i> ( $N = 3$ , CL = 37.4%)								
2MASS J04315411–0632100	$r$ -I	-2.18	-0.05	-0.05	+0.05	-0.10	+0.30	-1.88
2MASS J00532781–0253169*	$r$ -I	-2.16	-0.30	+0.40	-0.05	-0.24	+0.39	-1.77
2MASS J15211026–0607566	$r$ -II	-2.00	-0.20	+0.34	-0.18	+0.10	+0.93	-1.07
$\mu \pm \sigma$ ([X/Y])		-2.11±0.08	-0.18±0.10	+0.23±0.20	-0.06±0.09	-0.08±0.14	+0.54±0.28	-1.57±0.36
Cumulative fraction value		0.04		0.56	0.16	0.28	0.76	
<i>CDTG-28</i> ( $N = 4$ , CL = 36.5%)								
2MASS J12292696–0442325	$r$ -I	-2.23	-0.40	+0.28	0.00	-0.22	+0.46	-1.77
BPS BS 16089–0013	$r$ -I	-2.70	+0.40	+0.66	+0.16	-0.13	+0.46	-2.24
2MASS J17060555+0412354*	$r$ -I	-2.71	-0.10	+0.60	-0.57	+0.05	+0.50	-2.21
2MASS J00002416–1107454*	$r$ -I	-2.43	-0.27	+0.30	-0.04	-0.24	+0.51	-1.92
$\mu \pm \sigma$ ([X/Y])		-2.54±0.22	-0.18±0.32	+0.46±0.18	+0.03±0.25	-0.17±0.12	+0.48±0.02	-2.04±0.21
Cumulative fraction value		0.23		0.45	0.60	0.20	0.04	
<i>CDTG-29</i> ( $N = 5$ , CL = 35.9%)								
2MASS J19310426–3707397*	$r$ -I	-2.21	-0.45	+0.05	-0.70	-0.40	+0.40	-1.81
2MASS J17541561–5148268*	$r$ -I	-2.14	-0.60	-0.11	-0.20	-0.05	+0.50	-1.64
2MASS J18294359–4924253	$r$ -II	-1.22	-0.61	-0.22	-0.11	+0.29	+0.89	-0.33
SMSS J183225.29–334938.4*	$r$ -II	-1.74	-0.22	-0.20	+0.26	+0.50	+1.08	-0.66
SMSS J183128.71–341018.4*	$r$ -II	-1.83	+0.01	+0.03	+0.97	+0.53	+1.25	-0.58
$\mu \pm \sigma$ ([X/Y])		-1.84±0.36	-0.41±0.26	-0.09±0.12	-0.02±0.59	+0.23±0.38	+0.83±0.34	-0.83±0.75
Cumulative fraction value		0.45		0.18	0.97	0.85	0.88	
<i>CDTG-30</i> ( $N = 3$ , CL = 12.4%)								

Table 4 continued

Table 4 (continued)

Name	Class	[Fe/H]	[C/Fe]	[C/Fe] <sub>c</sub>	[Sr/Fe]	[Ba/Fe]	[Eu/Fe]	[Eu/H]
2MASS J16592172–6827199*	r-I	−2.80	−0.60	−0.05	−0.30	−0.20	+0.40	−2.40
2MASS J07411443–4339360	r-I	−1.74	+0.05	+0.07	+0.02	+0.13	+0.50	−1.24
2MASS J15260106–0911388	r-II	−2.83	−0.82	−0.06	+0.90	+0.69	+1.70	−1.13
$\mu \pm \sigma$ ([X/Y])		$-2.46 \pm 0.51$	$-0.46 \pm 0.37$	$-0.01 \pm 0.06$	$+0.21 \pm 0.51$	$+0.21 \pm 0.37$	$+0.87 \pm 0.59$	$-1.59 \pm 0.57$
Cumulative fraction value		0.81		0.07	0.92	0.84	0.98	

NOTE—Single (\*) mark indicates the 27 stars with relative distance errors in the range  $20\% < \epsilon < 30\%$ . See text for details.

NOTE—Means ( $\mu$ ), standard deviations ( $\sigma$ ), and cumulative fraction values for the elemental abundances in each CDTG with at least 3 measured abundances are listed. When the number of available measured elemental abundances is 4 or more, biweight estimates of these quantities are reported, in order to decrease the influence of potential outliers.

Table 1. Positions, Magnitudes, Distances, Radial Velocities, and Proper Motions for the Initial Sample

Name	RA	DEC	V mag	$d_{Gaia}$ (err)	$d_{SH}$ (err)	Rad Vel	PM <sub>RA</sub>	PM <sub>DEC</sub>
	(J2000)	(J2000)		(kpc)	(kpc)	(km s <sup>−1</sup> )	(mas yr <sup>−1</sup> )	(mas yr <sup>−1</sup> )
2MASS J00002259–1302275	00:00:22.60	−13:02:27.5	12.88	5.71 (1.54)*	4.78 (1.47)**	−104.4	−2.61	−9.45
2MASS J00002416–1107454	00:00:24.16	−11:07:45.4	12.04	3.76 (0.68)	3.51 (0.79)*	−110.4	−0.63	−23.48
SMSS J000113.96–363337.9	00:01:13.99	−36:33:38.1	13.91	8.02 (2.24)*	7.28 (2.03)*	243.3 <sup>a</sup>	8.35	−5.16
HD 224930	00:02:11.18	+27:04:40.0	5.67	0.01 (0.00)	0.01 (0.00)	−35.6	723.11	−933.75
2MASS J00021668–2453494	00:02:16.70	−24:53:49.5	13.49	4.86 (0.74)	5.11 (1.36)*	80.1	−3.61	−8.09
BPS CS 22957–0036	00:03:31.20	−04:44:19.0	14.41	1.26 (0.09)	1.20 (0.15)	−154.5 <sup>b</sup>	38.64	−22.27
HD 20	00:05:15.48	−27:16:18.8	9.01	0.50 (0.01)	0.50 (0.02)	−56.5	132.43	−39.92
2MASS J00073817–0345509	00:07:38.17	−03:45:50.9	11.65	2.86 (0.56)	2.72 (0.65)*	−146.3	2.30	−16.04
BPS CS 31070–0073	00:08:51.83	+05:26:17.1	14.53	...	1.44 (0.57)**	−86.0 <sup>c</sup>	19.87	−12.43
2MASS J00093394–1857008	00:09:33.94	−18:57:00.8	11.18	1.26 (0.08)	1.29 (0.08)	−71.4	39.33	−37.43
2MASS J00101758–1735387	00:10:17.52	−17:35:38.4	11.50	0.68 (0.02)	0.68 (0.02)	191.8	34.31	−54.97
HE 0010–3422	00:12:55.90	−34:05:44.2	15.48	...	7.27 (5.23)**	158.8 <sup>d</sup>	3.54	−8.00
2MASS J00154806–6253207	00:15:48.06	−62:53:20.7	11.03	2.06 (0.10)	2.07 (0.12)	207.8	24.90	−8.70
2MASS J00172430–3333151	00:17:24.30	−33:33:15.1	12.24	2.64 (0.30)	2.49 (0.41)	−18.3	−4.71	−9.24
2MASS J00182832–3900338	00:18:28.32	−39:00:33.8	11.21	3.10 (0.36)	3.05 (0.41)	350.8	5.12	−4.30
BPS CS 22882–0001	00:20:25.30	−31:39:04.0	14.77	6.27 (1.49)*	8.04 (1.44)	28.0 <sup>e</sup>	8.80	−6.72
2MASS J00223225–4839449	00:22:32.25	−48:39:44.9	11.06	3.90 (0.45)	4.01 (0.62)	245.0	18.19	−14.02
BPS CS 30339–0052	00:22:50.14	−34:07:20.7	15.34	...	5.00 (4.31)**	33.0 <sup>f</sup>	0.66	−0.67
BPS CS 29497–0004	00:28:06.92	−26:03:04.2	14.01	3.41 (0.35)	3.58 (0.81)*	105.1 <sup>g</sup>	9.47	0.39
2MASS J00305267–1007042	00:30:52.67	−10:07:04.2	12.77	3.60 (0.56)	3.26 (0.91)*	−74.2	19.79	−4.55
2MASS J00400685–4325183	00:40:06.90	−43:25:18.4	12.32	7.93 (1.73)*	7.33 (1.29)	47.1	3.05	−8.35
2MASS J00405260–5122491	00:40:52.60	−51:22:49.1	11.21	0.15 (0.00)	0.15 (0.00)	123.3	211.49	−197.32
2MASS J00413026–4058547	00:41:30.26	−40:58:54.7	11.29	3.22 (0.36)	3.21 (0.44)	354.8	2.64	−4.37
2MASS J00442897–1017497	00:44:28.97	−10:17:49.7	10.82	2.02 (0.30)	2.01 (0.33)	−3.0	8.76	−28.59
2MASS J00452379–2112161	00:45:23.80	−21:12:16.1	12.52	3.43 (0.48)	3.28 (0.64)	21.2	4.41	−6.56
2MASS J00452879–5846450	00:45:28.79	−58:46:45.0	10.66	2.28 (0.11)	2.29 (0.14)	187.9	−16.32	−23.26
2MASS J00453930–7457294	00:45:39.30	−74:57:29.6	11.71	1.61 (0.06)	1.63 (0.06)	−31.8	3.29	−46.99
HE 0045–2430	00:47:40.58	−24:14:02.1	15.09	3.86 (0.49)	3.95 (1.59)**	144.5 <sup>h</sup>	22.40	−7.50
2MASS J00482431–1041309	00:48:24.31	−10:41:30.9	10.78	2.21 (0.18)	2.22 (0.21)	−92.2	−2.64	−25.35
2MASS J00512646–1053170	00:51:26.50	−10:53:17.3	10.85	0.26 (0.00)	0.26 (0.00)	56.5	−32.03	−181.34
2MASS J00524174–0902235	00:52:41.76	−09:02:24.0	11.03	1.58 (0.09)	1.52 (0.10)	−238.1	−15.59	−24.72
2MASS J00532781–0253169	00:53:27.81	−02:53:16.9	10.39	2.91 (0.97)**	2.76 (0.73)*	−195.3	18.03	−16.96
2MASS J00541965–0611555	00:54:19.65	−06:11:55.5	13.01	4.33 (0.68)	4.31 (1.19)*	−131.5	8.07	−5.92
HE 0057–4541	00:59:59.28	−45:24:53.6	14.90	5.57 (0.71)	6.49 (1.75)*	13.4 <sup>i</sup>	0.16	−12.66
BPS CS 22953–0003	01:02:15.86	−61:43:45.8	13.69	3.79 (0.20)	3.96 (0.35)	209.0 <sup>e</sup>	−3.82	−15.77
BPS CS 22183–0031	01:09:05.08	−04:43:21.2	13.58	2.53 (0.19)	2.51 (0.34)	8.0 <sup>e</sup>	21.52	−9.34
2MASS J01094330–5907230	01:09:43.30	−59:07:23.0	12.22	3.14 (0.22)	3.14 (0.29)	60.9	15.59	−10.68
2MASS J01165010–6307441	01:16:50.16	−63:07:44.4	11.66	1.37 (0.04)	1.39 (0.05)	122.7	42.58	−13.24
2MASS J01202234–5425582	01:20:22.30	−54:25:58.2	12.62	1.42 (0.04)	1.44 (0.07)	68.7	33.02	3.87
2MASS J01213447–2528002	01:21:34.47	−25:28:00.2	11.72	4.87 (0.74)	4.67 (0.84)	19.6	8.08	−14.14
2MASS J01293113–1600454	01:29:31.10	−16:00:45.5	11.63	1.87 (0.16)	1.77 (0.17)	139.1	11.74	−42.71
2MASS J01311599–4016510	01:31:15.99	−40:16:51.0	11.10	2.18 (0.14)	2.20 (0.17)	−58.2	8.77	−26.32
2MASS J01321981–3040512	01:32:19.81	−30:40:51.2	10.73	0.46 (0.01)	0.46 (0.01)	−98.0	38.82	−77.41
2MASS J01371888–1729037	01:37:18.88	−17:29:03.7	9.75	2.10 (0.24)	2.16 (0.27)	−209.9	6.22	−25.56
2MASS J01373857–2618131	01:37:38.57	−26:18:13.1	11.40	1.95 (0.13)	1.94 (0.16)	−92.0	6.91	−15.11
2MASS J01425422–5032488	01:42:54.20	−50:32:48.9	11.32	0.66 (0.01)	0.67 (0.01)	157.6	60.70	−100.94
2MASS J01425445–0904162	01:42:54.45	−09:04:16.2	9.56	1.38 (0.11)	1.39 (0.14)	−64.8	4.49	−20.75
2MASS J01493760–4551222	01:49:37.60	−45:51:22.2	10.38	1.39 (0.05)	1.40 (0.06)	70.1	51.07	−5.10
2MASS J01530024–3417360	01:53:00.20	−34:17:36.1	9.53	0.30 (0.00)	0.30 (0.00)	22.7	22.19	−212.06
2MASS J01553180–4919420	01:55:31.80	−49:19:41.8	12.74	1.60 (0.07)	1.61 (0.12)	130.8 <sup>h</sup>	24.27	24.76
2MASS J01555066–6400155	01:55:50.70	−64:00:15.7	12.65	4.34 (0.45)	4.14 (0.57)	240.0	11.47	−11.28

Table 1 continued

















Table 1 (continued)

Name	RA	DEC	V mag	$d_{Gaia}$ (err)	$d_{SH}$ (err)	Rad Vel	PM <sub>RA</sub>	PM <sub>DEC</sub>
	(J2000)	(J2000)		(kpc)	(kpc)	(km s <sup>-1</sup> )	(mas yr <sup>-1</sup> )	(mas yr <sup>-1</sup> )
HE 2347–1334	23:50:26.83	–13:17:39.2	12.64	...	3.65 (2.42)**	–54.2	1.08	–5.66
BPS CS 29499–0058	23:52:15.90	–25:58:18.7	13.74	1.08 (0.03)	1.08 (0.05)	143.0 <sup>e</sup>	–6.75	–55.16
BPS CS 22945–0058	23:52:37.80	–66:05:01.7	14.93	1.57 (0.06)	1.60 (0.13)	23.4 <sup>b</sup>	30.74	–22.23
BPS CS 22945–0056	23:53:19.80	–65:29:39.5	14.04	5.66 (0.59)	6.11 (0.88)	222.0 <sup>e</sup>	–5.49	–10.80
BPS CS 29517–0025	23:54:28.84	–13:59:56.7	14.17	4.33 (0.68)	5.77 (1.07)	–186.0 <sup>e</sup>	10.21	–6.74
SDSS J235718.91–005247.8	23:57:18.96	–00:52:50.1	15.66	0.52 (0.01)	0.55 (0.03)	–9.5 <sup>w</sup>	49.75	–172.41

NOTE—Sources for (non-*Gaia*) radial-velocity information:

NOTE—<sup>a</sup> Jacobson et al. (2015), <sup>b</sup> Roederer et al. (2014), <sup>c</sup> T. C. Beers, private comm., <sup>d</sup> Hansen et al. (2015), <sup>e</sup> Beers et al. (1992), <sup>f</sup> Beers & Sommer-Larsen (1995), <sup>g</sup> Barklem et al. (2005), <sup>h</sup> Ezzeddine et al. (2020), <sup>i</sup> Hansen et al. (2018), <sup>j</sup> Aoki et al. (2002), <sup>k</sup> Bonifacio et al. (2009), <sup>l</sup> Kunder et al. (2017), <sup>m</sup> Xing et al. (2019), <sup>n</sup> Carrera et al. (2013), <sup>o</sup> Cohen et al. (2013), <sup>p</sup> Holmbeck et al. (2020), <sup>q</sup> Aoki et al. (2005), <sup>r</sup> Frebel et al. (2006), <sup>s</sup> Sakari et al. (2018), <sup>t</sup> Howes et al. (2015), <sup>u</sup> Howes et al. (2016), <sup>v</sup> Allende Prieto et al. (2000), <sup>w</sup> Aoki et al. (2010)

NOTE—Source for (non-*Gaia*) proper motions: <sup>1</sup> Kharchenko & Roeser (2009)

NOTE—Single (\*) and double (\*\*) marks indicate stars with relative distance errors in the range  $20\% < \epsilon \leq 30\%$ , and  $\epsilon > 30\%$ , respectively.

## REFERENCES

- Abate, C., Pols, O. R., Stancliffe, R. J., et al. 2015, *A&A*, 581, A62, doi: [10.1051/0004-6361/201526200](https://doi.org/10.1051/0004-6361/201526200)
- Abbott, B. P., Abbott, R., Abbott, T. D., et al. 2017, *PhRvL*, 119, 161101, doi: [10.1103/PhysRevLett.119.161101](https://doi.org/10.1103/PhysRevLett.119.161101)
- Abomalima, A., & Frebel, A. 2018, *ApJS*, 238, 36, doi: [10.3847/1538-4365/aadfe9](https://doi.org/10.3847/1538-4365/aadfe9)
- Aguado, D. S., Myeong, G. C., Belokurov, V., et al. 2021, *MNRAS*, 500, 889, doi: [10.1093/mnras/staa3250](https://doi.org/10.1093/mnras/staa3250)
- Allen, D. M., Ryan, S. G., Rossi, S., Beers, T. C., & Tsangarides, S. A. 2012, *A&A*, 548, A34, doi: [10.1051/0004-6361/201015615](https://doi.org/10.1051/0004-6361/201015615)
- Allende Prieto, C., Rebolo, R., García López, R. J., et al. 2000, *AJ*, 120, 1516, doi: [10.1086/301533](https://doi.org/10.1086/301533)
- An, D., & Beers, T. C. 2020, *ApJ*, 897, 39, doi: [10.3847/1538-4357/ab8d39](https://doi.org/10.3847/1538-4357/ab8d39)
- Anders, F., Khalatyan, A., Chiappini, C., et al. 2019, *A&A*, 628, A94, doi: [10.1051/0004-6361/201935765](https://doi.org/10.1051/0004-6361/201935765)
- Aoki, W., Beers, T. C., Honda, S., & Carollo, D. 2010, *ApJ*, 723, L201, doi: [10.1088/2041-8205/723/2/L201](https://doi.org/10.1088/2041-8205/723/2/L201)
- Aoki, W., Norris, J. E., Ryan, S. G., Beers, T. C., & Ando, H. 2002, *PASJ*, 54, 933, doi: [10.1093/pasj/54.6.933](https://doi.org/10.1093/pasj/54.6.933)
- Aoki, W., Honda, S., Beers, T. C., et al. 2005, *ApJ*, 632, 611, doi: [10.1086/432862](https://doi.org/10.1086/432862)
- Arcones, A., Scheck, L., & Janka, H.-T. 2006, *A&A*, 467, 231, doi: [10.1051/0004-6361:20066983](https://doi.org/10.1051/0004-6361:20066983)
- Arnould, M., Goriely, S., & Takahashi, K. 2007, *Phys. Rept.*, 450, 97, doi: [10.1016/j.physrep.2007.06.002](https://doi.org/10.1016/j.physrep.2007.06.002)
- Arthur, D., & Vassilvitskii, S. 2007, in Proceedings of the Eighteenth Annual ACM-SIAM Symposium on Discrete Algorithms, SODA '07 (USA: Society for Industrial and Applied Mathematics), 1027–1035
- Barklem, P. S., Christlieb, N., Beers, T. C., et al. 2005, *A&A*, 439, 129, doi: [10.1051/0004-6361:20052967](https://doi.org/10.1051/0004-6361:20052967)
- Beers, T. C., & Christlieb, N. 2005, *ARA&A*, 43, 531, doi: [10.1146/annurev.astro.42.053102.134057](https://doi.org/10.1146/annurev.astro.42.053102.134057)
- Beers, T. C., Flynn, K., & Gebhardt, K. 1990, *AJ*, 100, 32, doi: [10.1086/115487](https://doi.org/10.1086/115487)
- Beers, T. C., Preston, G. W., & Shectman, S. A. 1985, *AJ*, 90, 2089, doi: [10.1086/113917](https://doi.org/10.1086/113917)
- . 1992, *AJ*, 103, 1987, doi: [10.1086/116207](https://doi.org/10.1086/116207)
- Beers, T. C., & Sommer-Larsen, J. 1995, *ApJS*, 96, 175, doi: [10.1086/192117](https://doi.org/10.1086/192117)
- Belokurov, V., Erkal, D., Evans, N. W., Koposov, S. E., & Deason, A. J. 2018, *MNRAS*, 478, 611, doi: [10.1093/mnras/sty982](https://doi.org/10.1093/mnras/sty982)
- Binney, J. 2012, *MNRAS*, 426, 1324, doi: [10.1111/j.1365-2966.2012.21757.x](https://doi.org/10.1111/j.1365-2966.2012.21757.x)
- Bisterzo, S., Gallino, R., Straniero, O., Cristallo, S., & Käppeler, F. 2010, *MNRAS*, 404, 1529, doi: [10.1111/j.1365-2966.2010.16369.x](https://doi.org/10.1111/j.1365-2966.2010.16369.x)
- Bonifacio, P., Spite, M., Cayrel, R., et al. 2009, *A&A*, 501, 519, doi: [10.1051/0004-6361/200810610](https://doi.org/10.1051/0004-6361/200810610)
- Brauer, K., Ji, A. P., Frebel, A., et al. 2019, *ApJ*, 871, 247, doi: [10.3847/1538-4357/aafafb](https://doi.org/10.3847/1538-4357/aafafb)
- Burbidge, E. M., Burbidge, G. R., Fowler, W. A., & Hoyle, F. 1957, *Reviews of Modern Physics*, 29, 547, doi: [10.1103/RevModPhys.29.547](https://doi.org/10.1103/RevModPhys.29.547)

- Burris, D. L., Pilachowski, C. A., Armand roff, T. E., et al. 2000, *ApJ*, 544, 302, doi: [10.1086/317172](https://doi.org/10.1086/317172)
- Cain, M., Frebel, A., Gull, M., et al. 2018, *ApJ*, 864, 43, doi: [10.3847/1538-4357/aad37d](https://doi.org/10.3847/1538-4357/aad37d)
- Cain, M., Frebel, A., Ji, A. P., et al. 2020, *ApJ*, 898, 40, doi: [10.3847/1538-4357/ab97ba](https://doi.org/10.3847/1538-4357/ab97ba)
- Cameron, A. G. W. 1957, *PASP*, 69, 201, doi: [10.1086/127051](https://doi.org/10.1086/127051)
- Carollo, D., Chiba, M., Ishigaki, M., et al. 2019, *ApJ*, 887, 22, doi: [10.3847/1538-4357/ab517c](https://doi.org/10.3847/1538-4357/ab517c)
- Carrera, R., Pancino, E., Gallart, C., & del Pino, A. 2013, *MNRAS*, 434, 1681, doi: [10.1093/mnras/stt1126](https://doi.org/10.1093/mnras/stt1126)
- Cayrel, R., Depagne, E., Spite, M., et al. 2004, *A&A*, 416, 1117, doi: [10.1051/0004-6361:20034074](https://doi.org/10.1051/0004-6361:20034074)
- Choplan, A., Hirschi, R., Meynet, G., et al. 2018, *Astronomy & Astrophysics*, 618, A133, doi: [10.1051/0004-6361/201833283](https://doi.org/10.1051/0004-6361/201833283)
- Christlieb, N., Gustafsson, B., Korn, A. J., et al. 2004, *ApJ*, 603, 708, doi: [10.1086/381237](https://doi.org/10.1086/381237)
- Christlieb, N., Schörck, T., Frebel, A., et al. 2008, *A&A*, 484, 721, doi: [10.1051/0004-6361:20078748](https://doi.org/10.1051/0004-6361:20078748)
- Cohen, J. G., Christlieb, N., Thompson, I., et al. 2013, *ApJ*, 778, 56, doi: [10.1088/0004-637x/778/1/56](https://doi.org/10.1088/0004-637x/778/1/56)
- Comaniciu, D., & Meer, P. 2002, *IEEE Transactions on Pattern Analysis and Machine Intelligence*, 24, 603
- Côté, B., Eichler, M., Arcones, A., et al. 2019, *ApJ*, 875, 106, doi: [10.3847/1538-4357/ab10db](https://doi.org/10.3847/1538-4357/ab10db)
- Cowan, J. J., & Rose, W. K. 1977, *ApJ*, 212, 149, doi: [10.1086/155030](https://doi.org/10.1086/155030)
- Cowan, J. J., Sneden, C., Burles, S., et al. 2002, *ApJ*, 572, 861, doi: [10.1086/340347](https://doi.org/10.1086/340347)
- Dardelet, L., Ritter, C., Prado, P., et al. 2014, in *XIII Nuclei in the Cosmos (NIC XIII)*, 145
- Denissenkov, P. A., Herwig, F., Battino, U., et al. 2017, *ApJ*, 834, L10, doi: [10.3847/2041-8213/834/2/l10](https://doi.org/10.3847/2041-8213/834/2/l10)
- Drout, M. R., Piro, A. L., Shappee, B. J., et al. 2017, *Science*, 358, 1570, doi: [10.1126/science.aaq0049](https://doi.org/10.1126/science.aaq0049)
- Everall, A., Evans, N. W., Belokurov, V., & Schönrich, R. 2019, *MNRAS*, 489, 910, doi: [10.1093/mnras/stz2217](https://doi.org/10.1093/mnras/stz2217)
- Ezzeddine, R., Rasmussen, K., Frebel, A., et al. 2020, *ApJ*, 898, 150, doi: [10.3847/1538-4357/ab9d1a](https://doi.org/10.3847/1538-4357/ab9d1a)
- Frebel, A. 2018, *Annual Review of Nuclear and Particle Science*, 68, 237, doi: [10.1146/annurev-nucl-101917-021141](https://doi.org/10.1146/annurev-nucl-101917-021141)
- Frebel, A., Christlieb, N., Norris, J. E., et al. 2006, *ApJ*, 652, 1585, doi: [10.1086/508506](https://doi.org/10.1086/508506)
- Frey, B. J., & Dueck, D. 2007, *Science*, 315, 972, doi: [10.1126/science.1136800](https://doi.org/10.1126/science.1136800)
- Fulbright, J. P. 2000, *AJ*, 120, 1841, doi: [10.1086/301548](https://doi.org/10.1086/301548)
- Gaia Collaboration, Prusti, T., de Bruijne, J. H. J., et al. 2016, *A&A*, 595, A1, doi: [10.1051/0004-6361/201629272](https://doi.org/10.1051/0004-6361/201629272)
- Gaia Collaboration, Brown, A. G. A., Vallenari, A., et al. 2018, *A&A*, 616, A1, doi: [10.1051/0004-6361/201833051](https://doi.org/10.1051/0004-6361/201833051)
- Hampel, M., Stancliffe, R. J., Lugaro, M., & Meyer, B. S. 2016, *ApJ*, 831, 171, doi: [10.3847/0004-637x/831/2/171](https://doi.org/10.3847/0004-637x/831/2/171)
- Hansen, C. J., Primas, F., Hartman, H., et al. 2012, *A&A*, 545, A31, doi: [10.1051/0004-6361/201118643](https://doi.org/10.1051/0004-6361/201118643)
- Hansen, T., Hansen, C. J., Christlieb, N., et al. 2015, *ApJ*, 807, 173, doi: [10.1088/0004-637x/807/2/173](https://doi.org/10.1088/0004-637x/807/2/173)
- Hansen, T. T., Holmbeck, E. M., Beers, T. C., et al. 2018, *ApJ*, 858, 92, doi: [10.3847/1538-4357/aabacc](https://doi.org/10.3847/1538-4357/aabacc)
- Hawkins, K., & Wyse, R. F. G. 2018, *MNRAS*, 481, 1028, doi: [10.1093/mnras/sty2282](https://doi.org/10.1093/mnras/sty2282)
- Hayek, W., Wiesendahl, U., Christlieb, N., et al. 2009, *A&A*, 504, 511, doi: [10.1051/0004-6361/200811121](https://doi.org/10.1051/0004-6361/200811121)
- Helmi, A., Babusiaux, C., Koppelman, H. H., et al. 2018, *Nature*, 563, 85, doi: [10.1038/s41586-018-0625-x](https://doi.org/10.1038/s41586-018-0625-x)
- Helmi, A., & de Zeeuw, P. T. 2000, *MNRAS*, 319, 657, doi: [10.1046/j.1365-8711.2000.03895.x](https://doi.org/10.1046/j.1365-8711.2000.03895.x)
- Helmi, A., Veljanoski, J., Breddels, M. A., Tian, H., & Sales, L. V. 2017, *A&A*, 598, A58, doi: [10.1051/0004-6361/201629990](https://doi.org/10.1051/0004-6361/201629990)
- Helmi, A., White, S. D. M., de Zeeuw, P. T., & Zhao, H. 1999, *Nature*, 402, 53, doi: [10.1038/46980](https://doi.org/10.1038/46980)
- Herwig, F. 2005, *ARA&A*, 43, 435, doi: [10.1146/annurev.astro.43.072103.150600](https://doi.org/10.1146/annurev.astro.43.072103.150600)
- Hill, V., Plez, B., Cayrel, R., et al. 2002, *A&A*, 387, 560, doi: [10.1051/0004-6361:20020434](https://doi.org/10.1051/0004-6361:20020434)
- Hollek, J. K., Frebel, A., Roederer, I. U., et al. 2011, *ApJ*, 742, 54, doi: [10.1088/0004-637X/742/1/54](https://doi.org/10.1088/0004-637X/742/1/54)
- Holmbeck, E. M., Frebel, A., McLaughlin, G. C., et al. 2019a, *ApJ*, 881, 5, doi: [10.3847/1538-4357/ab2a01](https://doi.org/10.3847/1538-4357/ab2a01)
- Holmbeck, E. M., Sprouse, T. M., Mumpower, M. R., et al. 2019b, *ApJ*, 870, 23, doi: [10.3847/1538-4357/aaefef](https://doi.org/10.3847/1538-4357/aaefef)
- Holmbeck, E. M., Beers, T. C., Roederer, I. U., et al. 2018, *ApJ*, 859, L24, doi: [10.3847/2041-8213/aac722](https://doi.org/10.3847/2041-8213/aac722)
- Holmbeck, E. M., Hansen, T. T., Beers, T. C., et al. 2020, *ApJS*, 249, 30, doi: [10.3847/1538-4365/ab9c19](https://doi.org/10.3847/1538-4365/ab9c19)
- Honda, S., Aoki, W., Kajino, T., et al. 2004, *ApJ*, 607, 474, doi: [10.1086/383406](https://doi.org/10.1086/383406)
- Horowitz, C. J., Arcones, A., Côté, B., et al. 2019, *Journal of Physics G: Nuclear and Particle Physics*, 46, 083001, doi: [10.1088/1361-6471/ab0849](https://doi.org/10.1088/1361-6471/ab0849)
- Hotokezaka, K., Beniamini, P., & Piran, T. 2018, *International Journal of Modern Physics D*, 27, 1842005, doi: [10.1142/S0218271818420051](https://doi.org/10.1142/S0218271818420051)
- Howes, L. M., Casey, A. R., Asplund, M., et al. 2015, *Nature*, 527, 484, doi: [10.1038/nature15747](https://doi.org/10.1038/nature15747)

- Howes, L. M., Asplund, M., Keller, S. C., et al. 2016, *MNRAS*, 460, 884, doi: [10.1093/mnras/stw1004](https://doi.org/10.1093/mnras/stw1004)
- Ishigaki, M. N., Aoki, W., & Chiba, M. 2013, *ApJ*, 771, 67, doi: [10.1088/0004-637X/771/1/67](https://doi.org/10.1088/0004-637X/771/1/67)
- Ivans, I. I., Simmerer, J., Sneden, C., et al. 2006, *ApJ*, 645, 613, doi: [10.1086/504069](https://doi.org/10.1086/504069)
- Jacobson, H. R., Keller, S., Frebel, A., et al. 2015, *ApJ*, 807, 171, doi: [10.1088/0004-637x/807/2/171](https://doi.org/10.1088/0004-637x/807/2/171)
- Ji, A. P., Frebel, A., Chiti, A., & Simon, J. D. 2016, *Nature*, 531, 610–613, doi: [10.1038/nature17425](https://doi.org/10.1038/nature17425)
- Ji, A. P., Simon, J. D., Frebel, A., Venn, K. A., & Hansen, T. T. 2019, *ApJ*, 870, 83, doi: [10.3847/1538-4357/aaf3bb](https://doi.org/10.3847/1538-4357/aaf3bb)
- Johnson, C. I., McWilliam, A., & Rich, R. M. 2013, *ApJL*, 775, L27, doi: [10.1088/2041-8205/775/1/L27](https://doi.org/10.1088/2041-8205/775/1/L27)
- Johnson, J. A., & Bolte, M. 2002, *ApJ*, 579, 616, doi: [10.1086/342829](https://doi.org/10.1086/342829)
- Keegans, J., Fryer, C. L., Jones, S. W., et al. 2019, *MNRAS*, 485, 620, doi: [10.1093/mnras/stz368](https://doi.org/10.1093/mnras/stz368)
- Kharchenko, N. V., & Roeser, S. 2009, *VizieR Online Data Catalog*, I/280B
- Kilpatrick, C. D., Foley, R. J., Kasen, D., et al. 2017, *Science*, 358, 1583, doi: [10.1126/science.aag0073](https://doi.org/10.1126/science.aag0073)
- Kirby, E. N., Cohen, J. G., Guhathakurta, P., et al. 2013, *ApJ*, 779, 102, doi: [10.1088/0004-637x/779/2/102](https://doi.org/10.1088/0004-637x/779/2/102)
- Koppelman, H., Helmi, A., & Veljanoski, J. 2018, *ApJ*, 860, L11, doi: [10.3847/2041-8213/aac882](https://doi.org/10.3847/2041-8213/aac882)
- Koppelman, H. H., Helmi, A., Massari, D., Price-Whelan, A. M., & Starkenburg, T. K. 2019a, *A&A*, 631, L9, doi: [10.1051/0004-6361/201936738](https://doi.org/10.1051/0004-6361/201936738)
- Koppelman, H. H., Helmi, A., Massari, D., Roelenga, S., & Bastian, U. 2019b, *A&A*, 625, A5, doi: [10.1051/0004-6361/201834769](https://doi.org/10.1051/0004-6361/201834769)
- Kunder, A., Kordopatis, G., Steinmetz, M., et al. 2017, *AJ*, 153, 75, doi: [10.3847/1538-3881/153/2/75](https://doi.org/10.3847/1538-3881/153/2/75)
- Lai, D., Bolte, M., Johnson, J., et al. 2008, *ApJ*, 681, 1524, doi: [10.1086/588811](https://doi.org/10.1086/588811)
- Lattimer, J. M., & Schramm, D. N. 1974, *ApJL*, 192, L145, doi: [10.1086/181612](https://doi.org/10.1086/181612)
- Li, H., Aoki, W., Zhao, G., et al. 2015, *PASJ*, 67, 84, doi: [10.1093/pasj/psv053](https://doi.org/10.1093/pasj/psv053)
- Limberg, G., Rossi, S., Beers, T. C., et al. 2020, *arXiv e-prints*, arXiv:2011.08305. <https://arxiv.org/abs/2011.08305>
- Lindgren, L., Hernández, J., Bombrun, A., et al. 2018, *A&A*, 616, A2, doi: [10.1051/0004-6361/201832727](https://doi.org/10.1051/0004-6361/201832727)
- Lloyd, S. 1982, *IEEE Transactions on Information Theory*, 28, 129, doi: [10.1109/TIT.1982.1056489](https://doi.org/10.1109/TIT.1982.1056489)
- Malzer, C., & Baum, M. 2019, *arXiv e-prints*, arXiv:1911.02282. <https://arxiv.org/abs/1911.02282>
- Mardini, M. K., Li, H., Placco, V. M., et al. 2019, *ApJ*, 875, 89, doi: [10.3847/1538-4357/ab0fa2](https://doi.org/10.3847/1538-4357/ab0fa2)
- Mashonkina, L., Christlieb, N., & Eriksson, K. 2014, *A&A*, 569, A43, doi: [10.1051/0004-6361/201424017](https://doi.org/10.1051/0004-6361/201424017)
- Masseron, T., Johnson, J. A., Lucatello, S., et al. 2012, *ApJ*, 751, 14, doi: [10.1088/0004-637x/751/1/14](https://doi.org/10.1088/0004-637x/751/1/14)
- McInnes, L., Healy, J., & Astels, S. 2017, *The Journal of Open Source Software*, 2, doi: [10.21105/joss.00205](https://doi.org/10.21105/joss.00205)
- McMillan, P. J. 2017, *MNRAS*, 465, 76, doi: [10.1093/mnras/stw2759](https://doi.org/10.1093/mnras/stw2759)
- McWilliam, A. 1998, *AJ*, 115, 1640, doi: [10.1086/300289](https://doi.org/10.1086/300289)
- McWilliam, A., Preston, G. W., Sneden, C., & Searle, L. 1995, *AJ*, 109, 2757, doi: [10.1086/117486](https://doi.org/10.1086/117486)
- Meynet, G., Ekström, S., & Maeder, A. 2006, *A&A*, 447, 623, doi: [10.1051/0004-6361:20053070](https://doi.org/10.1051/0004-6361:20053070)
- Morrison, H. L., Flynn, C., & Freeman, K. C. 1990, *AJ*, 100, 1191, doi: [10.1086/115587](https://doi.org/10.1086/115587)
- Myeong, G. C., Evans, N. W., Belokurov, V., Amorisco, N. C., & Koposov, S. E. 2018a, *MNRAS*, 475, 1537, doi: [10.1093/mnras/stx3262](https://doi.org/10.1093/mnras/stx3262)
- Myeong, G. C., Evans, N. W., Belokurov, V., Sand ers, J. L., & Koposov, S. E. 2018b, *MNRAS*, 478, 5449, doi: [10.1093/mnras/sty1403](https://doi.org/10.1093/mnras/sty1403)
- Myeong, G. C., Vasiliev, E., Iorio, G., Evans, N. W., & Belokurov, V. 2019, *MNRAS*, 488, 1235, doi: [10.1093/mnras/stz1770](https://doi.org/10.1093/mnras/stz1770)
- Naidu, R. P., Conroy, C., Bonaca, A., et al. 2020, *ApJ*, 901, 48, doi: [10.3847/1538-4357/abaef4](https://doi.org/10.3847/1538-4357/abaef4)
- Nishimura, N., Takiwaki, T., & Thielemann, F.-K. 2015, *ApJ*, 810, 109, doi: [10.1088/0004-637x/810/2/109](https://doi.org/10.1088/0004-637x/810/2/109)
- Pignatari, M., Gallino, R., Meynet, G., et al. 2008, *ApJ*, 687, L95, doi: [10.1086/593350](https://doi.org/10.1086/593350)
- Placco, V. M., Frebel, A., Beers, T. C., & Stancliffe, R. J. 2014, *ApJ*, 797, 21, doi: [10.1088/0004-637x/797/1/21](https://doi.org/10.1088/0004-637x/797/1/21)
- Placco, V. M., Holmbeck, E. M., Frebel, A., et al. 2017, *ApJ*, 844, 18, doi: [10.3847/1538-4357/aa78ef](https://doi.org/10.3847/1538-4357/aa78ef)
- Placco, V. M., Santucci, R. M., Yuan, Z., et al. 2020, *ApJ*, 897, 78, doi: [10.3847/1538-4357/ab99c6](https://doi.org/10.3847/1538-4357/ab99c6)
- Preston, G. W., Thompson, I. B., Sneden, C., Stachowski, G., & Shectman, S. A. 2006, *AJ*, 132, 1714, doi: [10.1086/507519](https://doi.org/10.1086/507519)
- Queiroz, A. B. A., Anders, F., Santiago, B. X., et al. 2018, *MNRAS*, 476, 2556, doi: [10.1093/mnras/sty330](https://doi.org/10.1093/mnras/sty330)
- Queiroz, A. B. A., Anders, F., Chiappini, C., et al. 2020, *A&A*, 638, A76, doi: [10.1051/0004-6361/201937364](https://doi.org/10.1051/0004-6361/201937364)
- Rasmussen, K. C., Zepeda, J., Beers, T. C., et al. 2020, *arXiv e-prints*, arXiv:2010.04214. <https://arxiv.org/abs/2010.04214>
- Roederer, I. U., Cowan, J. J., Karakas, A. I., et al. 2010, *ApJ*, 724, 975, doi: [10.1088/0004-637x/724/2/975](https://doi.org/10.1088/0004-637x/724/2/975)



- Roederer, I. U., Hattori, K., & Valluri, M. 2018a, *AJ*, 156, 179, doi: [10.3847/1538-3881/aadd9c](https://doi.org/10.3847/1538-3881/aadd9c)
- Roederer, I. U., Preston, G. W., Thompson, I. B., Shectman, S. A., & Sneden, C. 2014, *ApJ*, 784, 158, doi: [10.1088/0004-637x/784/2/158](https://doi.org/10.1088/0004-637x/784/2/158)
- Roederer, I. U., Preston, G. W., Thompson, I. B., et al. 2014, *AJ*, 147, 136, doi: [10.1088/0004-6256/147/6/136](https://doi.org/10.1088/0004-6256/147/6/136)
- Roederer, I. U., Sakari, C. M., Placco, V. M., et al. 2018b, *ApJ*, 865, 129, doi: [10.3847/1538-4357/aadd92](https://doi.org/10.3847/1538-4357/aadd92)
- Roederer, I. U., Mateo, M., Bailey, John I., I., et al. 2016, *AJ*, 151, 82, doi: [10.3847/0004-6256/151/3/82](https://doi.org/10.3847/0004-6256/151/3/82)
- Roerdink, J. B. T. M., & Meijster, A. 2000, *Fundamenta Informatica*, 41, 187–228, doi: [10.3233/FI-2000-411207](https://doi.org/10.3233/FI-2000-411207)
- Ryan, S. G., Norris, J. E., & Beers, T. C. 1996, *ApJ*, 471, 254, doi: [10.1086/177967](https://doi.org/10.1086/177967)
- Sakari, C. M., Placco, V. M., Farrell, E. M., et al. 2018, *ApJ*, 868, 110, doi: [10.3847/1538-4357/aae9df](https://doi.org/10.3847/1538-4357/aae9df)
- Sartoretti, P., Katz, D., Cropper, M., et al. 2018, *A&A*, 616, A6, doi: [10.1051/0004-6361/201832836](https://doi.org/10.1051/0004-6361/201832836)
- Schatz, H., Toenjes, R., Pfeiffer, B., et al. 2002, *ApJ*, 579, 626, doi: [10.1086/342939](https://doi.org/10.1086/342939)
- Schönrich, R., McMillan, P., & Eyer, L. 2019, *MNRAS*, 487, 3568, doi: [10.1093/mnras/stz1451](https://doi.org/10.1093/mnras/stz1451)
- Sestito, F., Longeard, N., Martin, N. F., et al. 2019, *MNRAS*, 484, 2166, doi: [10.1093/mnras/stz043](https://doi.org/10.1093/mnras/stz043)
- Sestito, F., Martin, N. F., Starkenburg, E., et al. 2020, *MNRAS*, doi: [10.1093/mnrasl/slaa022](https://doi.org/10.1093/mnrasl/slaa022)
- Shappee, B. J., Simon, J. D., Drout, M. R., et al. 2017, *Science*, 358, 1574, doi: [10.1126/science.aaq0186](https://doi.org/10.1126/science.aaq0186)
- Siegel, D. M., Barnes, J., & Metzger, B. D. 2019, *Nature*, 569, 241, doi: [10.1038/s41586-019-1136-0](https://doi.org/10.1038/s41586-019-1136-0)
- Simon, J. D. 2018, *ApJ*, 863, 89, doi: [10.3847/1538-4357/aacdfb](https://doi.org/10.3847/1538-4357/aacdfb)
- Siqueira Mello, C., Hill, V., Barbuy, B., et al. 2014, *A&A*, 565, A93, doi: [10.1051/0004-6361/201423826](https://doi.org/10.1051/0004-6361/201423826)
- Sneden, C., Johnson, J., Kraft, R. P., et al. 2000, *ApJL*, 536, L85, doi: [10.1086/312742](https://doi.org/10.1086/312742)
- Sneden, C., Cowan, J. J., Lawler, J. E., et al. 2003, *ApJ*, 591, 936, doi: [10.1086/375491](https://doi.org/10.1086/375491)
- Sobeck, J. S., Kraft, R. P., Sneden, C., et al. 2011, *AJ*, 141, 175, doi: [10.1088/0004-6256/141/6/175](https://doi.org/10.1088/0004-6256/141/6/175)
- Thielemann, F.-K., Eichler, M., Panov, I., & Wehmeyer, B. 2017, *Annual Review of Nuclear and Particle Science*, 67, 253, doi: [10.1146/annurev-nucl-101916-123246](https://doi.org/10.1146/annurev-nucl-101916-123246)
- Travaglio, C., Gallino, R., Arnone, E., et al. 2004, *ApJ*, 601, 864, doi: [10.1086/380507](https://doi.org/10.1086/380507)
- Valentini, M., Chiappini, C., Bossini, D., et al. 2019, *A&A*, 627, A173, doi: [10.1051/0004-6361/201834081](https://doi.org/10.1051/0004-6361/201834081)
- Vasiliev, E. 2018, *MNRAS*, 482, 1525, doi: [10.1093/mnras/sty2672](https://doi.org/10.1093/mnras/sty2672)
- Wanajo, S. 2013, *ApJ*, 770, L22, doi: [10.1088/2041-8205/770/2/L22](https://doi.org/10.1088/2041-8205/770/2/L22)
- Ward, J. H. J. 1963, *Journal of the American Statistical Association*, 58, 236, doi: [10.1080/01621459.1963.10500845](https://doi.org/10.1080/01621459.1963.10500845)
- Watson, D., Hansen, C. J., Selsing, J., et al. 2019, *Nature*, 574, 497, doi: [10.1038/s41586-019-1676-3](https://doi.org/10.1038/s41586-019-1676-3)
- Westin, J., Sneden, C., Gustafsson, B., & Cowan, J. J. 2000, *ApJ*, 530, 783, doi: [10.1086/308407](https://doi.org/10.1086/308407)
- Winteler, C., Käppeli, R., Perego, A., et al. 2012, *ApJ*, 750, L22, doi: [10.1088/2041-8205/750/1/L22](https://doi.org/10.1088/2041-8205/750/1/L22)
- Xing, Q.-F., Zhao, G., Aoki, W., et al. 2019, *Nature Astronomy*, 3, doi: [10.1038/s41550-019-0764-5](https://doi.org/10.1038/s41550-019-0764-5)
- Yuan, Z., Chang, J., Banerjee, P., et al. 2018, *ApJ*, 863, 26, doi: [10.3847/1538-4357/aacd0d](https://doi.org/10.3847/1538-4357/aacd0d)
- Yuan, Z., Myeong, G. C., Beers, T. C., et al. 2020, *ApJ*, 891, 39, doi: [10.3847/1538-4357/ab6ef7](https://doi.org/10.3847/1538-4357/ab6ef7)

